2017

Polymer Fibre Artificial Muscle

Shazed Md Aziz
University of Wollongong

UNIVERSITY
OF WOLLONGONG
AUSTRALIA

Polymer Fibre Artificial Muscle

By

Shazed Md Aziz

School of Mechanical, Materials, Mechatronic and Biomedical Engineering

Intelligent Polymer Research Institute

Wollongong, Australia

"This thesis is presented as part of the requirements for the award of the degree

Doctor of Philosophy

from the

University of Wollongong Australia"

August 2017

DECLARATION

I, Shazed Md Aziz, declare that this thesis, submitted in fulfilment of the requirements for awarding the degree of Doctor of Philosophy at the School of Mechanical, Materials, Mechatronic and Biomedical Engineering at the University of Wollongong, is entirely my own, unless otherwise stated, referenced or acknowledged. This document has not been submitted for qualifications at any other academic institution.

Shazed Md Aziz

August 2017

ACKNOWLEDGEMENTS

I would like to begin by thanking my supervisors Prof. Geoffrey M. Spinks, Dr. Javad Foroughi and Dr. S. Naficy for the way in which they have mentored me during my Ph.D. studies and their interest in my education. Specially, I am much thankful to my principal supervisor Prof. Geoffrey M. Spinks for giving me the opportunity to join his research group, and for his constant support, guidance, idea and encouragement throughout the Ph.D. program. His expertise and knowledge in artificial muscle technology will certainly prove to be priceless throughout the rest of my scientific career. I am also thankful to Prof. Hugh R. Brown for his support as a research advisor with his extraordinary scientific knowledge on fundamental of polymers. I am truly grateful for all their assistance and guidance throughout a well-defined and fruitful research project.

I am also appreciative of all my friends at the Intelligent Polymer Research Institute who have made these past four years a pleasurable experience. I would like to thank all of those who have contributed to this project and I would like to acknowledge the technical supports provided by the workshop of Australian Institute of Innovative Materials (AIIM) during the construction of custom built mechanical and electrical apparatuses / devices.

Last but not least, I owe my sincere gratitude to my family, friends, and colleagues thus far and everything yet to come, especially my belated parents, and wife, Bidita Binte Salahuddin, and my sister, Khaleda Naznin for their priceless help, guidance, and endless encouragement and blessing.

ABSTRACT

Large-scale torsional actuation occurs in twisted fibres and yarns as a result of volume change induced electrochemically, thermally, photonically, and other means. When formed into spring-like coils, the torsional actuation within the fibre or yarn generates powerful tensile actuation per muscle weight. For further development of these coil actuators and for the practical application of torsional actuators, it is important to standardise methods for characterising both the torsional stroke (rotation) and torque generated. This thesis introduces such a method for use in the free rotation of a one-end-tethered fibre, when operating against an externally applied torque (isotonic) and during actuation against a return spring fibre (variable torque). The torsion mechanics approach has been verified and allows the prediction of torsional stroke under any external loading condition based on the fundamental characteristics of the actuator: free stroke and stiffness. The second thesis aim was to develop a better understanding of the link between fibre / yarn volume change and the induced torsional actuation. The developed theoretical analysis was based on experimental investigation of the effects of fibre diameter and inserted twist on the torsional stroke and torque measured when heating and cooling nylon 6 fibres over a certain temperature range. The results show that the torsional stroke depends only on the amount of twist inserted into the fibre and is independent of fibre diameter. The torque generated is larger in fibres with more inserted twist and with larger diameters. These results are successfully modelled using a single-helix approximation of the twisted fibre structure. Apart from nylon 6 fibre, thermally-induced torsional actuation of twisted fibres made from polyethylene and polypropylene were also studied experimentally and theoretically. The single-helix model accurately predicts the torsional stroke based on the measured fibre length and diameter change during heating. The degree of actuation was found to be greater in the

order of nylon 6, polyethylene and polypropylene, respectively, due to their volume change occurred respective to the applied temperature chance. Generated blocked torques was also correctly predicted by the single-helix model when combined with the measured fibre torsional stiffness. However, it has been found that these actuators require multiple heat/cool cycles (referred to as 'training' cycles) prior to obtaining a fully reversible actuation response. The effect of annealing conditions applied to twisted nylon 6 fibre was investigated and it is shown that annealing at near-melting temperature eliminates the need for the training cycles. Furthermore, the effect of an applied external torque on the torsional actuation is also investigated and torsional creep is shown to be affected by the temperature and load. Finally, to show the applicability of torsional actuators, a new concept for contractile artificial muscles is introduced in which the torsional rotation of a twisted nylon 6 fibre drives a twist to writhe conversion in a serially attached elastomeric spandex yarn. The core idea originated from the torsional muscle with a return spring fibre connected in series. A spandex yarn is attached to the twisted fibre and thermally induced torsional rotation of the twisted fibre caused formation of coils in the spandex yarn and caused an overall muscle contraction. Torsional rotation of twisted fibre and resultant spandex coil geometry are utilized to theoretically predict the amount of muscle contraction by means of a modified single-helix theory. Once again a theoretical model was developed and a good agreement was found between measured and calculated results. The thesis concludes with suggestions for further work that include both theoretical and practical areas.

LIST OF PUBLICATIONS

1. S. Aziz, S. Naficy, J. Foroughi, H.R. Brown, G.M. Spinks, Characterisation of torsional actuation in highly twisted yarns and fibres, *Polymer Testing*, 46 (2015) 88-97.
2. S.H. Kim, M.D. Lima, M.E. Kozlov, C.S. Haines, G.M. Spinks, S. Aziz, C. Choi, H.J. Sim, X. Wang, H. Lu, D. Qian, J.D.W. Madden, R.H. Baughman, S.J. Kim, Harvesting temperature fluctuations as electrical energy using torsional and tensile polymer muscles, *Energy & Environmental Science*, 8(11) (2015) 3336-3344.
3. S. Aziz, S. Naficy, J. Foroughi, H.R. Brown, G.M. Spinks, Controlled and scalable torsional actuation of twisted nylon 6 fibre, *Journal of Polymer Science Part B: Polymer Physics*, 54(13) (2016) 1278-1286.
4. J. Foroughi, G.M. Spinks, S. Aziz, A. Mirabedini, A. Jeiranikhameneh, G.G. Wallace, M.E. Kozlov, R.H. Baughman, Knitted carbon-nanotube-sheath/spandex-core elastomeric yarns for artificial muscles and strain sensing, *ACS Nano*, 10(10) (2016) 9129-9135.
5. A. Mirabedini, S. Aziz, G.M. Spinks, J. Foroughi, Wet-spun biofibre for torsional artificial muscles, *Soft Robotics*, Accepted (2017).
6. S. Aziz, S. Naficy, J. Foroughi, H. R. Brown and G.M. Spinks, Comparison of torsional actuation in twisted polymer fibres: polyethylene, polypropylene and polyamide-6, *Polymer*, Awaiting Revision (2017).
7. S. Aziz, S. Naficy, J. Foroughi, H. R. Brown and G.M. Spinks, Thermo-mechanical effects in the torsional actuation of twisted nylon 6 fibre, *Journal of Applied Polymer Science*, DOI: 10.1002/app.45529 (2017).

TABLE OF CONTENTS

LIST OF ABBERVIATIONS

SMA	Shape memory alloy
EAP	Electroactive polymer
PZT	Lead zirocondate titanate
PVDF	Polyvinylidene fluoride
FRC	Fibre reinforced composite
LED	Light emitting diode
PPy	Polypyrrole
CNT	Carbon nanotube
SEBS	Polystyrene-poly(ethylene–butylene)-polystyrene copolymer
$TEABF_4$	Tetraethylammonium tetrafluoroborate
ITAP	Incandescent tension annealing process
T_g	Glass transition temperature
d_o	Diameter of the fibre before actuation
d	Diameter of the fibre after actuation
D	Diameter of the coil before actuation
D'	Diameter of the coil after actuation
L	Length of coil before actuation
ΔL	Change in coil length
Δn	Change in number of twist for a certain length of fibre
ΔT	Change of twist
Δd	Change in fibre diameter
α_f	Twist angle to the fibre axis
V	Volume

r	Non-actuated fibre radius
r'	Actuated fibre radius
l_s	Length of twisted fibre string
λ	Length ratio
$\phi(L_A)_{free}$	Free rotation of a one-end-tethered fibre
$\phi(L_A)_{\text{isotonic}}$	Fibre rotation under external torque
$\phi(L_A)_{return\ spring}$	Fibre rotation against return spring
$\tau_{blocked}$	Blocked torque
τ_{ext}	External torque
S_A	Non-actuated fibre torsional stiffness
S'_A	Actuated fibre torsional stiffness
k_A	Torsional modulus of actuated fibre
k'_A	Torsional modulus of non-actuated fibre
G	Shear modulus
E	Elastic modulus
J	Polar moment of inertia
λ	Ratio factor
N_c	Number of coil
τ_c	Critical torque before coil formation
n_c	Critical twist before coil formation
α_c	Coil bias angle
L_S	Coil string length

LIST OF FIGURES

CHAPTER 1

CHAPTER 2

CHAPTER 3

CHAPTER 4

CHAPTER 5

CHAPTER 6

LIST OF TABLES

CHAPTER 1

CHAPTER 2

CHAPTER 3

CHAPTER 4

CHAPTER 6

CHAPTER 1 Torsional Artificial Muscles

1.1 Introduction

New discoveries in smart materials fuel the continual advancement of artificial muscles that mimic the performance of skeletal muscles. One major advantage of artificial muscles over conventional actuators such as electric motors and combustion engines is their potential for miniaturisation without the sacrifice of power generated per mass. Artificial muscles have been developed that can reversibly simulate muscle-like motions such as contraction, expansion, bending, and rotation [1-4]. Many different materials have been developed for artificial muscles, including shape memory alloys (SMAs) [5-15], electroactive polymers (EAPs) [4, 16-21] and piezoelectric and dielectric materials [22-26]. The performance of artificial muscles can be evaluated against a number of parameters, including force and displacement generated and speed of response. In many of these areas, artificial muscle performance surpasses that of natural skeletal muscle, making them significantly attractive to use in applications where a muscle-like response is required. Commercial development and use of these materials are at the primary stage, and only a few types are commercially exposed. However, there is need for continued improvement in artificial muscles systems since applications areas can be expanded by reducing overall system mass and volume, reducing driving voltages, increasing actuation rates, cycle-life and power density [1, 27, 28].

Like natural skeletal muscle, artificial muscles are characterised by a reciprocating or oscillatory type of motion that may be evident as tensile, bending, torsional or a combination of these processes. Figure 1 summarises the general actuation types of artificial muscles. Simple volume change materials can generate tensile actuation strokes [Figure 1.1(a)] and the coupling of an active volume change material to a flexible support structure converts the volume change into a bending displacement [Figure 1.1(b)]. Examples include bimetallic strips and similar laminate structures.

Helically twisted fibres or yarns can generate torsional rotation depending on their volume changes once activated [Figure 1.1(c)]. Additionally, twist induced coiled fibres can generate contractile motion when the degree of inserted twists changes [Figure 1.1(d)]. This thesis specifically concentrates on these 'torsional' artificial muscles and aims to better understand the mechanism of torsional actuation occurring in heat-activated twisted polymer fibres.

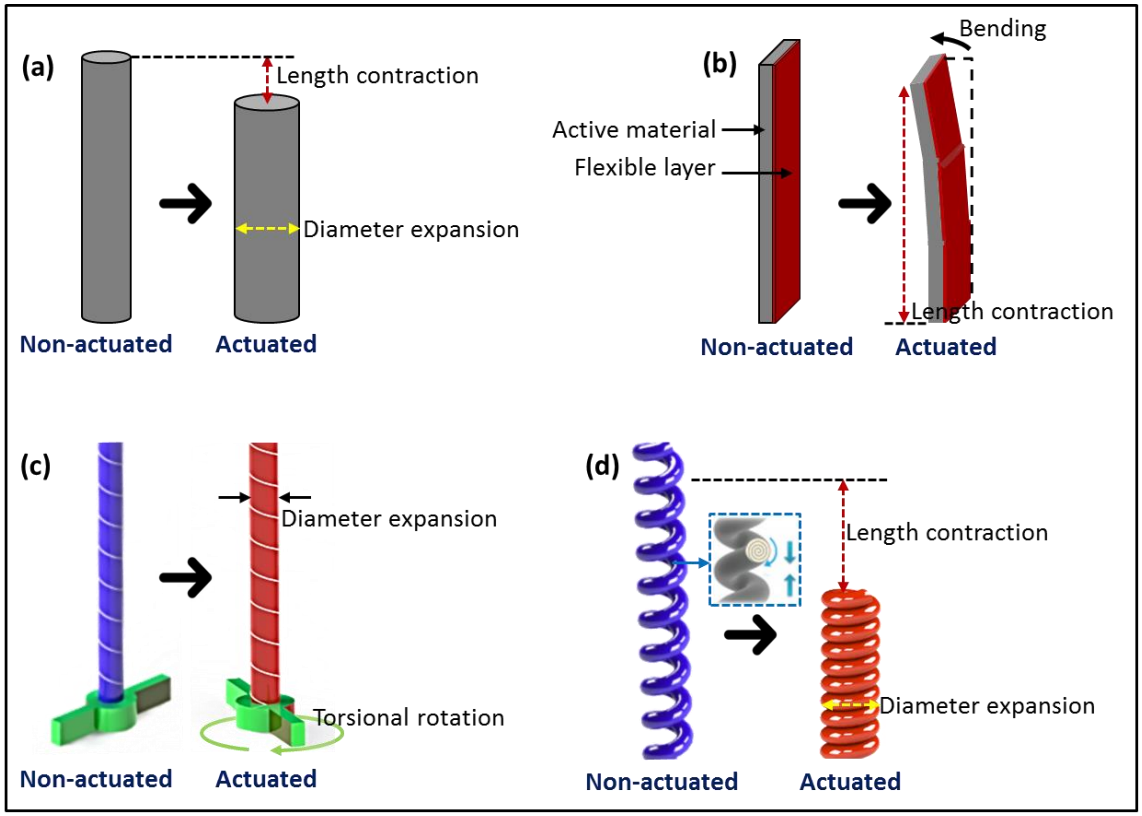

Figure 1.1. Actuation capabilities of differently structured materials; (a) linear actuation, (b) bending motion, (c) torsional rotation, and (d) torsion induced linear actuation.

Torsional actuation of a material can be defined as in 'torsion mechanics' which describes the angular rotation of one part of a slender beam when a torque is applied and where the rotation occurs around the beam long axis. Torsional actuators show such

rotations in fibres, wires, films and strips in certain materials when exposed to various stimuli. Most recent interest has considered the torsional actuation in highly twisted fibres and yarns mainly because of the large torsional rotations generated, but earlier work has examined torsional actuation in tubes and ribbons or strips. Figure 1.2 charts the recent evolution of torsional actuators which shows an increase of published work over the past decade.

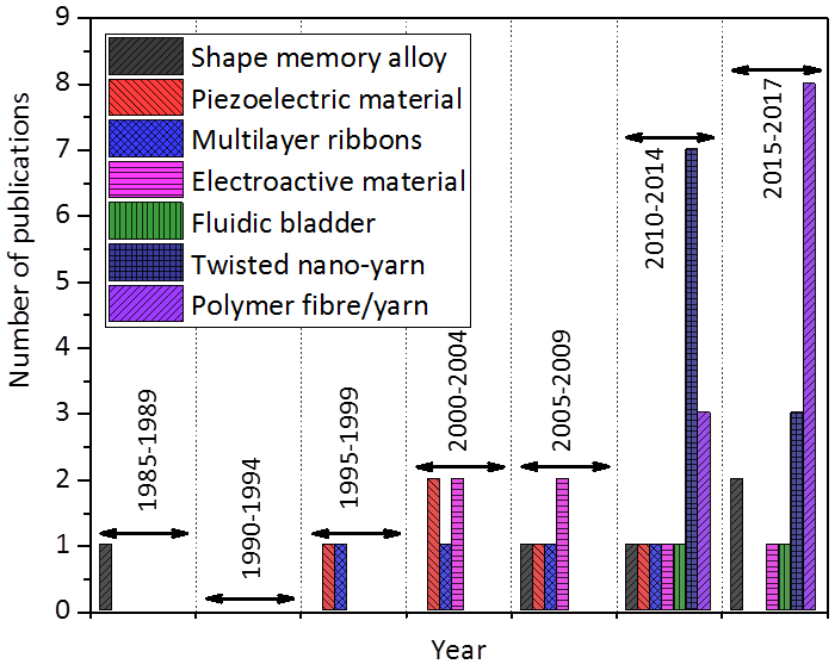

Figure 1.2. Development progression of torsional actuators constructed of different materials.

Torsional actuation can be used to develop useful oscillatory rotations, but the most significant application area is in tensile actuation of coil structures that is driven by torsion in the coil fibre or wire. The well-established spring mechanics shows that stretching a coiled fibre that is tethered to prevent end rotation produces a change in the fibre's twist as given by:

$$\Delta T = \frac{N\Delta L}{l^2} \tag{1.1}$$

Where ΔT is the change in twist (turns/m) of the fibre of length l that forms a coil of N turns and when the coil length changes by ΔL. Coils made from torsionally actuating fibres generate large coil tensile actuations. Tensile strokes as high as ~50% were reported for twisted and coiled nylon 6,6 fibres, delivering power densities over 5.3 kW/kg with 2.48 kJ/kg contractile work capacity and greatly exceeding that produced by natural skeletal muscle (39 J/kg) [29, 30].

Applications that exploit the rotating action of torsional actuators have employed tethering at either one end or both ends. The latter requires some asymmetry in the actuator to allow rotation and most typically this has been achieved by connecting the actuating material in series to a non-actuating material. The non-actuating material also operates as a 'return spring' mechanism that can improve the reversibility of the actuation when the actuating stimulus is removed. The mechanics of torsional actuation is first described in terms of reversible rotation for an actuating fibre tethered at one end only. A vertically hanging fibre of length l that is clamped at the top end and free to rotate at the opposite end can be treated as a torsional shaft. The rotation of the free end with regard to the clamped end is $\phi(l) = \tau / S$, where τ is the torque applied to the free end and S is the torsional rigidity of the fibre. The actuating fibre generates an internal torque causing a rotation per yarn length of $\Delta\theta$ at the free end. The rotation at any distance x from the tethered end to the free fibre end is:

$$\phi(\mathrm{x}) = \mathrm{x}\Delta\theta \qquad (1.2)$$

Torsional rotation of a fibre clamped at both ends and subjected to constant tensile load is measured using a paddle attached to the fibre at a distance x from the starting point. Clamping at both ends does not allow any rotation at either end hence rotation is only possible if the fibre is actuated along only part of its length. Here, rotation of the

actuating segment of the fibre mechanically introduces rotation to the non-actuating segment, thereby generating an increasing opposing torque in the non-actuating segment as the torsional rotation proceeds. Therefore, tethering the fibre at both ends restricts rotation at all points along the fibre compared to the free rotation by producing this equal and opposite residual torques in the actuating and non-actuating segments. The net rotation, $\phi(\mathrm{x})$ occurring at any point x along the actuating segment is given by:

$$\phi(\mathrm{x}) = \mathrm{x}\Delta\theta\left(\frac{\beta}{\beta+\gamma}\right) \tag{1.3}$$

where β is the ratio of the torsional modulus of the actuating and non-actuating segments; γ is the ratio of the actuating segment length to non-actuating segment length; and x varies from zero to *l*, where *l* is the length of the actuating segment.

These principles of torsional mechanics provide a framework for the comparison of various reported torsional actuators. The inherent torsional actuation properties are described by $\Delta\theta$, the torsional stiffness and the rates of response. Where available these parameters are described below for different torsional actuators and related to the different functional mechanisms of actuation. These principles then provide guidance for the design of actuator systems and provide knowledge about their current and potential applications.

1.2 Shape Memory Alloy (SMA) Torsional Actuators

Shape memory alloys (SMAs) are a group of metallic materials that offers the ability to recover a former length or shape when heated. Although a wide range of alloys exhibits the shape memory effect, only those that can recover from a large amount of plastic strain are of practical interest. Among several industrially developed SMAs (such as Cu–Zn–Al, Cu–Al–Ni, and Ni–Ti), the most common SMA is Ni–Ti (Nitinol) alloy

used for its high ductility and fatigue and corrosion resistance [13, 31-33]. In addition, Nitinol offers design flexibility in the form of rods [34, 35], tubes [11], sheets [9, 36], strips [37], wires [6, 12, 38-40], and coils [41, 42].

Torsional actuation has been demonstrated in both thin SMA strips and wires. Tobushi et al. [43] have conducted torsion, recovery torque and torsion fatigue tests with a TiNi SMA thin strip to evaluate the basic torsion characteristics based on thermal recovery. When the strip was twisted, torque and recovery torque was found to be increased in proportion to the angle of twist and temperature. A rotation of 90^{o} was achieved through shape recovery in a 40 mm long strip operated in the one-end-tethered mode. Another work was conducted with similar TiNi tape, however, used a return spring mechanism for achieving two-way actuation [44]. Here the twisted strip was connected to a superelastic alloy strip that acted as a return spring in the two-end-tethered configuration. A linear relationship was observed between torque and angle of twist per unit length of the strip under a constant loading process. The alternating torsion, the initial and reverse twisting were found to be symmetric with respect to an origin.

Gabriel et al. [45] demonstrated a micro-scale rotary actuator using SMA wire. The TiNi wire was twisted to various amounts and clamped at both ends. Torsional actuation was induced by electrical Joule heating. Both ends of the wire were connected to one terminal of a current source with a third terminal connected to the centre of the wire [Figure 1.3(a)]. The current sources (i_1 and i_2) connected to the rod are pulse-width modulated, and differentially varying the durations of the pulses causes differential heating of the two SMA halves and hence causes an angular deflection about the longitudinal axis at the centre of the SMA wire. In one experiment, a 100 mm long, 100 μm diameter piece of SMA wire was twisted to 320 turns per metre and heated by

passing a current of 200 mA. A maximum torsional stroke of ~0.65° per mm was achieved [Figure 1.3(b)] [45].

Similar torsional actuation mechanisms have recently been reported [8, 46] where a twisting SMA rod was embedded in an elastomeric sheet. These composite actuator systems used the SMA rod as a one-end-tethered torsional actuator and the elastomer sheet as a 'return spring' mechanism to enable two-way actuation [Figure 1.3(c)]. Joule heating of the SMA wire generated twisting of the elastomer sheet to ~1° per mm of 3 mm thick sample [Figure 1.3(d)] [8]. Increasing actuator thicknesses to 5 and 7 mm where the width and length of the actuator were fixed at 15 and 70 mm reduced the torsional stroke, but the blocked torque remained unchanged.

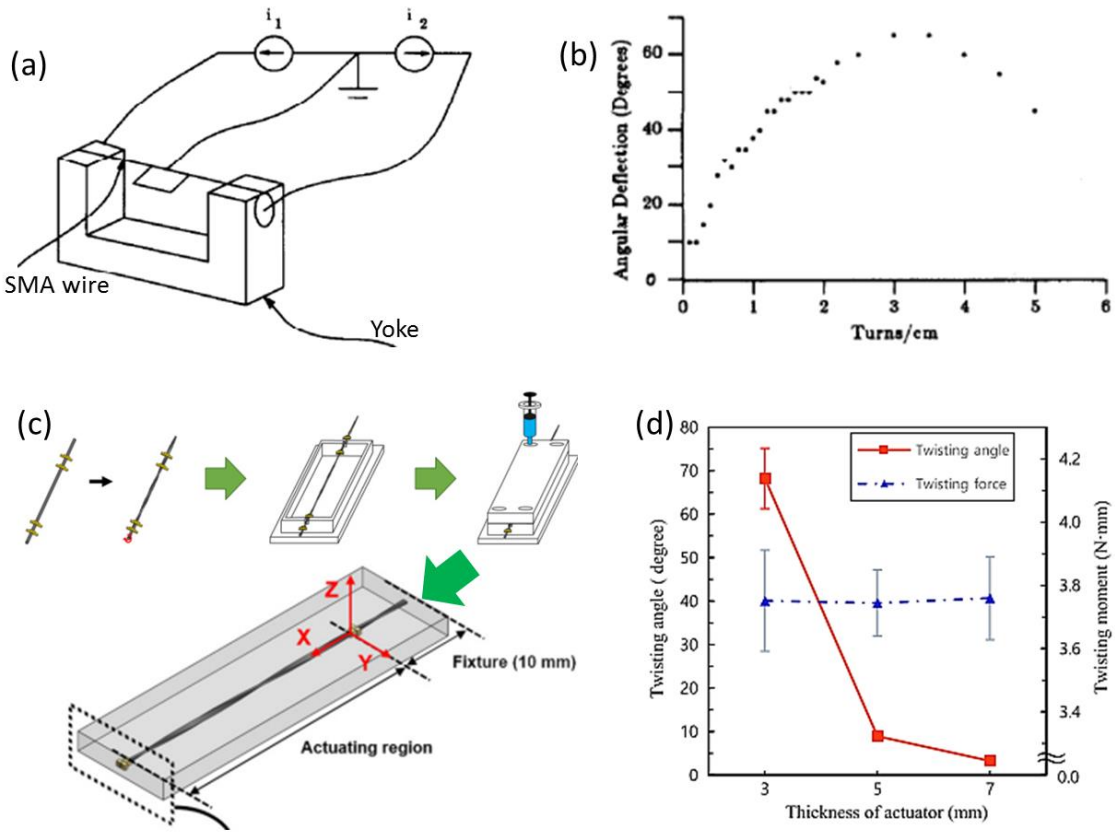

Figure 1.3. Micro-rotary actuator; (a) schematic illustration showing clamping yoke, torsionally strained SMA wire and electronics for differential heating, (b) angular deformation vs. pre-clamped twist (turns/cm) for a 10 mm long, 100 µm diameter piece

of SMA wire being heated by a 200 mA current [45]. Soft twisting actuator; (c) fabrication method of a twisting actuator by clamping the SMA wire with torsional strain, then positioning the SMA wire onto the mold, and finally, lose the upper mold and inject siloxane elastomer, (d) twisting angle and twisting moment depending on the elastomer layer thickness [8].

Despite having a significant number of advantages, control challenges exist in SMA actuators due to their undesired nonlinear characteristics. Conventional solutions using digital encoders remain unfeasible at this scale. Therefore, miniature and low-weight sensors need to be integrated for accurate measurement of torsional actuation. Moreover, power consumption is another concern with SMA actuators, that becomes more significant as the number of actuators grows [47]. Another major limitation is having low (maximum of ~4.5° per mm) rotational angle which makes the SMA torsional actuators less feasible for a real-life application.

1.3 Piezoelectric Torsional Actuators

Piezoelectric and electrostrictive materials are a natural choice for precision displacement transducers or actuators. They utilise the strain induced piezoelectric effect by an electric field to provide static structural deformation [48-50]. A number of materials show piezoelectricity such as piezoelectric ceramics (lead zirocondate titanate, PZT), piezoelectric polymers (polyvinylidene fluoride, PVDF), and piezoelectric ceramic/polymer composites. Actuators made of piezoelectric ceramic materials are now being widely used for numerous applications, such as precision positioning, noise and vibration sensing and cancellation, ultrasonic motors, and controlling hydraulic valves.

Due to their increasing demand, piezoelectric torsional actuators have been studied for many years. Morita et al. [51] developed a torsional actuator from multilayered and assembled piezo-ceramic cylinder which was able to harvest shear strain directly. However, the manufacturing process of the actuator was fairly complex and seems challenging to be used in mini or micro-sized torsional actuators. Therefore, Kim et al. [52] presented the design, test and improvement of a piezoelectric torsional actuator using piezoceramics and a torsion bar which was comparatively easy to construct. The proposed cylindrical actuator directly invokes the shear mode of the piezoelectric material; hence, no complicated additional mechanism is needed [Figure 1.4(a)]. However, a small angular displacement of 0.18° was achieved from a 25 mm long tube. Glazounov et al. [53] described a similar kind of actuator where the conversion of shear piezoelectric strain of a tubular structure were converted into angular displacement. The tube structure actuator consisted of an even number of piezoelectric ceramic segments which were poled in such a way that the remanent polarization, P_r, is directed along the length of each segment. The joints between the segments act as electrodes to apply electric driving field, E_1. The segments were electrically connected in parallel and provide coherent shear strain, S_5, by the applied electric field in all the segments. Due to the cylindrical structure of the actuator, the shear strain was directly transformed into the angular displacement, β [Figure 1.4(b)]. In another work, Pan et al. reported a torsional actuator with helical electrodes [54] that holds a very simple structure [Figure 1.4(c)]. A tubular PZT was wrapped with a pair of parallel electrodes on its surface to transform into a torsional actuator. When this helically structured assembly is put into use, usually one end is fixed to a steady object and another end is kept freely movable. A small torsional angle of about 1.7° was observed from a 40 mm long tube when the driving voltage changes from −500 to +500 V [Figure 1.4(d)]. This helical structure is

very suitable for fabricating tiny torsional actuators using piezoelectric hollow or solid fibres, which can be produced by several conventional methods, for example, microfabrication by co-extrusion and viscous-suspension-spinning process [51, 55].

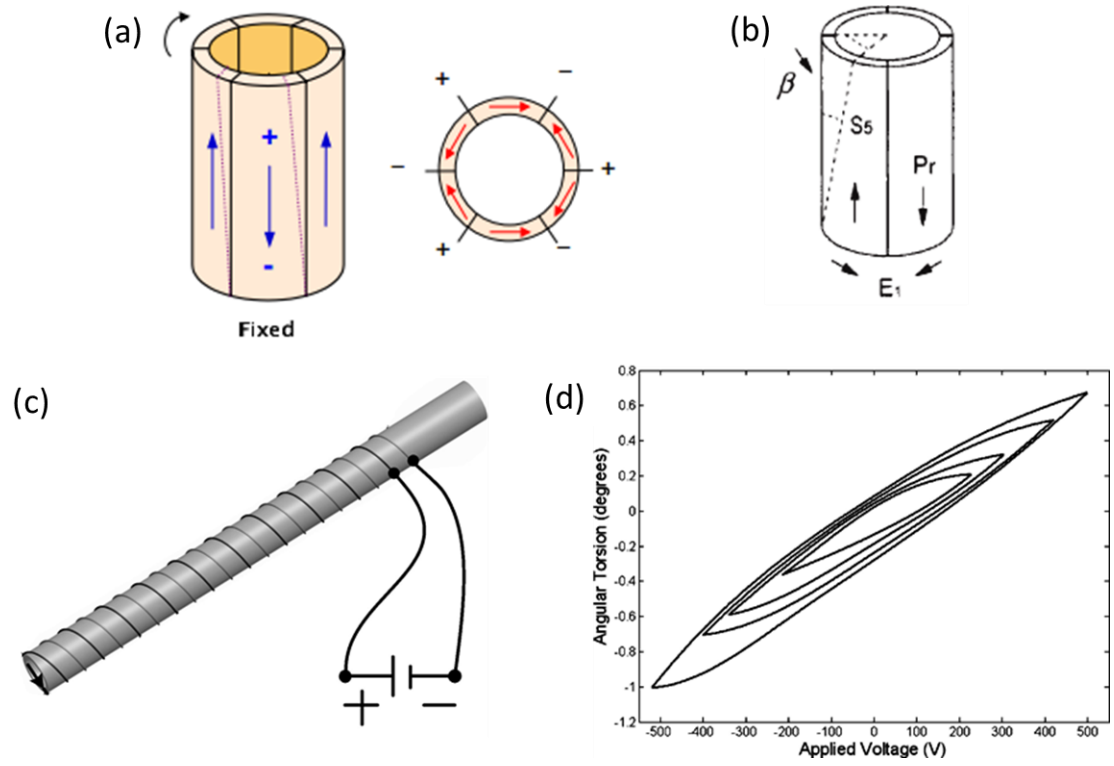

Figure 1.4. Tubular piezoelectric torsional actuator. (a) Piezoceramic based torsion bar (front and op view) [52]. (b) Piezoelectric ceramic segments are bonded together to form a tube structured torsional actuator [53]. (c) Proposed helical electrode actuator model for controlled performance and (d) static torsional rotation [54].

Apart from tubular piezoelectric torsional actuators, Finio et al. [56] have modelled a twisting sheet based piezoelectric actuator to achieve controlled performance that can be applicable in the micro-robotic field. Twisting motion was obtained with a single piezoelectric layer by laminating antisymmetric top and bottom fibre reinforced composite (FRC) layers [Figure 1.5(a)]. An actuator of specific dimension can attain a rotation angle of θ_{twist} [Figure 1.5(b)] by applying a voltage across the piezoelectric

layer, using the conductive FRC layers as electrodes. A theoretical model was developed which successfully predicts torsional rotation, torque and energy density of piezoelectric twisting actuator; and optimises these values by accounting actuator geometry such as reinforced fibre orientation angle γ [56].

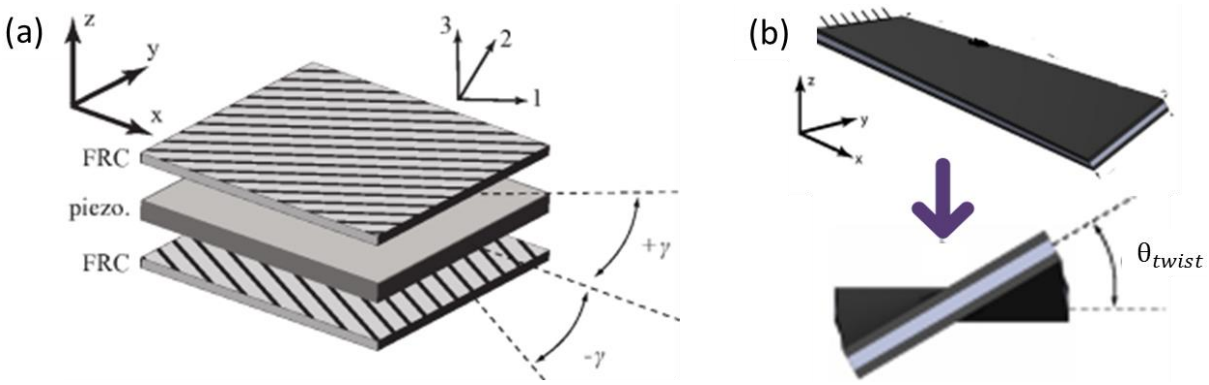

Figure 1.5. Multilayer piezoelectric torsional actuator. (a) The fibre directions of the two FRC layers oriented at angle ± γ to the longitudinal axis of the actuator, and (b) a 3-D and end-on view of a twisting actuator with twist angle $\boldsymbol{\theta_{twist}}$ [56].

Despite of significant number of works conducted and published there still remain several restrictions of piezoelectric materials which limit their usability in modern day torsional actuator systems [57, 58]. For example, piezoelectric ceramics are stiff and brittle, and cannot be coated onto non-uniform surfaces, which restricts the design flexibility in the transducer. Similar to SMA torsional actuators they also produce very small material deformation compared to charge input; hence they are not suitable in many of those applicable fields where large torsional movement is required, specifically, in impact rotating motors and robotics [50, 59, 60].

1.4 Multilayer Torsional Ribbons

The mechanical principles of residual stress or strain-induced bending of multilayer structures have been exploited to manufacture micro- and macroscale torsional actuators. For instance, net shape helically structures made of bimorph strip were successfully developed by Pearce et al. [61], Mohammadi et al. [62] and Bell et al. [63]. The helical ribbons were produced by inducing a bending action within the bimorph structure where the bending direction did not coincide with the long axis of the bimorph ribbon. The bending angle can be controlled by manipulating the anisotropic properties of one of the bimorph layers. For example, epitaxial deposition of InAs/GaAs using AlAs as a sacrificial layer dictated that the ⟨100⟩ direction is the preferred roll-up direction when the patterned bilayers were released by wet etching. Helical ribbons with different pitches and helix angles form depending on the misorientation angle of the ribbon's geometric axes and the bending direction [(Figure 1.6(a)]. The angle between the patterned stripe and the closest ⟨100⟩ direction determines the pitch between turns of the resulting helical structures. This is illustrated by the images in Figure 1.6(b).

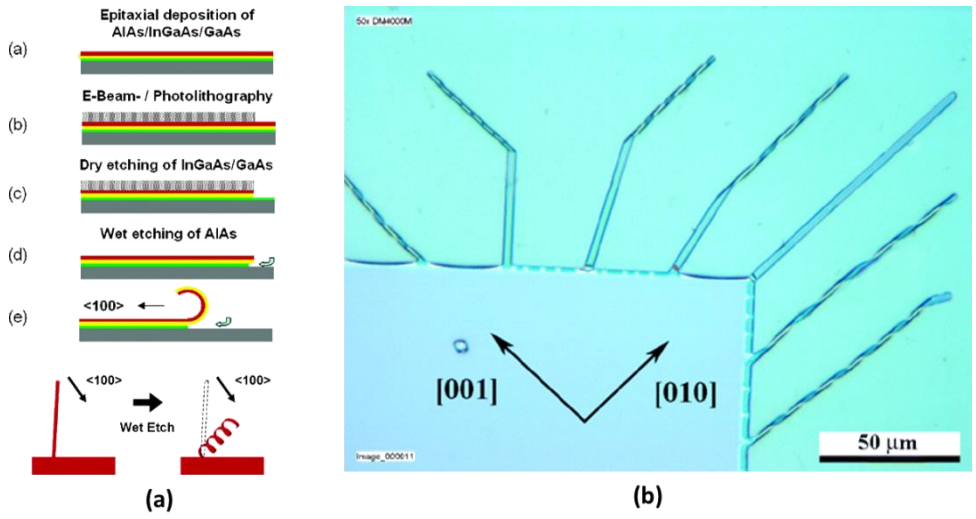

Figure 1.6. (a) Basic process sequence and schematic top view: initial planar bilayer, patterned through conventional microfabrication technique. (b) Digital microscope

image with released helical structures. The different orientations of the initial pattern result in helical structures with different pitches [63].

In another work, Liu et al. [64] built a micro-scale torsional muscle actuated by the phase transition of VO_2, with a simple bimorph design. The rotational actuator was constructed by releasing a long "V"-shaped Cr/VO_2 bimorph structure where VO_2 thin films were initially grown by pulsed laser deposition on Si substrates with a thick thermal oxide. The exposed area of VO_2 was etched away by reactive ion etching (RIE). Then the "V"-shaped Cr/VO_2 area was shielded by photoresist with the same pattern, and the exposed SiO_2 and the underneath Si were deep-etched by RIE. Upon removal of the photoresist and under-etching of the SiO_2 layer beneath the Cr/ VO_2, "V"-shaped Cr/ VO_2 bimorph ribbon were released [Figure 1.7(a)]. The final structure is a suspended bimorph helix consisting of two symmetric coils naturally connected to the two Cr electrode pads. Figure 1.7(b) shows a single coil being actuated by global heating with the specific rotation amplitude of ~1000° per mm of coil length which is reduced by half from that of a dual coil [Figure 1.7(c)]. This system includes all the functions including torsional actuator, memristor, and proximity sensor, showing great possibilities in applications that require a high level of functionality integration in a tiny space. The torsional muscles simulate active neuromuscular systems with all-inorganic materials by sensing a distanced remote substance and responding by rotating to a different configuration [64].

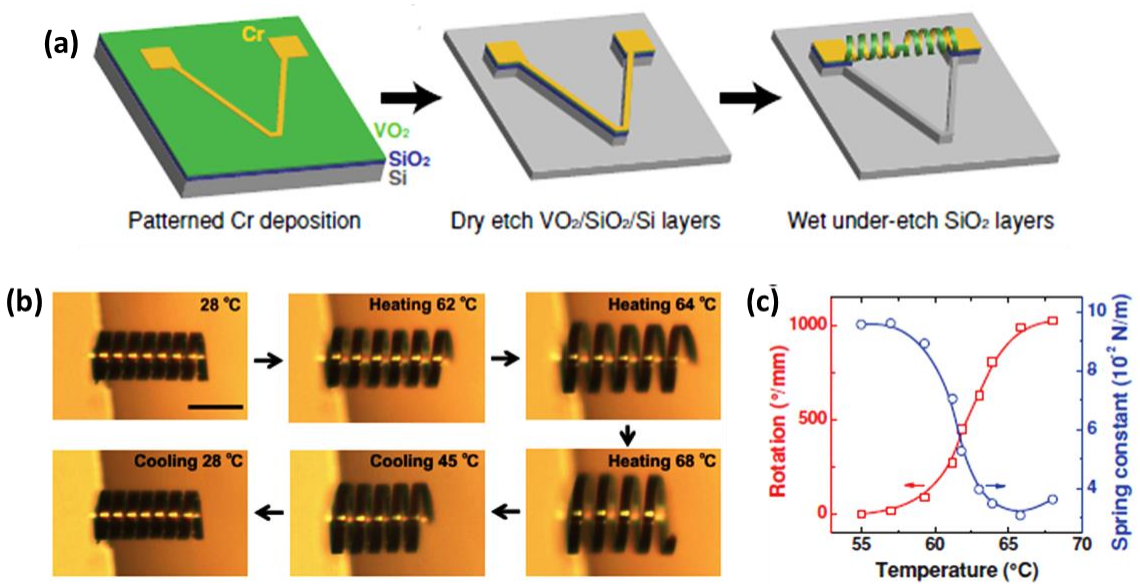

Figure 1.7. Fabrication of VO_2 based bimorph coils. (a) Schematic of the microfabrication process of a dual coil. (b) Rotation of a single coil removed from as-fabricated dual coil operated at various temperatures in a heating/cooling cycle. (c) Temperature dependence of specific rotation and spring constant in the heating half-cycle [64].

Overall, multilayer bimorphs strips were able to provide significant torsional deformation; however, since the spring constant varies with the change in strip geometry additional tuning is necessary by optimizing the dimensions of the bimorphs as well as the spring length. Additionally, they must be constrained from translational movement perpendicular to the axial direction which adds to system complexity.

1.5 Electroactive Polymer (EAP) Torsional Actuators

Electroactive Polymers (EAPs) are functional materials that are often used as actuators in adaptive structures, in particular when large deformations are required. In EAPs, electric energy is directly converted into mechanical work and some EAPs can create large strains of more than 10%. Typical EAPs are described briefly below followed by examples of their application to generate torsional actuation.

Dielectric elastomer EAPs have been widely studied in recent years for developing electroactive actuators due to their excellent overall performance, including large elongation, high energy density, good energy conversion efficiency and fast response [4, 65]. Application of an electric field by means of compliant electrodes on both sides of an elastomer film results in its deformation according to Maxwell's pressure and the nearly incompressible properties of the material. Considerable strains can be achieved in comparison to other common actuators, such as piezoelectric devices [25]. Dielectric elastomers are frequently being used as actuators in many technological fields such as mobile mini- and micro-robots, micro-pumps, micro air vehicles, disk drive, prosthetic devices, flat panel loudspeakers and optical fibre positioning [65-67].

Conducting polymers are another class of EAPs which structurally feature a conjugated backbone and are electronically conductive. Upon oxidation or reduction of the polymer, conductivity is increased and leads to a charge imbalance which results in a flow of ions into the material so as to balance charge. Conducting polymer actuators are generally designed by immersing the polymer in a bulk liquid electrolyte environment [68, 69]. The ions or dopants enter the polymer from a surrounding electrolyte medium which typically remains in the form of gel, solid, or liquid. Contraction or expansion of the polymer occurs due to the mass transfer of ions between the polymer and the electrolyte. Typical volume changes are about 10%, and length changes are hence on the order of 3% [70, 71]. Nevertheless, the dimensional changes of a single piece of conductive polymer during redox can directly be exploited to produce better linear motion [28]. On the other hand, a conjugated-polymer layer bonded to a non-swelling layer [72] or another conjugated-polymer layer, but with different swelling [73, 74] results in significant bending motion. These configurations have been explored in

various biomedical [72], biological [75], microfluidic [76, 77] and robotic [78, 79] applications.

1.5.1 Developed EAP Torsional Actuators

A dielectric elastomer actuating motors that continuously rotate a shaft have been described by Anderson et al. [80, 81] and Heim et al. [82]. A variation described recently by Wache et al. describes oscillatory torsional motion of dielectric elastomer actuators [83]. The governing principle behind this new rotational motion is the creation of asymmetric electrodes, which induce a twisting of the actuator centre (Figure 1.8). The two different kinds of samples were investigated and their working principle is shown in Figure 1.9(a). In the first kind, the rigid external frames supporting a free standing, pre-stretched film of VHB acrylic elastomer have a square shape with an inner side where four rectangular electrodes located at the corners of the frame. Left scheme on Figure 1.9(a) shows this first configuration and illustrates how the application of a voltage causes a change in the configuration and produces a rotation of the cross placed in the middle of the film. In the second assembly [right scheme of Figure 1.9(a)], the elastomer film is enclosed by circular frames instead of the square ones, with a fixed inner diameter. The samples were fixed in a dark chamber with continuous illumination applied by light emitting diodes (LEDs). A rotation of the cross is observed depending on the intensity of the field applied, and among the tested configurations, a maximum rotation of 10° was achieved [Figure 1.9(b)].

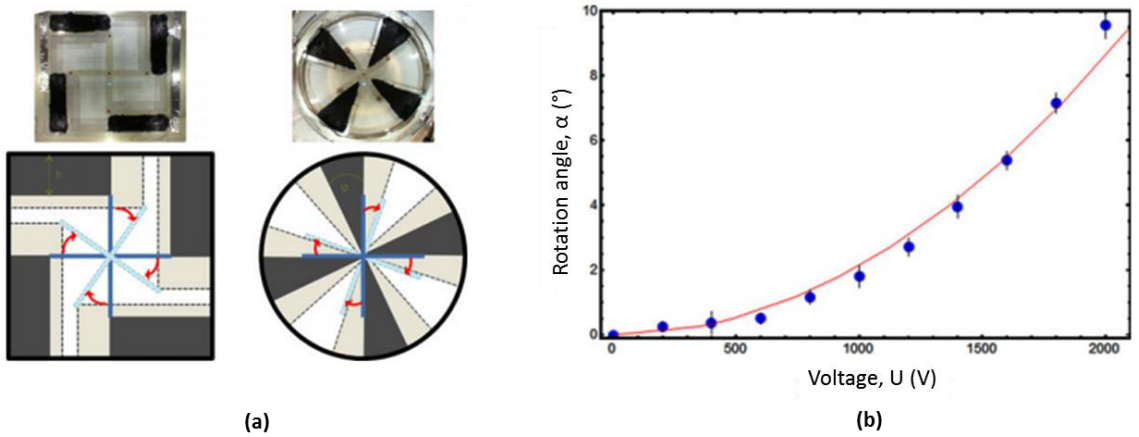

Figure 1.8. Dielectric elastomer actuators, (a) photographs and sketches of their working principle based on asymmetry for both configurations, left: square, right: circle. Dark grey represents the initial electrode and light grey represents the activated/expanded electrode and (b) evolution of the output angle with voltage for a circular device with rods and electrode angles equal to 55°[83].

A few studies have reported the development of rotary actuators based on conductive polymers. Hunter et al. applied a polyaniline-based linear actuator to rotate a crank for rotary motion in one direction. Fang et al. proposed a novel conjugated-polymer-based reversible oscillatory torsional actuator by embedding helically wound fibres into a conjugated-polymer tube (Figure 1.10) [84]. In this configuration, the fibres are confined and have little room for extension. Therefore, they impose directional constraints for swelling of the material matrix, which causes complex deformation resulted by the fibre-matrix orientation. The torsion, elongation, and dilation of the tube are predicted by developing and utilising a nonlinear elasticity-based theoretical model. A prototype for the proposed torsional actuator was constructed by helically embedding platinum fibres into a polypyrrole (PPy) hollow tube during the PPy deposition. Application of a positive charge between the fibre-directed PPy tube and an electrolyte causes the movement of anions in the electrolyte toward the PPy/electrolyte interface.

This results in a double layer of charges on the interface and then, diffusion of highly concentrated ions in the double layer into the PPy [Figure 1.9(a)]. Application of a negative voltage causes the PPy to be reduced, and the previously absorbed ions will be returned back to the electrolyte. Mass transfer of ions in and out of the polymer causes swelling and deswelling of the tube, which subsequently leads to result in torsion [Figure 1.9(b)]. The measured maximum peak-to-peak torsion was about ~0.01° per mm of actuator length [Figure 1.9(c)].

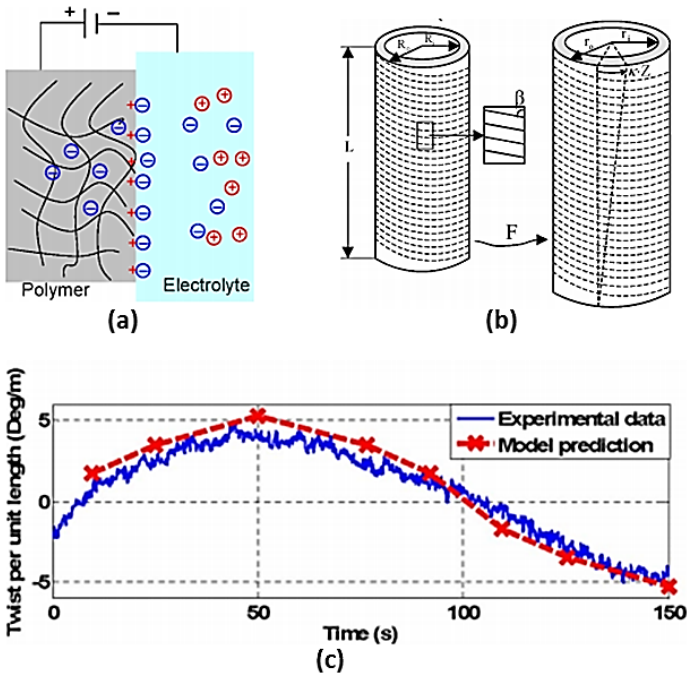

Figure 1.9. Conjugated polymer torsional actuator; (a) Illustration of double-layer charging and diffusion for a polymer film in contact with an electrolyte, (b) Illustration of the actuator configuration in original and deformed configuration and (c) Torsion result under a 0.005-Hz sinusoidal voltage input [84].

1.5.2 Limitations of EAP Actuators

Despite having several advantages, EAPs have a number of issues yet to be addressed to use them as practical actuator systems [85]. In past two decades, some dielectric elastomer actuators have demonstrated extensions up to three times their initial lengths,

satisfactory efficiencies and specific energy densities. However, in most experiments actuator life was a serious concern. In some applications dielectric elastomers still lack several important properties such as low voltage operation [86]. Use of conductive polymers as actuators require significantly less voltage; however, the response time of these actuators is high, and a low actuation force is generated which limits the practical applications [87, 88]. Both the EAPs torsional actuators described here showed very small torsional rotation when operated as oscillatory torsional actuators.

1.6 Fluidic Torsional Actuators

Fluidic artificial muscles, also familiar as McKibben muscles, have been extensively studied in both analytical and experimental aspects [89-92]. Fluidic artificial muscles are constructed in a very simple way and consist of internal elastomer bladder surrounded by a helically braided outer sleeve. Commonly, one end of the muscle is connected to a fluid port through which pressurised working fluid flow in and out of the muscle, while the other end of the muscle is closed by a plug, crimp or another blocking device. These muscles work by using pressurised fluid to expand the internal elastic tube such that the outer braided sleeve of inextensible fibres causes linear contraction of the whole muscle unit.

Pneumatic or air filled muscle is the most common type of fluidic artificial muscle and these systems have demonstrated many of the distinctive features found in a real muscle [89, 93-96]. Some researchers [91, 97-99] have also investigated hydraulic artificial muscles and shown that an antagonistic pair of the hydraulic actuator is able to deliver force to weight ratios more than six times higher than a traditional double-acting hydraulic cylinder while attaining similar tensile stroke and maximum force output [91]. These attractive features make fluidic artificial muscles a suitable actuation choice for

bioinspired robot designs [97, 100-102], powered prosthetics [103-106], or robots designed to interact closely with humans [96, 99, 107].

While axial movement of fluidic artificial muscles has been studied and developed fairly comprehensively, much less research has been conducted to construct simple fluidic actuators that can provide rotary actuation [108, 109]. In one example, Sanan et al. [108] have assembled two differently shaped structures [two shapes S1 and S2 in Figure 1.10(a)] into a single configuration (having shape S) along a shared geometric centre to make pneumatic torsional actuators. The two helices in Figure 1.10(a) are joined along the central axis of the two shapes. The final merged structure is shown in Figure 1.10(b). The fabric used to make the muscle was inextensible; therefore, the common central axis length remained constant and accordingly the length of the whole actuator was held constant during the movement. Consequently, the motion between the ends of the torsion shape actuator moves toward pure rotating motion with negligible axial movement. One of the prototypes developed a torsional rotation of nearly 0.4° per mm of actuator length.

Despite having novelty in this particular work, an issue was overlooked is the structural role of the actuator if it is to be used in a soft-bodied robot. In particular, the load bearing central axis structure needs to be sufficiently stiff to linear and bending forces but compliant to torsional loads, hence, the design requires a careful investigation and selection of the central axis material.

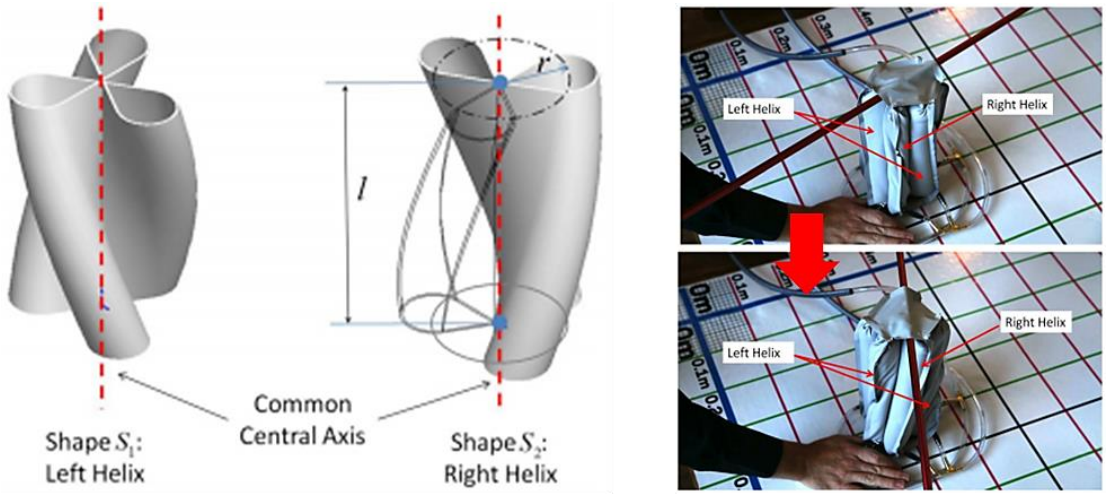

Figure 1.10. Pneumatic torsional actuator; (a) two oppositely oriented helix that make up the rotary shape actuator (each leaf of the helices is wrapped around the common central axis of the actuator of length *l*, as helix with a pitch circle radius *r*, and one leaf of the right helix has been shown transparent for illustrative purposes) and (b) physical realization of the torsion shape actuator (the relative arrangement of the two helices can be seen as labelled in the two pictures) [108].

In another work, Connolly et al. [109] demonstrated that a wide range of motions, including linear extension, radial expansion, and rotational motion can be achieved from fibre-reinforced soft fluidic artificial muscles by simply controlling the fibre angle [109]. To illustrate the effect of fibre angles (ranged from 0° to 90°) on the response of the actuators, a numerical study was conducted by using finite element analysis. To verify the finite element results, numerical predictions and experimental data were compared for two actuators having fibre angles of -3° and 70° (Figure 1.11). Understating the effect of tailoring the fibre angle provides a quantitative prediction of motion of the soft actuators and exploration of the design space for this class of actuators. A small magnitude of torsional rotation of ~1.75° per mm of actuator length was reported in this work. Another limitation includes the requirement of the fluidic

pump to the actuator set-up which makes it unsuitable for macro- or microscopic operations.

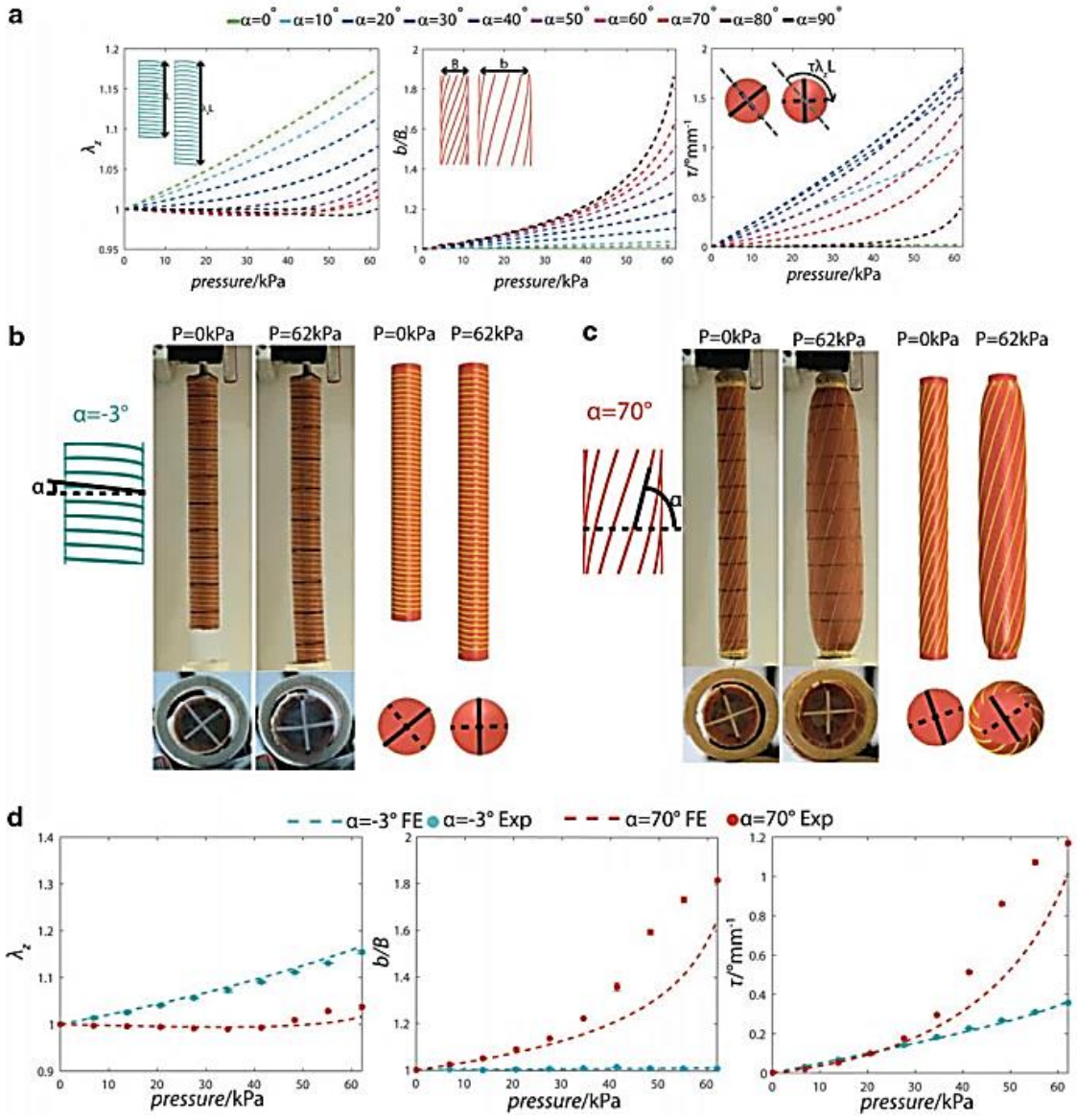

Figure 1.11. Fluidic actuators with one set of fibres. (a) finite element results showing extension (λ_z), expansion (b/B), and twist per unit length (τ) as a function of the applied pressure for a range of different fibre angles. The positive fibre orientation was considered in the clockwise direction which induces twist in the counter-clockwise direction (negative twist), (b) photographs from experimental characterization (left) and snapshots from finite element simulation (right) for an actuator with fibre angle α = -3° (both front views and bottom views are shown), (c) photographs from experimental characterization (left) and snapshots from finite element simulation (right) for an

actuator with fibre angle α = 70° and (d) Comparison between finite element simulations and experiments for two actuators with fibre angle α = - 3° and α = 70° [109].

1.7 Twisted Nano-Yarn Torsional Actuators

High speed and large stroke torsional actuation have recently been realised by using twisted nano-yarn based actuators. Researchers have discovered electrochemical torsional actuation of the multi-walled carbon nanotube yarn [110] and then further functional improvements were achieved by utilising several actuation methods [111-117]. Metallic nano-wire [118] and graphene oxide nano-yarn [119] was also used to fabricate high strength torsional actuator with fast actuation. The actuation mechanism was described in terms of volumetric changes of yarns once activated.

1.7.1 Torsional Carbon Nanotube (CNT) Artificial Muscles

Linear and bending modes of CNT actuators are well known by using different stimuli such as electricity, fuels, light, or heat [120]. Electrostatic attraction and repulsion between two nanotubes have been used for cantilever-based nano-tweezers [121] and mechanically functional switches and logic elements [122, 123]. On the macroscale, electrically powered [124-129] and fuel-powered [130, 131] electrochemical CNT actuators provide a small expansion stroke and over a hundred times higher stress generation than natural muscle. CNTs also have been used as additives that act in conjunction with organic polymers to provide photo-responsive [132], shape memory [133, 134], electrochemical [135] and electromechanical [136, 137] actuators. Fennimore et al. demonstrated electromechanically powered torsional and rotational motors by using a single multi-walled nanotube as a low-friction shaft with attached magnetic rotor where repeated rotation of 360° was achieved without having any wear or fatigue [138].

Foroughi et al. were first to demonstrate an electrolyte-filled twist-spun multi-walled CNT yarn acted as a torsional artificial muscle. They used a conventional three-electrode electrochemical set-up, and produce a reversible 250° rotation per mm of sample length and 590 revolutions per minute [110]. The muscles operated by electrochemical double-layer charge injection, as demonstrated in carbon nanotube supercapacitors based reports [111, 139-142]. Immersion of a twisted multi-walled CNT yarn and a counter electrode in an electrolyte and applying a voltage between these electrodes causes the yarn to rotate in the untwist direction. To improve reversibility, the yarn was tethered at both ends to prohibit end rotation and a paddle was attached near yarn centre with only one-half of the yarn immersed in the electrolyte and used as a torsional muscle. Despite having a smaller torsional rotation than the same length of CNT yarn that was tethered at only one end, the reversibility of the actuation was improved because the non-actuating section of the yarn functioned as a torsional return spring to rotate the paddle to its initial angle (Figure 1.12).

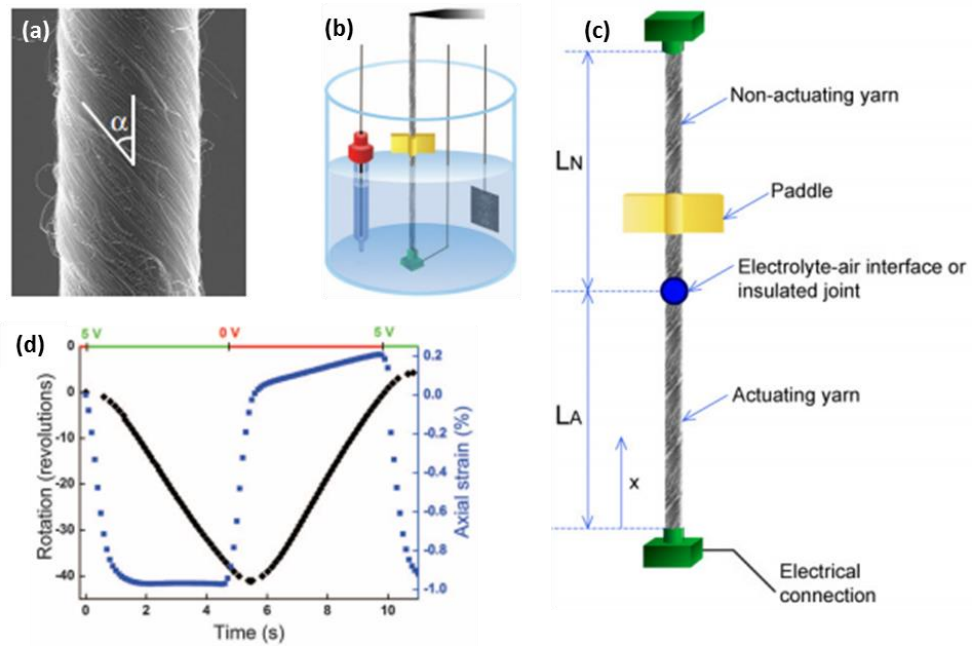

Figure 1.12. Torsional CNT artificial muscle; (a) Scanning electron micrograph of a carbon nanotube yarn that was symmetrically twist-spun (twist angle, α) from a multi-

walled CNT forest, (b) Illustration of electrochemical cell configurations used for characterizing torsional actuation or the combination of torsional and tensile actuation, where the Ag/Ag^+ reference electrode, actuating yarn electrode, and Pt mesh counter-electrode are shown from left to right, (c) both end tethered yarn configuration with actuating yarn length, L_A and non-actuating yarn length, L_N, and (d)) Torsional rotation (black) and axial length actuation (blue) versus time for a yarn (length = 120 mm, diameter = 12 mm, α = 40°) [110].

Electrochemical actuation of CNT yarn relies on the use of electrolytes; hence, the actuating system is restricted to a wet environment or the use of gel-based electrolytes. Electrolytes also put a narrow boundary on operating temperature, application of voltage, and rate of actuation. Furthermore, special packaging is needed which adds extra weight and volume, and reduces the work density of the actuator system. To overcome these limitations, Lima et al. have designed guest-filled, electrolyte-free, twisted CNT yarn muscles that provide high speed torsional and tensile stroke, in which a muscle spins a rotor at an average 11,500 revolutions per minute or provides ~3% tensile actuation at 1200 cycles per minute [117]. Electrically, chemically, or photonically induced volume change of guest material generates torsional rotation and tensile contraction of the CNT yarn host. However, these wax-infiltrated, electro-thermally powered artificial muscles are torsionally underdamped, thereby experiencing dynamic oscillations that complicate positional control.

Chun et al. developed an ultrafast hybrid CNT yarn muscle that produced a torsional rotation of 9,800 revolutions per minute without noticeable oscillation by using a similar mechanism in spider silk to reduce uncontrolled spinning of the spider at the end of dragline silk [112]. A viscoelastic material, containing paraffin wax and polystyrene-poly(ethylene–butylene)-polystyrene copolymer (SEBS), was used as the yarn guest

material to produce an overdamped dynamic oscillating response. The thermally-induced volume increase of the wax/polymer composite within the CNT yarn causes the yarn length to contract and the yarn to partially untwist to generate torsional rotation.

In another article, Lee at al. demonstrated electrochemically induced, all-solid-state torsional and tensile artificial yarn muscles using a spinnable CNT sheet and received large torsional rotation (53°/mm) without using the relatively complicated three-electrode electrochemical system, a liquid electrolyte, or heavy packaging [116]. Anode and cathode yarns were fabricated by infiltrating the solid electrolyte (poly(vinylidene fluoride-co-hexa- fluoropropylene), PVdF-*co*-HFP, containing tetraethylammonium tetrafluoroborate ($TEABF_4$) with propylene carbonate (PC) to obtain an electrical insulation electrolyte layer on the yarn surface. These two yarns were then plied together using an opposite twist direction of yarn plying than for the initially introduced yarn twist. Penetration of ions and solvating species from exterior electrolytes into the anode and cathode yarns causes the increase in hybrid yarn volume and produces yarn untwist and yarn contraction. Torsional actuation study of CNT yarn has also been conducted by utilising environmental temperature variation [143]. In the example studied, twisted CNT yarn was employed as the backbone for torsional actuation driven by the volume change of infiltrated a phase change material (PCM). When the specific volume of CNT yarn varies drastically at the phase-transition temperature, torsional actuation has occurred. A maximum of 8°/mm rotation was observed when the temperature varies from 27 to 40°C.

More recently, solvent or vapour driven torsional multi-walled CNT yarn muscles have been reported by a few researchers. Chen et al. [144] showed that a compact coil of multiple twisted multi-walled CNT yarns consisting of nanoscale gaps between the

nanotubes and micrometre-scale gaps among the twisted fibres contribute to the rapid response and large actuation stroke of the actuating fibres. Upon exposure to ethanol vapour, a coil of 20 multi-walled CNT yarn reversibly rotated a 570 times heavier paddle by 380° per mm of muscle length with a maximum rotational speed of ~6361 rpm (Figure 1.13). A maximum tensile contraction of ~10% was also generated during the rotation.

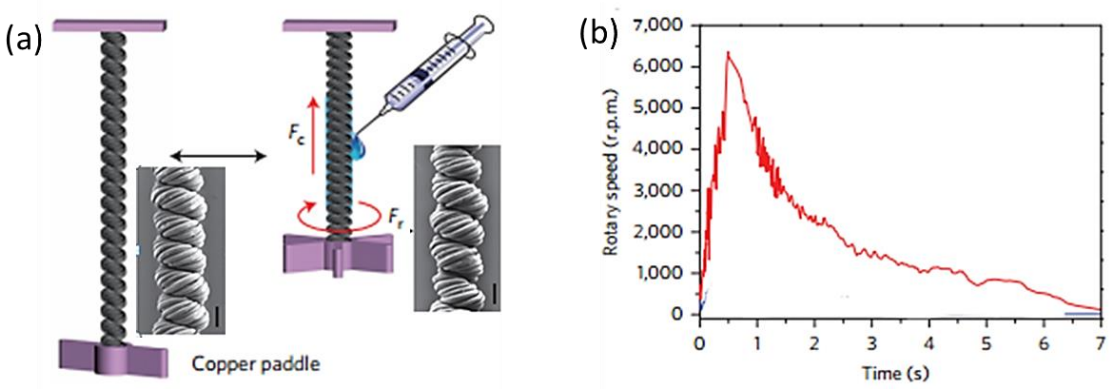

Figure 1.13. Actuation performances of helical coiled multi-walled CNT yarn; (a) Schematic illustration of the contractive and rotary actuators. A copper paddle with a mass of 75 mg was fixed at the end of the sample. Contractive (Fc) and rotary (Fr) forces were generated simultaneously on coming into contact with a solvent. To measure the contractive force, the two ends were clamped. (b) Rotary speeds generated by the coiled sample upon the absorption of ethanol. The coiled sample was made from 20 twisted yarns [144].

In another work, Di et al. [113] demonstrated an incandescent tension annealing process (ITAP) for stabilising both twisted and coiled multi-walled CNT yarns with respect to unwanted irreversible untwist, thereby avoiding the need to tether torsional artificial muscles, and increasing the mechanical loads that can be driven by these muscles. This ITAP involves thermally annealing twisted CNT yarns at a temperature of about 2000°C while these yarns are under tensile loads (Figure 1.14). When exposed to

acetone vapour, a 24-mm-long, 100-μm-thick coiled ITAP yarn reversibly rotated a 6100 times heavier rotor by 630° (corresponding to a rotation of 26° per mm of muscle length). The maximum rotational speed of the rotor was 44 rpm, and the muscle lifted a weight corresponding to a 2.9 MPa load by about 0.7% of the yarn length [Figure 1.15(d)].

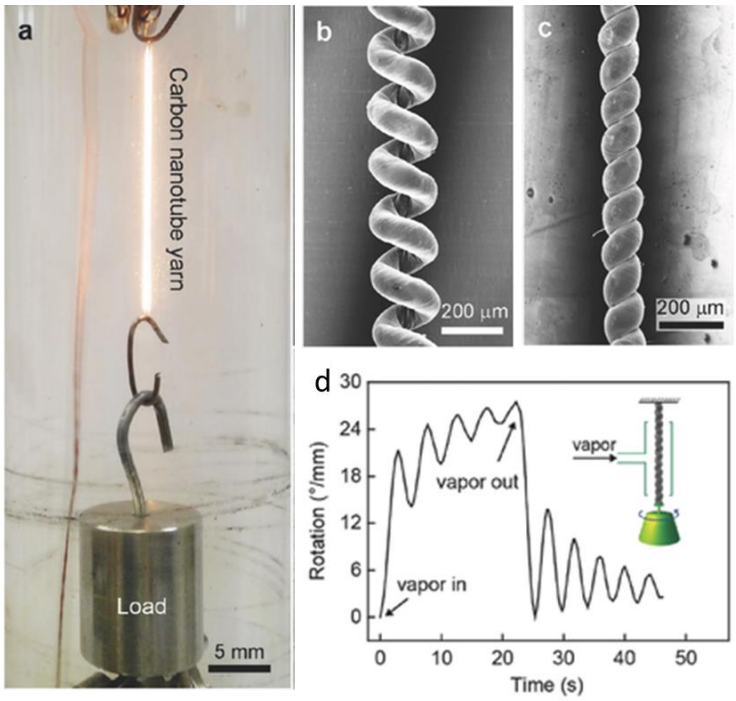

Figure 1.14. Acetone vapour induced torsional CNT artificial muscle; (a) Setup for applying ITAP to multi-walled CNT yarns. SEM images of the effects of an applied freely rotating load on b) a nontethered, non-ITAP coiled yarn and c) a nontethered, coiled ITAP yarn, showing that the ITAP stabilises the coiled yarn with respect to untwisting. a) Weight rotation in degrees (normalised to yarn length) versus time for a one-end-tethered, coiled ITAP yarn (inset, with 24 mm length and 100 μm yarn diameter) when driven by acetone vapour absorption/desorption [113].

Multi-walled CNT twisted yarns have been the most extensively studied for torsional actuator showing high performance in terms of large torsional strokes and high speed

actuation. A summary of works on torsional CNT yarn artificial muscles is provided in Table 1.1.

Table 1.1. Torsional CNT yarn artificial muscles and corresponding performances.

Materials	Tethering system	Actuation principle	Maximum reversible torsional rotation		Tensile contraction (%)
			Stroke (degree/ mm)	(Speed) rpm	
Multi-walled CNT yarn [110]	Two-end	Electrochemical double-layer charge injection	~250	~590	~1
Host: Multi-walled CNT yarn Guest: Paraffin wax [117]	Two-end	Thermal, electro-thermal, or photo-thermal	~180	~11,500	~3
Host: Multi-walled CNT yarn Guest: Paraffin wax + SEBS copolymer [112]	Two-end	Electro-thermal	~85	~9,800	Not reported
Electrolyte (PVdF-*co*-HFP + $TEABF_4$ + PC) infiltrated twisted CNT yarn [116]	One-end	Electrochemical	~53	Not reported	~0.7
PCM (icosane) infiltrated CNT yarn [143]	Two-end	Thermal	~8	~0.1	Not reported
Incandescent tension annealed coiled multi-walled CNT yarn [113]	One-end	Chemical (acetone vapour)	~26	~44	0.7
Multi-walled CNT fibre [114]	Two-end	Electromechanical	Not reported	~2700	~2
Hierarchically made multi-walled CNT yarn coil [144]	One-end	Chemical (ethanol vapour)	~380	~6361	~10

Compared with other torsionally actuating materials, CNT yarn demonstrate several advantages such as actuation under low voltages, ultra-high speed response, and millions of cycle-life which mainly originates from unique electronic properties, large surface area, and excellent chemical and thermal stability of CNT yarns. Torsional CNT artificial muscles have potential application in microfluidic mixing [110], torsional motors [117], torsional pumps [112], and micro-electromechanical systems [110, 116, 145].

1.7.2 Metallic Nanowire Torsional Actuator

CNT yarns have been promising as torsional or tensile actuators; however, they usually exhibit low mechanical strength and electrical or thermal conductivity. Mirvakili et al. [118] demonstrated a torsional actuator based on twisted metal nanowires yarns that are strong, pliable, and more conductive than CNT yarns. Niobium nanowire fibres were extracted by etching a copper-niobium nano-composite material made by severe plastic deformation [118, 146]. When impregnated with paraffin wax, the niobium nanowire yarns produce fast rotational actuation as the wax is heated. Similar to wax impregnated CNT yarns, heated and expanded wax untwists the yarn, which then re-twists upon cooling. Normalised to yarn length, 12° per mm of torsional rotation was achieved along with twist rates in excess of 1800 revolutions per minute when 23 times larger paddle is used for measurement (Figure 1.15). The tensile modulus of 19 ± 5 GPa was measured for the niobium nanowire yarns, which is very similar to that of multi-walled CNTs.

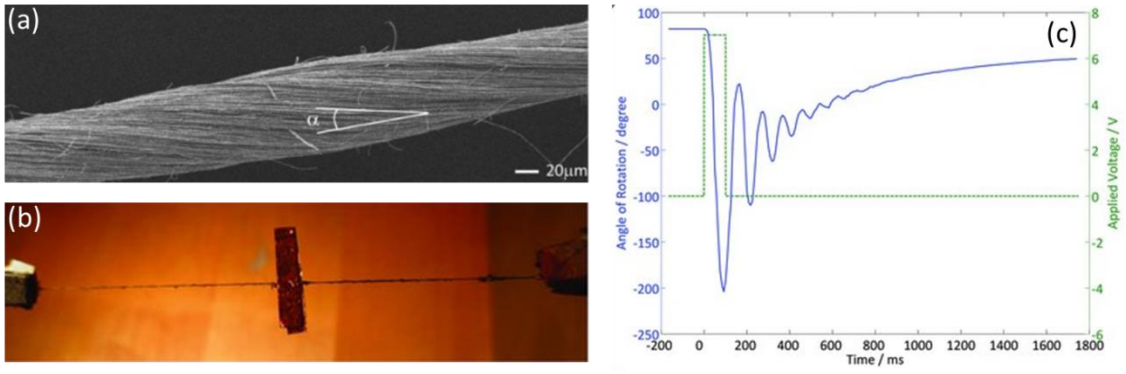

Figure 1.15. Niobium nanowire yarn torsional actuator. (a) As spun yarn with twist angle α of 13°. (b) Torsional actuation configuration, with the right half of the yarn infiltrated with wax and melting induced by current pulses. The central paddle is used to determine rotation. (c) The angle of rotation versus time upon pulse voltage actuation of the niobium nanowire yarn [118].

Niobium nano-yarns are promising candidates for being used in small, tightly wound magnetic coils and for flexible metal contacts, where conventional commercial wires are not adequately acquiescent. In thermally induced torsional actuation, the higher conductivity of niobium nanowire yarns allows heating to be attained with lower voltages than are required in CNT yarns, making them of possible importance in portable devices such as implantable drug delivery systems, guided catheters, and miniature valves [118].

1.7.3 Graphene-Fibre Torsional Actuator

The significant potential of graphene fibres stems from the characteristic they combine the high mechanical strength and flexibility of fibres with the extraordinary electronic and thermal properties of graphene [147-149]. These fibres with in-line oriented graphene sheets offer the great capability to develop unconventional fibre-based devices. Recently, a spinning technique for constructing graphene fibres directly from graphene oxide has stimulated research in this field, as this delivers a large-scale and

inexpensive route to fibres with a variety of different functionalities that could be useful in textiles for wearable electronics [150, 151]. Expanding the scope of graphene fibres and exploring the unconventional potential of graphene fibres, Cheng et al. reassembled the intrinsic configuration of graphenes within the fibre body and achieved a novel moisture-driven rotational motor by twisting the as-spun graphene oxide fibre hydrogel [119, 152]. This twisted configuration with rearranged graphene sheets within the fibres offers excellent performance as a reversible rotary actuator showing a rotary speed of up to ~5190 revolutions per minute under relative humidity fluctuation (Figure 1.16).

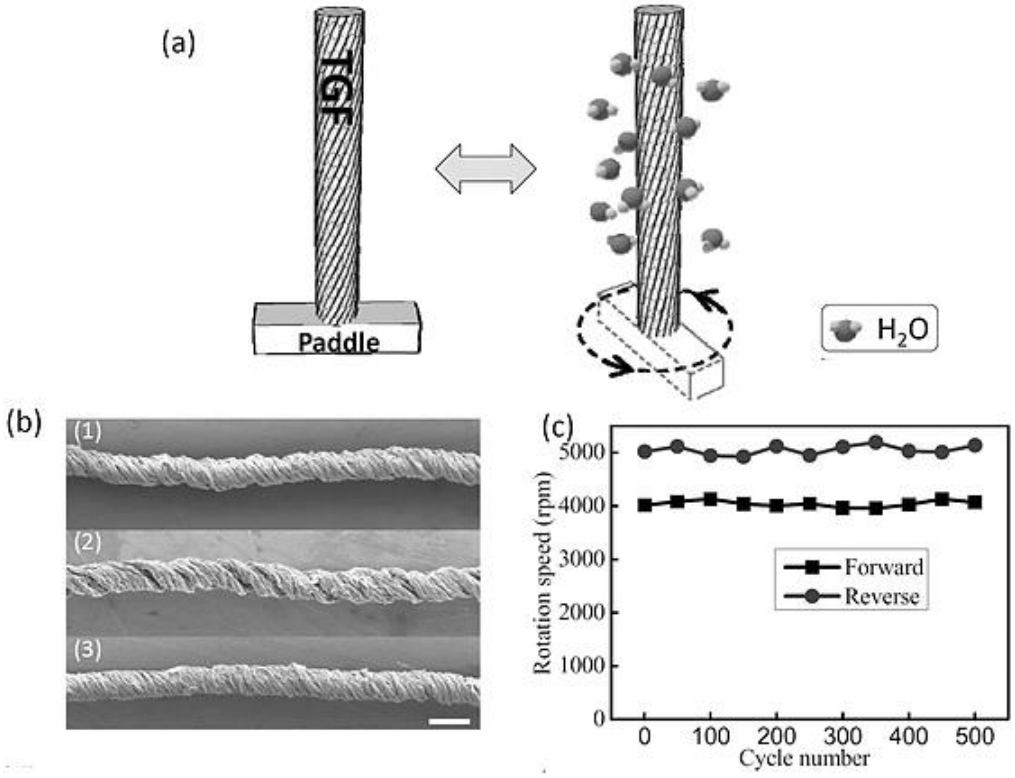

Figure 1.16. Torsional twisted graphene fibre actuator; (a) Schematic rotation of a twisted graphene oxide fibre with a paddle at the low (left) and high (right) humidity. When the moisture increases (right), the twisted graphene oxide fibre can drive the paddle rotating fast; then the paddle can reverse to the initial state when the moisture decreases (left), (b) SEM images of the initially twisted graphene oxide fibre at relative humidity = 20% (1), after exposure to high humidity of 85% (2), and the final state of twisted graphene oxide fibre as the humidity goes back to the initial relative humidity =

20% (3); scale bar: 100 μm, and (c) The durability test of twisted graphene oxide fibre (>5000 turns per meter) undergoing repeated relative humidity changes, showing forward (the environment humidity changed from relative humidity = 20% to 85%) and backward (relative humidity = 85% to 20%) rotation speed versus cycle numbers [119].

Torsional rotation of ~588° per mm was observed by using a 200 mm long twisted sample. Although the amount of measured rotation is more than twice CNT yarn torsional actuator (~250° per mm) [110], this one-end-tethered system may have limited practical usability due to the uncontrolled mobility to any direction.

1.8 Polymer Fibre/Yarn Based Torsional Muscle

Stimuli-responsive fibres and yarns are of great interest in the field of artificial muscles. These fibres can experience a volume and/or shape change when externally stimulated resulting in a tensile expansion/contraction [153-158], bending [158-160] or torsional rotation [88, 155, 158, 161]. Potential applications for these fibres are many and include microfluidic mixing, micro-scale robots and massage-sleeve exoskeletons for relaxation-clothing.

1.8.1 Twisted Fibre Muscles

Recently, Haines et al. demonstrated that low-cost, high-strength oriented polymer fibres can be transformed into tensile and torsional muscles by inserting twist in the fibre [155]. As reported, commercially produced fibres including polyethylene and nylon fishing line, and polyester sewing thread were used as the precursors. As with CNT yarn muscles [110, 117], the twist was inserted into these polymer fibres to make them chiral, which enables them to function as torsional muscles. Tensile stroke was greatly amplified by inserting such a large amount of twist that some twist converted to fibre coiling [162, 163]. A thermally-induced tensile contraction of the overtwisted coils

was found to surpass the maximum *in vivo* stroke of human skeletal muscles (~20%) [1] [Figure 1.17(a)]. A similar kind of actuation was also obtained by introducing heat to the fibres by using different ways such as Joule heating by means of electrically conductive filaments [154] [164] or coatings [155, 157], air heating [153, 155, 165], photo-thermal stimulation [155] or electrochemical stimulation [155].

There are several advantages of using heat-activated polymer fibre muscles compared to other stimulus. For example, electrochemically charged fibres of conducting polymers can generate large strokes but have low cyclability and need a multi-electrode electrochemical system, which adds to system weight and cost [28, 72]. Electric field induced electrostrictive polymer rubbers [25, 166] are attractive because of their large strokes and high performances but is difficult to use as an artificial muscle because of the required high electric fields. In contrast, thermally-induced twisted polymer fibres or yarns are able to deliver large amounts of mechanical work as torsional actuators with high cyclability and cycle rate. These single piece systems do not require any special assembly and are suitable for manufacturing light weight and low cost actuator. Specifically, a constant torque torsional actuation experiment was conducted by using an 0.86 mm diameter, 55 mm long, twisted nylon 6 fibre. Under a temperature fluctuation from 20° to 160°C, this torsional actuator rotated a 2.8 mm diameter axle by 286° and lifted a 1 kg weight by 7 mm. The mechanical work done by the actuator was calculated to be 2.1 kJ/kg [Figure 1.17(b)] based on the mass of the nylon fiber and this work ouput is similar to the 2.48 kJ/kg generated during tensile actuation of a coiled nylon 6,6 fibre. It was found that thermal contraction of coiled polymer fibre muscles principally arises from thermally-induced fibre untwist, which generates a torque that decreases inter-coil separation. This thermally-induced fibre untwist (ΔT, measured in turns per initial fibre length) produces the torsional actuation of twisted fibres and

amplifies the length change of coiled fibres by changing coil bias angle from α_c to α_c', as described by the spring mechanics equation [167],

$$\Delta \boldsymbol{T} = \frac{\sin(\alpha_c')\cos(\alpha_c')}{\pi D'} - \frac{\sin(\alpha_c)\cos(\alpha_c)}{\pi D} \tag{1.4}$$

Here, D and D' are the diameters of coils, taken through the fibre centreline before and after heating, and the coil bias angle α_c is the angle between the fibre and the coil's cross-section. For a coil having N turns and length L fabricated from a precursor fibre of length l: $\sin(\alpha_c) = L/l$ and $\cos(\alpha_c) = \pi ND/l$. The expression suggest that when the change in fibre length l is negligible, stretching a coiled fibre which is tethered to prevent end rotation produces a change in the fibre twist of,

$$\Delta \boldsymbol{T} = \frac{N\Delta L}{l^2} \tag{1.5}$$

This expression predicts that the large contractions and expansions in coil length in twisted and coiled polymer fibres originate from fibre untwist during heating. This twist-driven coil contraction/expansion mechanism is best understood by using mandrel-made coils. Heating of a homochiral coiled fibre (twisted and coiled in the same direction), delivers an untwisting torque that pulls coils together, providing work by linear contraction. On the contrary, the length of a heterochiral muscle (twisted and coiled in the opposite direction) increases due to the fibre untwist during heating that pushes the coils apart [Figure 1.17(c)]. However, a comprehensive study on muscle stroke and specific work capacity based on fibre diameter and muscle fabrication parameters is yet to be performed which is critically important for the diverse family of targeted applications including humanoid robotics, powered prosthetic limbs, microfluidic actuators, giant-force-capacity exoskeletons, and smart textiles [154-156, 164, 168, 169].

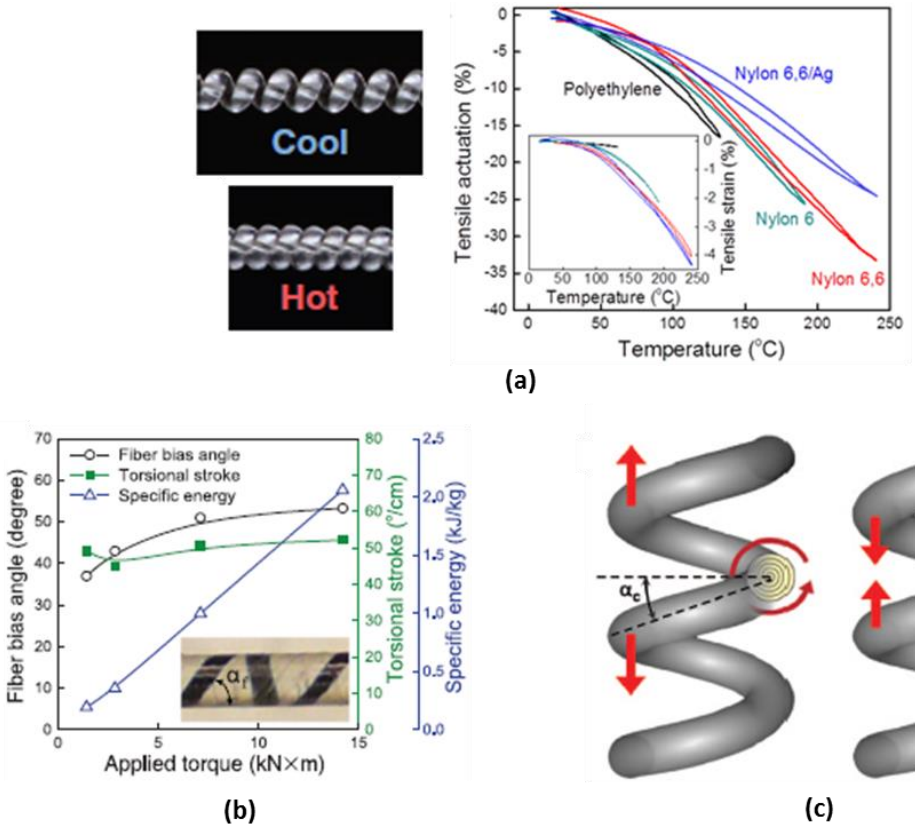

Figure 1.17. Actuation of oriented polymer fibre; (a) Comparison of the tensile actuation of braided polyethylene, nylon 6 monofilament, nylon 6,6 monofilament, and silver-coated nylon 6,6 multifilament fibres before twisting (inset) and after coiling by twist insertion, (b) the optically measured fibre bias angle induced by an applied torque and the torsional stroke and work during thermal actuation (between 20° and 160°C) as a function of this applied torque for a non-coiled torsional muscle made from 860 mm diameter nylon 6 fishing line (inset photograph was used to optically determine the fibre bias angle by measuring the displacement of a black line from its initial orientation parallel to the fibre axis) and (c) schematic illustration of the mechanism by which torsional fibre actuation drives large-stroke tensile actuation for heterochiral (left) and homochiral (right) coiled fibres [155].

1.8.2 Characterization Method of Torsional Fibre/Yarn Muscles

Real-world application of torsional artificial muscles necessitates an accurate and continuous characterization method that allows the torsional stroke and torque to be calculated for any externally applied environmental and mechanical condition. Previous

work has focused mainly on measuring torsional stroke, for example by securing the sample at one end and measuring the rotation of the free end. Occasionally a return spring mechanism has been used to improve reversibility of torsional actuation. Haines et al. demonstrated a test apparatus for measuring isotonic torsional stroke and the work output from a twisted polymer fibre [155]. Torque was applied to a nylon 6 monofilament fibre by attachment to a constant diameter axle (supported by two metal bearings), around which a polymer fibre holding the load ‘c’ (Figure 1.18) was wrapped. The constant torque caused by load ‘c’ was first used to increase fibre twist, compared with that for earlier measurements in a sequence, and then to enable thermally-induced actuation measurements under this torque. The same size load (labelled ‘d’ in Figure 1.20) was applied to keep the fibre under tension, thereby preventing coil formation.

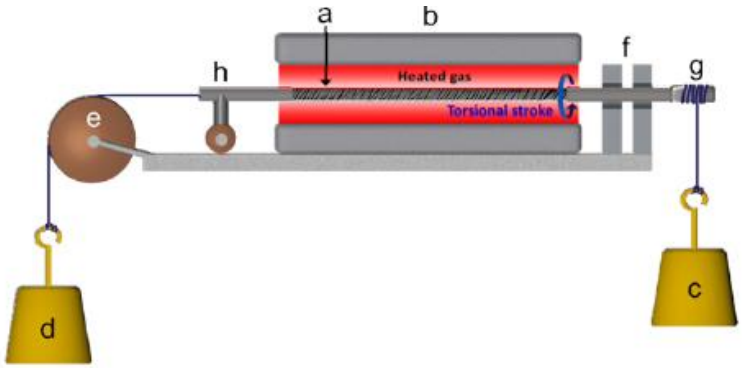

Figure 1.18. Schematic illustration of an apparatus for measuring torsional stroke and torsional work capacity as a function of applied torque during the torsional actuation of twisted polymer fibre muscles. Components are: polymer muscle (a), controlled temperature furnace (b), load (c) providing torque, tensile load (d) for muscle, pulley (e) to support this load, bearing-supported rod (f) connecting polymer muscle to axle (g) for applying torque, and a wheel-supported attachment (h) for the muscle, which enables horizontal movement of the muscle end [155].

1.8.3 Mechanism of Torsional Rotation

Torsional actuation of helically twisted oriented polymer fibres is associated with the thermal expansion coefficients of the non-twisted fibre to both radial and lengthwise direction. These synthetic polymer fibres exhibit anisotropic thermal expansion behaviour, i.e. their responses are different in different directions [170]. A large thermal contraction in the fibre axis direction has been reported for several semicrystalline polymers above their glass transition temperature (T_g) and this has been attributed to the rubber-elastic behaviour of the intercrystalline tie-molecules (TM) [171]. Highly oriented semicrystalline polymers are made up of crystalline lamellae embedded in an amorphous matrix, each lamella consisting of mosaic crystalline blocks connected by occasional 'tie molecules'. Upon drawing, the chain axes of the crystalline blocks become increasingly aligned along the draw direction. Simultaneously, the crystalline blocks are pulled out of the lamellae, and on further deformation, these blocks will align along the draw direction forming a periodic structure. The intercrystalline material may be thought of as consisting of the three components as shown in Figure 1.19.

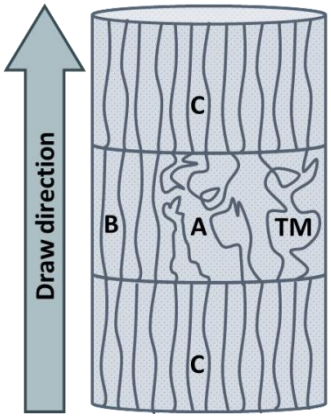

Figure 1.19. Schematic diagram showing the structure of a highly oriented semicrystalline polymer (A) amorphous region: this includes floating chains, cilia which are attached to a block at one end, and loops which start and end on the same block; (B) intercrystalline bridges: it has been proposed that tie-molecules may coalesce to form

bridges of a crystalline nature; (C) Chain-folded crystal blocks; (TM) tie-molecules, joining one crystalline block to another: these increases in both number and tautness with increasing amorphous content (redrawn from [171]).

According to Choi et al. [171], the axial thermal contraction of the highly oriented semicrystalline polymer fibres such as polyethylene and nylon originate from both crystalline and non-crystalline regions. Aligned crystal blocks and the crystalline bridges are formed between these regions with the polymer chain direction similar to the fibre drawing direction [172]. The main contribution to the negative thermal expansion in the draw direction comes from the rubber-elastic effect of the pre-stretched amorphous tie-molecules in the inter-crystalline regions. These polymer chains remain as highly extended after drawing due to the formation of the crystalline bridges. The inter-crystalline space is significantly sensitive to the moduli of the extended tie-molecules and the crystalline bridges and the volume fraction of each phase. According to the thermodynamics of rubber elasticity, the modulus of the amorphous tie-molecules increases due to the application of heat [173] and results in the contraction of crystalline bridges since the modulus of this region remains almost unchanged on heating. These mechanics are operated only at temperatures above the T_g of the polymer. Choi et al. have reported a thermal contraction coefficient up to $-40 \times 10^{-5}\ K^{-1}$ in the draw direction of highly oriented polymer fibre [171] that is much higher than the change in dimensions of the crystal lattice.

The untwisting phenomenon of oriented twisted polymer fibres can be explained based on these anisotropic thermal properties of highly oriented semicrystalline polymer fibres. Twisting of these fibres results in helically oriented chains. Thermally-induced length contraction of the oriented polymer chains now happens along the helical path

presented during twist insertion. The contraction of length in the direction of helically wrapped polymer chains can be accommodated within the twisted fibre by combinations of changes in axial fibre length (Δl), diameter (Δd), and number of twist (Δn). The relationship between twisted fibre length (l), diameter (d), precursor fibre axial chain length (λ) and the helical chain angle to the fibre axis (α_f) is modelled by a single helix [155]:

$$\frac{\Delta n}{n} = \frac{\Delta \lambda}{\lambda} \frac{1}{cos^2 \alpha_f} - \frac{\Delta d}{d} - \frac{\Delta l}{l} tan^2 \alpha_f \quad (1.6)$$

This equation predicts the untwisting of fibre when helically oriented polymer chain contracts (negative $\Delta\lambda$) and fibre diameter expands (positive Δd); therefore agreeing the anisotropic thermal behaviour of highly oriented polymer fibres.

Foroughi et al. have reported that the important characteristics related to the deformations of an electrochemically charged twisted CNT yarn can be approached by using this single helix-model [110]. Figure 1.20 illustrates a twisted single fibre having *n* rotations at a helix bias angle α_f to form a cylindrical shape of length l and radius *r*. The helical path length of fibre is l_s and the end rotation of fibre with respect to its starting point at the top is ϕ. The cylindrical radius (*r*) and volume (*V)* enclosed by the helically wound fibre can be expressed in terms of fibre length as [110]:

$$r^2 = (l_s^2 - l^2)/4\pi^2 n^2 \quad (1.7)$$

$$V = l(l_s^2 - l^2)/4\pi n^2 \quad (1.8)$$

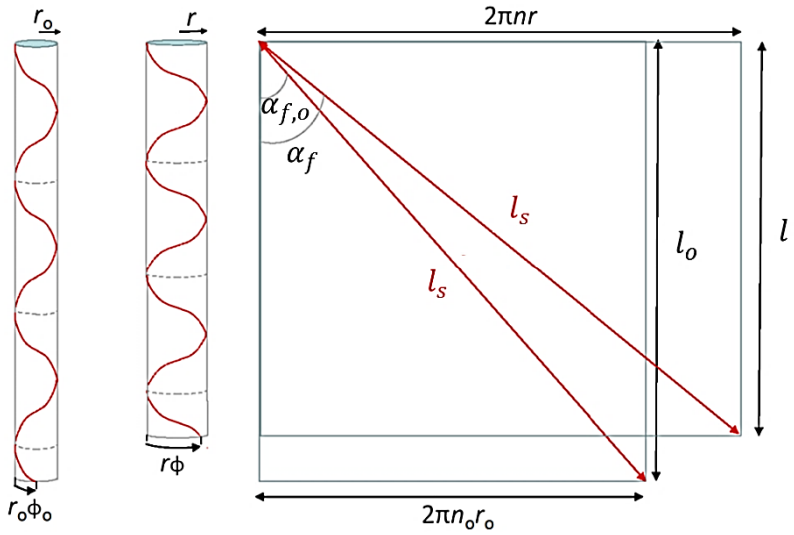

Figure 1.20. Single-helix model for a twist-spun CNT yarn, where helically wound fibre of constant length $\boldsymbol{l_s}$ forms a cylindrical volume of radius r_o and length $\boldsymbol{l_o}$ before actuation and *r and* $\boldsymbol{l}$ after actuation (left and middle illustrations). The fibre makes n_o turns along the cylinder length before actuation and *n* after actuation, and the rotation of the spring bottom end with respect to spring top is $\boldsymbol{\phi_o}$ before actuation and $\boldsymbol{\phi}$ after actuation (modified from [110]).

Rotation due to a change in the cylinder volume is indicated by a change in the number of twists, with a decrease in n indicating untwisting of the helix and an increase in n corresponding to an increase in twist. The ratio of the number of turns after a volume change to the initial number of turns is given by:

$$\frac{\boldsymbol{n}}{\boldsymbol{n_o}} = \left(\frac{\boldsymbol{V_o}}{\boldsymbol{V}}\frac{\boldsymbol{\lambda l_o l_s^2 - \lambda^3 l_o^3}}{\boldsymbol{l_o l_s^2 - l_o^3}}\right)^{\boldsymbol{1/2}} \tag{1.9}$$

where V_o and l_o are for the initial state, V and l are for the actuated state, and λ is the length ratio (l/l_o). Equation (1.9) is for a single helix that can approximate the outer shell of a twisted yarn, and may not quantitative predict the real fibre untwist during heating because of different axial and radial dimensional changes occurring internally in the twisted fibre. At the least, this equation provides a general explanation as to why the

twisted polymer fibre untwists when heated and the importance of the anisotropy of thermal expansion on this untwist.

The helix model approximates the mechanism of torsional actuation obtained from almost all kinds of helically twisted structures such as CNT yarns, metallic nanowire yarns, graphene oxide yarns and polymer fibres. For any stimuli applied to the actuators (i.e. thermal, chemical, moisture, electrochemical, electro-thermal, or photo-thermal) there results an overall volume change, which then drives the torsional actuation. However, Guo at al. [114] proposed a possible different actuation mechanism of electromechanical actuation of twisted CNT fibres. By quoting the Ampere's Law, it was attributed that these CNTs in a parallel arrangement produce electromagnetic forces as the current flows along the length of the CNTs. Although the electromagnetic force of a single CNT is very small, the combined effect of millions of CNTs in the cross-sectional area of a fibre can generate a force high enough to induce significant electromechanical lengthwise contraction and torsional rotation. By analogy of tensile actuators, the electromagnetic attractions are perpendicular to the CNTs, and the contraction stress attributes to the component force along the axial direction of the CNT fibre. Upon Joule heating, the produced tensile stress of CNT fibres of same cross-sectional CNT density was expected to be increased with the increasing twist bias angle. Unexpectedly, it was found that the stress first increased and then decreased with the increasing bias angle. This unwanted property was explained from the point of three-dimensional hopping conduction mechanism of the CNT fibre [174-176]. Haines et al. [154], on the other hand, have elaborately explained the torsional actuation mechanism of twisted fibres (polymers or CNTs) by using their thermal expansion anisotropy and the helical orientation. It was found that the twisted polymer fibres produce similar torsional actuation when either Joule heated or air heated. Since there is no

electromagnetic effect present in air heating process, the torsional response was solely seen as a result of the thermal expansion parameters. Twisting fibres of anisotropically expanding materials exposed a new phenomenon i.e. the thermal torsion effect. Any oriented fibre that expands radially more than it expands in length (before twisting) can produce untwist simply by inserting twist into the fibre. Although pure CNT yarns also provide anisotropic thermal expansion, by causing nanotube length contraction and yarn diameter expansion during heating, like for the in-plane and interplane expansions in graphite [177], this dimensional change is small and only able to produce useful actuation when the yarn is heated under very high temperature. By infiltrating a volume expanding guest within the confines of a twisted CNT yarn, a large, initially isotropic guest expansion can be transformed into an anisotropic yarn expansion by the helically aligned, high stiffness CNTs, thereby producing torsional actuation. A number of researchers have supported this mechanism, therefore, validates the acceptability of thermal expansion phenomenon of torsionally actuated fibres/yarns [110, 112, 113, 116, 117, 119, 144, 155].

1.9 Summary on Torsional Artificial Muscles

As-discussed, torsional actuators made of different materials and structures have different actuating mechanism and efficiencies. Table 1.2 summarises the maximum performances obtained from the torsional actuators of different material groups and structures.

Table 1.2. Summary table of torsional artificial muscles made of different materials and structures.

Kind of torsional actuator	Developed structures	Stimulus	Maximum stroke (degree / mm)
Shape memory alloy	Rod, tube, sheet, strip, wire, or coil	Joule heating	~4.5 [45]
Piezoelectric material	Bar, tube, twisted sheet, or fibre	Piezoelectric effect	~0.04 [54]
Multilayer torsional ribbon	Twisted or coiled bimorph strip	Global heating	~1000 [64]
Electroactive polymer	Films, or tube	Electrical energy	~0.01 [84]
Fluidic torsional actuator	Tubular elastomer with outer helical braided sleeve	Air, or water	~1.75 [109]
Carbon nanotube	Twisted or coiled yarn	Electrochemical, chemical, electromechanical, thermal, electro-thermal, or photo-thermal	~380 [144]
Metallic nanowire	Twisted yarn	Thermal	~12 [118]
Graphene fibre	Twisted fibre	Chemical (moisture activated)	~588 [119]
Polymer fibre	Twisted, or coiled fibre	Air heating, Joule heating, photo-thermal, or electrochemical	~300 [161]

A number functional prototype has been developed by using torsional artificial muscles. Tobushi et al. [43] have used the thermal recovery of a twisted thin strip of TiNi SMA to develop several prototype devices. A rotation of 90^{o} was achieved through shape

recovery in a 40 mm long strip operated in the one-end-tethered mode. This example was a one-way actuation and was used as a door opening mechanism [Figure 1.21(a)]. Another device used a return spring mechanism for two-way actuation to open and close window blinds in sunlight and darkness, respectively [44]. Here the twisted strip was connected to a superelastic alloy strip that acted as a return spring in the two-end-tethered configuration [Figure 1.21(b)]. Foroughi et al. [110] demonstrated a fluidic mixer by using a electrochemically actuated CNT yarn torsional artificial muscle to mix two laminar flowing liquids (dyed yellow and blue) that were joined at a T-junction in a fluidic circuit [Figure 1.21(c)]. A reversible paddle rotation of up to 180° was attained with a 65 mm long actuating yarn of 15 μm in diameter. The yarn rotated a 100 times wider paddle than the diameter of the yarn, and 80 times its mass, in the flowing liquids at a maximum rotation rate of 360° per second. Cheng et al. [119] constructed a humidity switch and an electric generator in which the application of vapour leads to a twisted graphene oxide fibre switching the magnetisation of a small magnet, which sequentially drives a small electric field in copper coils surrounding it [Figure 1.21(d)]. In the switch (1), twisted fibre in response to moisture (e.g., relative humidity = 85%) can rotate a paddle to press on the metal plate, as pointed out by the arrow, so that the electric circle powered by the battery will turn on the LED, as shown in the inset photo. The generator (2) contains four copper coils around the twisted fibre with a magnet. When the humidity changes, twisted fibre can reversibly rotate the magnet within the surrounding copper coils to generate electricity. Recently, Haines et al. [155] utilized twisted coiled nylon fibres to fabricate smart textile fabric, braided structure and window shutter. When heated, torsional actuation of twisted fibres drive linear movement of the coils and regulates textile porosity (1), braid lifting (2) and opening / closing of the window shutter (3), respectively.

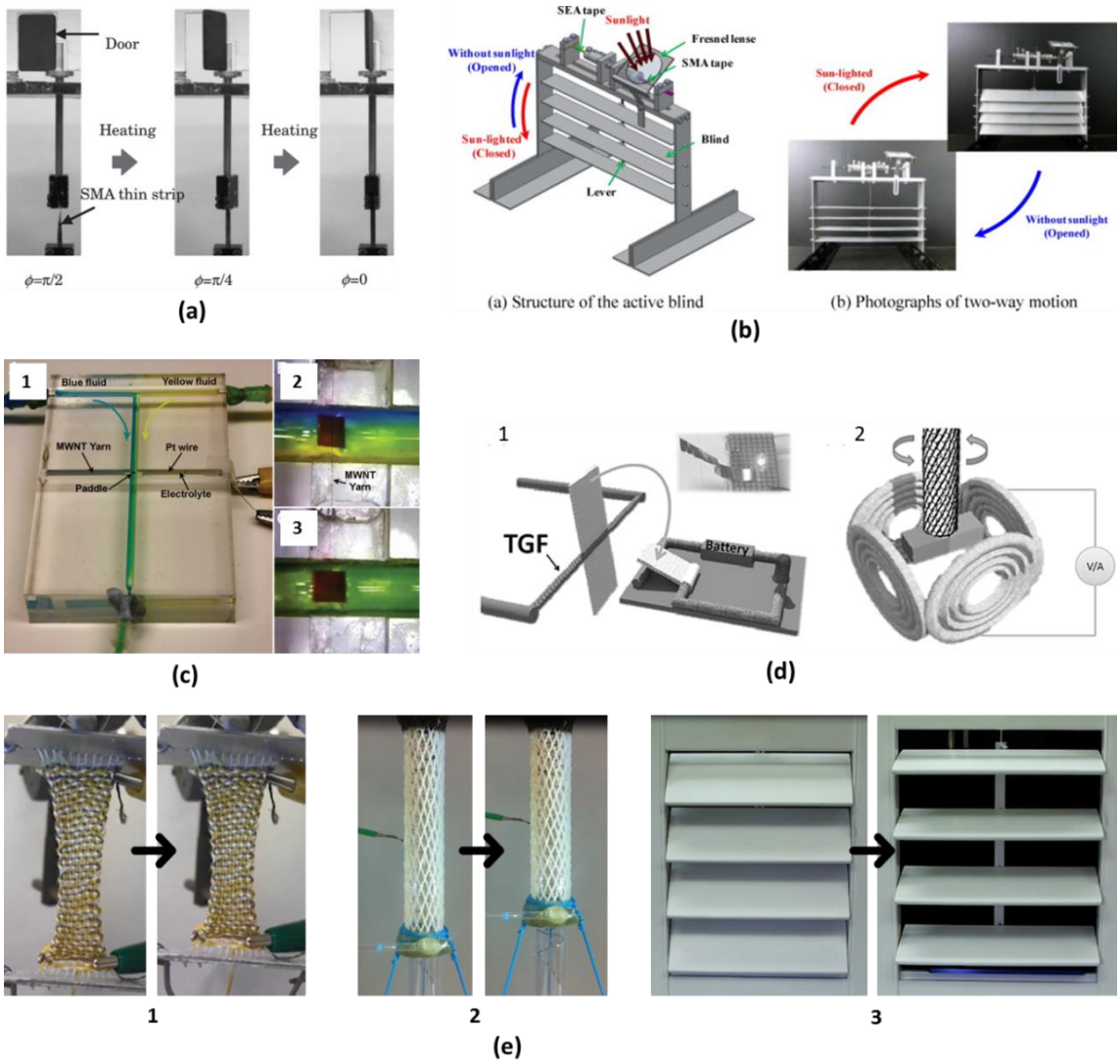

Figure 1.21. Functional prototypes made of torsional artificial muscles. (a) Joule heated SMA thin strip showing one-way rotary movement of a door (***ϕ*** denotes the angle of twist) [43]. (b) Solar-powered active blind model constructed of two-way rotary actuation of a SMA tape [44]. (c) Fluidic mixer operated by a multi-walled CNT yarn torsional actuator; 1. photograph of the prototype, 2. unmixed fluid, and 3. mixed fluid [110]. (d) The scheme of the designed humidity switch (1) and the alternating current generator (2) based on the humidity-responsive twisted graphene oxide fibres (TGF) [119]. (e) Prototypes made by using twist induced coiled nylon 6,6 fibres where thermally induced torsional rotation of the twisted structures causes linear movement of a; 1. textile fabric, 2. braided structure, and 3. window shutter [155].

1.10 Thesis Aims

To aid material development for torsional muscle and for coiled tensile muscles, the present work aims to study the fundamental understandings of torsional actuation in twisted highly oriented polymer fibres. Thermally-driven tensile actuation of twist-induced coiled polymer fibres has been investigated recently and found to be dependent on their untwisting/retwisting (torsional actuation) phenomenon due to the surrounding temperature change. These readily available and low cost materials make the actuators easily accessible and act as high performance artificial muscle. However, the actuation mechanism is not fully understood in terms of the anisotropic thermal responses on these twist drawn oriented fibres and their fabrication parameters such as sample diameter, twist density/bias angle, sample annealing temperature, moisture content and crystal content. The following chapters of this thesis document the early development of torsional actuators and their characterization techniques, the underlying mechanism of their responses and their use to develop a novel integrated torsion / tensile actuator system.

The first aim of the research described in this thesis was to develop a test method for assessing torsional actuation. The developed method included procedures to characterize torsional stroke and torque as well as provide an assessment of speed, reversibility and cycle life.

The second aim of this research project was to investigate the scale dependency of torsional stroke and generated torque in twisted polymer fibres. The single-helix approximation of the twisted fibre structure will be evaluated in terms of the quantitative prediction of the torsional stroke during fibre heating. The model was applied initially to twisted nylon 6 fibers of different diameters and different inserted

twist. Secondly, the model was applied to twisted polyethylene and polypropylene fibres to investigate the effects of different volume change anisotropies.

The third aim of this research project was to investigate methods used to thermally set the helical chain structure of twisted highly oriented semicrystalline nylon 6 fibre. Currently, the twisted polymer fibre torsional and tensile actuators require several unwanted 'training cycles' of heating and cooling prior to achieving fully reversible actuation. The specific aim was to employ several annealing techniques to modify the structure of twisted polymer fibres and investigate the effects on the reversibility of torsional actuation behaviour under different mechanical conditions.

The fourth and final aim of this research project was to develop an integrated artificial muscle which shows contractile behaviour of highly elastic yarn by coiling itself originated from thermally-induced torsional actuation of a twisted polymer fibre. The specific interest was to evaluate single-helix approximation of coiled yarn in terms of coil geometry, and combined with torsional actuation of twisted fibre to predict the overall muscle contraction.

CHAPTER 2 Characterisation of Torsional Actuation in Highly Twisted Yarns and Fibres

This chapter has been adapted from the article "S. Aziz, S. Naficy, J. Foroughi, H. R. Brown and G.M. Spinks, *Polymer Testing* 46:88-97 (2015)".

The introduction section in this chapter is a shortened version compared with the published article to avoid duplication with the comprehensive literature review of Chapter 1.

2.1 Introduction

As described in chapter one, practical application of torsional artificial muscles require a precise and continuous characterization technique that allows the torsional stroke and torque to be calculated for any externally applied environmental and mechanical condition. To aid material development for torsional muscle, the present work aims to develop a test method for assessing torsional actuation. Of interest is a procedure to characterize torsional stroke and torque as well as an assessment of speed, reversibility and cycle life. Previous work has focussed mainly on measuring torsional stroke, for example by tethering the sample at one end and measuring the rotation of the free end. Sometimes a return spring mechanism has been used to improve reversibility of torsional actuation. In these cases, the actuating yarn or fibre was attached to another non-actuating fibre, both ends were tethered and torsional rotation measured at the junction. An advantage of the two-end-tethered system is the ability to fix the location of the rotating element. In contrast, the free end of the one-end-tethered system can move in any direction and has limited practical utility.

What is needed is a measurement technique and analysis procedure that allows the torsional stroke and torque to be calculated for any imposed external loads. By analogy with tensile actuators, the characterisation method should provide the stroke-torque curve defining the free stroke (zero external torque), blocked torque (zero torsional rotation) and all combinations of non-zero stroke and torque. Such information has not yet been reported for any of the twisted fibre torsional muscles. Herein is described a method for measuring the rotation of a shaft attached to a near frictionless bearing and driven by a torsional actuator, *i.e.* the twisted fibre. The measurement system can measure both torsional stroke and torque, and the sample can either be operated with or without a return spring fibre.

The theoretical treatment of torsional actuation assumes that a given stimulus induces a free rotation that increases linearly with fibre length, and is here denoted θ and reported as degrees per mm of actuating fibre length. The actual rotation angle ϕ(*x*) varies linearly with distance *x* taken from the clamped end of a fibre so that the torsional stroke at the free end of a one-end-tethered fibre of length L_A is:

$$\phi(L_A)_{\text{free}} = L_A.\theta \tag{2.1}$$

If the fibre behaves as a linear elastic rod in torsion, then the blocked torque will be:

$$\tau_{blocked} = \phi(L_A)_{\text{free}} \times S_A \tag{2.2}$$

Here, S_A is the torsional stiffness of the actuating fibre, or the resistance to rotation. The torsional stiffness is more fundamentally related to the fibre diameter (*d*), length (*L*) and the fibre material's shear modulus (*G*) in the circumferential direction:

$$S = \frac{k}{L} = \frac{JG}{L} \tag{2.3}$$

Here, *k* is termed the 'torsional modulus' in standard torsion mechanics and should not be confused with other moduli, such as the shear modulus and Young's modulus that are true material properties. The torsional modulus depends both on material properties (shear modulus *G*) and the fibre dimensions. J is the polar moment of inertia of fibre and formulated in terms of sample diameter for a fibre of circular cross-section is:

$$J = \frac{\pi d^4}{32} \tag{2.4}$$

The stimulus used to initiate torsional actuation, for example heat, is likely to affect the material's torsional stiffness due to dimensional changes and modulus shift. Consequently, the blocked torque represented by Equation (2.2) uses the torsional stiffness of the fibre in the final actuated state after the stimulus has been applied

(hereafter denoted S'_A). A change in torsional stiffness will also contribute to the torsional stroke measured under isotonic (constant external torque) conditions. For a one-end-tethered fibre acting against an external torque τ_{ext} the torsional stroke will be given by:

$$\phi(L_A)_{\text{isotonic}} = L_A.\theta + \tau_{\text{ext}}\left(\frac{1}{S'_A} - \frac{1}{S_A}\right) \quad (2.5)$$

The second term in Equation (2.5) relates to the free end rotation resulting from a change in sample torsional stiffness from S_A to S'_A in the starting and final states, respectively.

When operated against a return spring, the external torque acting against the actuating fibre increases after the stimulus has been applied. The return spring is twisted as the actuating fibre torsionally actuates generating a restoring torque within the return spring fibre. The rotation at the end of the actuating fibre, corresponding to the junction between the actuating and non-actuating fibres, will be smaller than in free rotation so a residual torque remains in the actuating fibre. At equilibrium, the residual torque in the actuating fibre is exactly cancelled by the restoring torque generated in the return spring, non-actuating fibre. For the general case where the actuating fibre is subjected to a constant external torque and connected to a return spring fibre of torsional stiffness S_N, the torsional stroke (ϕ) at the junction between actuating and non-actuating fibres can be determined from the torque balance Equation:

$$S'_A\left[\left\{L_A.\theta + \tau_{\text{ext}}\left(\frac{1}{S'_A} - \frac{1}{S_A}\right)\right\} - \phi\right] = S_N.\phi \quad (2.6)$$

Re-arranging Equation (2.6) gives an expression for the expected torsional stroke at the junction between the actuating and non-actuating fibres:

$$\phi(L_A)_{return\ spring} = \left[L_A.\theta + \tau_{ext}\left(\frac{1}{S'_A} - \frac{1}{S_A}\right)\right]\left(\frac{S'_A}{S'_A+S_N}\right) \quad (2.7)$$

In the case where the external torque is zero, the stroke is given by:

$$\phi(L_A)_{return\ spring} = L_A.\theta\left(\frac{S'_A}{S'_A+S_N}\right) \quad (2.8)$$

Equation (2.8) reduces to Equation (2.1) in the absence of a return spring (S_N=0) and when the actuating fibre is tethered at only one end. Figure 2.1 illustrates the theoretical torsional stroke expected for the case of free rotation, isotonic torsional actuation and torsional actuation with a return spring. The torsional strokes are expressed as a fraction of the free rotation to emphasise the importance of the inherent torsional actuation parameter, θ, in determining the torsional stroke in all cases.

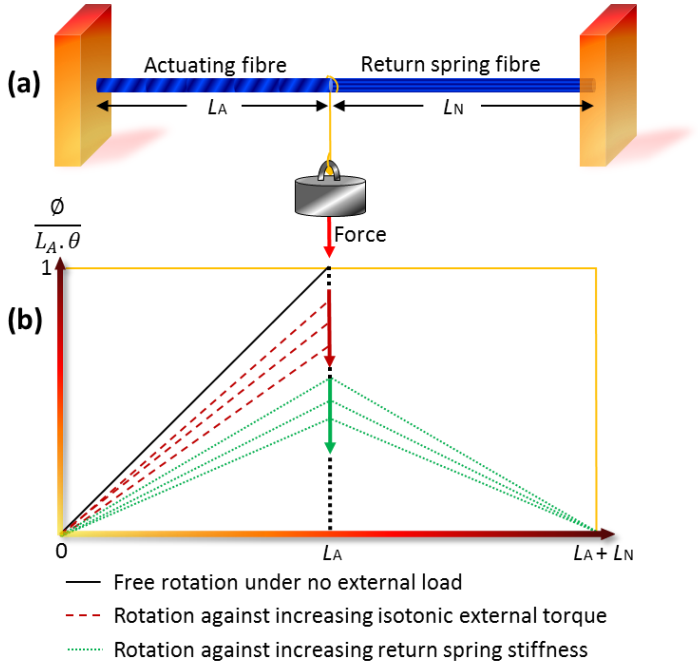

Figure 2.1. a) Illustration of different torsional actuation methods where the actuating element is optionally subjected to an external torque (presented as force applied by a hanging weight) and/or a return spring fibre; b) theoretical estimates of torsional stroke at each point along the length of an actuating fibre and return spring (non-actuating) fibre, if used, and operated in free rotation or isotonic rotation modes.

2.2 Experimental Methods

2.2.1 Muscle Fabrication

The fibre was attached to the motor at its upper end and supported by a fixed weight (~200 gm) hanging on the other end providing 10 MPa stress to the fibre. The incorporated weight was tethered contrary to the motor rotation, and hence each turn from the motor shaft caused the formation of one turn in the fibre. The muscle fibre taken for the actuation test was twisted until the onset of coiling. The supported weight on the fibre was crucial to have straight and uniformly twisted fibres, without permitting snarl formation prior to coiling. The non-coiled section of twisted fibre was then taken to an isothermal heating oven and annealed at 120°C, or ~70^{o}C above glass transition (T_g) [178, 179], for 30 minutes with both ends clamped to prevent loss of twist. Heating at a temperature over T_g helps the newly introduced twisted shape to be permanently set. After removal from the oven, the fibre was relaxed at room temperature for 2 hours while still clamped. Figure 2.2 shows a schematic diagram of twist insertion and the preparation of fishing line muscle to be used for actuation tests.

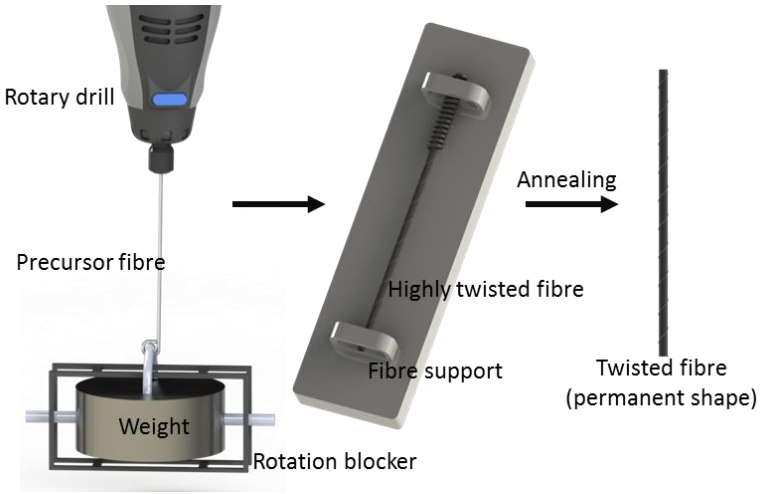

Figure 2.2. Schematic illustration of twist insertion in nylon 6 (graphics are not to scale).

Twist insertion per length of precursor fibre was determined by using a rotation counter. Fibre bias angle (α_f**,** relative to fibre axis) due to the twist insertion was calculated from the number of turns/meter using Equation (2.9) [110].

$$\alpha_f = tan^{-1}(\pi dT) \tag{2.9}$$

Here, *d* is the fibre diameter and *T* is the amount of turns inserted per initial fibre length.

Additionally, the fibre bias angle was observed directly using an optical microscope (LEICA M205 A). The observed bias angle was in close agreement with the value calculated using Equation (2.9) from the measured number of turns/meter inserted into the twisted fibre.

2.2.2 Thermally-Powered Torsional Actuation Test

Experiments were conducted using an in-house-produced torsional actuation test apparatus with a heating chamber (Figure 2.3). The heating process was operated through Nichrome 80/20 heating wire and driven by an electrical current source. Twisted nylon fibre was positioned in the heating zone to evaluate the torsional actuation performance during heating and cooling cycles. A thermocouple was positioned close to the sample to estimate sample temperature.

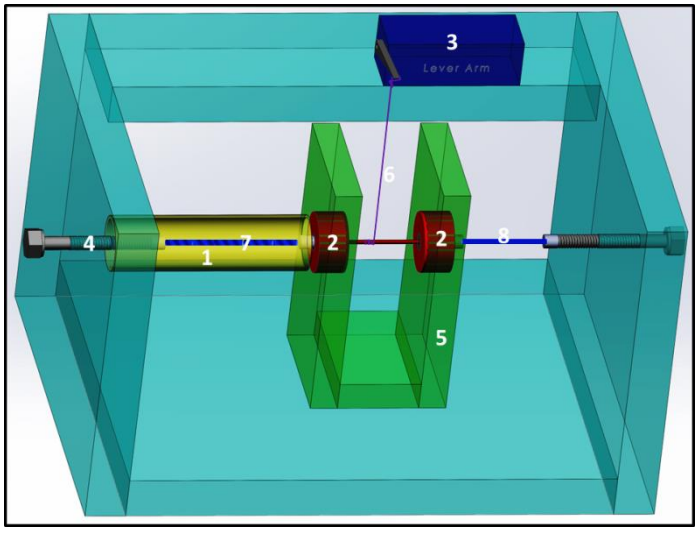

Figure 2.3. CAD model of torsional actuation test apparatus; (1) heating zone, (2) ultra-low friction air bearings, (3) lever arm force/distance transducer, (4) movable fibre gripping clamp, (5) support for air bearings, (6) connecting fibre between lever arm force/distance transducer and bearing shaft, (7) actuating muscle fibre, and (8) fibre acting as return spring keeping the actuating muscle straight and well positioned.

A slow heating process (3.5°C/min) was maintained by using a programmable controller (Electro Chemical Engineering Pty Ltd, Australia) to increase temperature at a uniform rate from 25°C to 60°C. Figure 2.4 shows the integrated experimental set-up consisting of test apparatus, programmable power supply and dual-mode lever arm system (Aurora Scientific, Canada). In all cases, it was found that a small number of heating and cooling cycles were needed before the torsional actuation became fully reversible. Data measurements were conducted after the completion of these 'training cycles'. Samples were equilibrated in ambient laboratory conditions before testing and separate studies between carefully dried and water-saturated samples showed negligible difference in actuation behaviour.

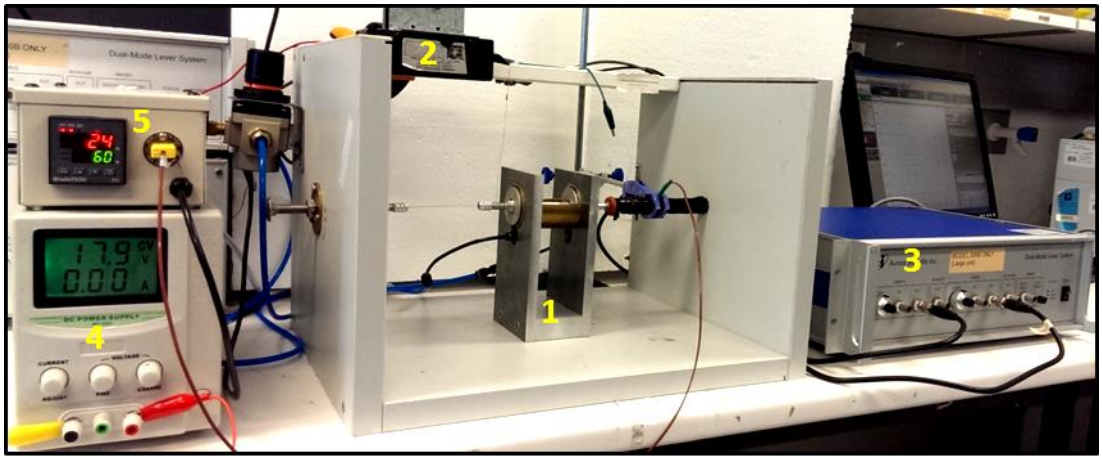

Figure 2.4. Torsional actuation testing set-up; (1) test apparatus, (2) lever arm force/distance transducer, (3) lever arm controller, (4) DC power supply, (5) programmable temperature controller.

Initial interest was to quantify the amount of torsional stroke generated by the twisted fibre in a certain range of temperature. The fibre was tethered to a rigid support at one end and the other end was clamped to an aluminium shaft (radius, r_s) passing through a pair of aligned air bearings (OAVRL13MM supplied by CGB Precision Products Pty Ltd, USA) mounted on aluminium supports. These compressed air assisted bearings are able to provide almost frictionless rotation, so that torsional motion can freely occur with negligible external disturbance to the actuated fibre. The amount of thermally powered free torsional stroke generated by the twisted fishing line was observed optically by using a microscopic camera system (ISSCO-OPTEK). The camera was positioned and focused axially to the air bearing and videography of bearing rotation was exported to a geometric tool (GeoGebra mathematics software) to quantify the amount of fibre rotation.

The optical method for determining torsional stroke could not provide real-time data, so the test apparatus was modified by introducing a dual-mode lever arm force/distance transducer (Aurora 305B). The air bearing shaft was partially wrapped with a high

stiffness thin polyethylene fibre (DYNEEMA 180 μm diameter) and connected to the lever arm operated in isotonic mode (constant force) and positioned so that the connecting fibre was perpendicular to the shaft. Torsional actuation of the twisted fibre rotated the connecting shaft which caused proportional displacement of the lever arm that was then expressed as the torsional stroke (degree). Calibration of lever arm displacement to shaft rotation was performed in terms of shaft circumference and angular movement that caused the linear motion of vertically placed lever arm. The lever arm applied a small and constant normal force (F_N) to the shaft resulting in a constant torque ($\tau_S=F_N.r_s$). Unless otherwise stated, the external force opposed the rotation of the twisted fibre when the latter was heated.

The same apparatus was also used to evaluate the torque generated during heating/cooling of the twisted nylon fibre. In this case the lever arm was operated in the isometric mode (constant length) to prevent shaft rotation and provide a measure of the blocked torque. Torque/stroke curves could also be obtained by first measuring the blocked torque and then allowing the shaft to rotate by gradually reducing the applied force to zero while measuring the amount of shaft rotation.

Of further interest was to assess the amount of torsion when the actuating fibre was attached to a 'return spring', as has been typically used in previous studies. As shown in Figure 2.2, a return spring fibre can be included by attachment to the air bearing shaft and a second end tethering point. Tension is sometimes also applied using the return spring fibre.

2.2.3 Fibre characterization

The torsional rigidity (S) [180], torsional modulus ($k=JG$) [110] and shear modulus (G) [181] of both the twisted (actuated) fibre and return spring fibre were determined by

measuring the shaft rotation resulting from mechanical increase of torque applied by the lever arm. Torsional rotation (ϕ) versus torque (τ) curves from multiple samples of different lengths was used to determine torsional rigidity of fibre, as in Equation (2.2).

2.3 Results

2.3.1 Characteristic Properties of Twisted Fibre

A nylon 6 fibre of 550 µm diameter (d) was used for twist insertion. Figure 2.5 shows optical micrographs at different stages of the twisting process. Figure 2.5(a) represents the precursor fibre and Figures 2.5(b) and (c) show, respectively, the coiled and non-coiled portions of fibre after insertion of 450±5 turns per metre of initial fibre length. The highly twisted, but non-coiled section of muscle fibre was extracted for further analysis. Fibre diameter was found to have increased during twisting by ~10% from ~551 µm to ~597 µm. The bias angle of inserted twist was calculated from Equation (2.9) and found to be 35.3°. Figure 2.5(d) shows optical measurements of the fibre bias angle showing 36.0° from the fibre axis, which is in close agreement with the calculated value.

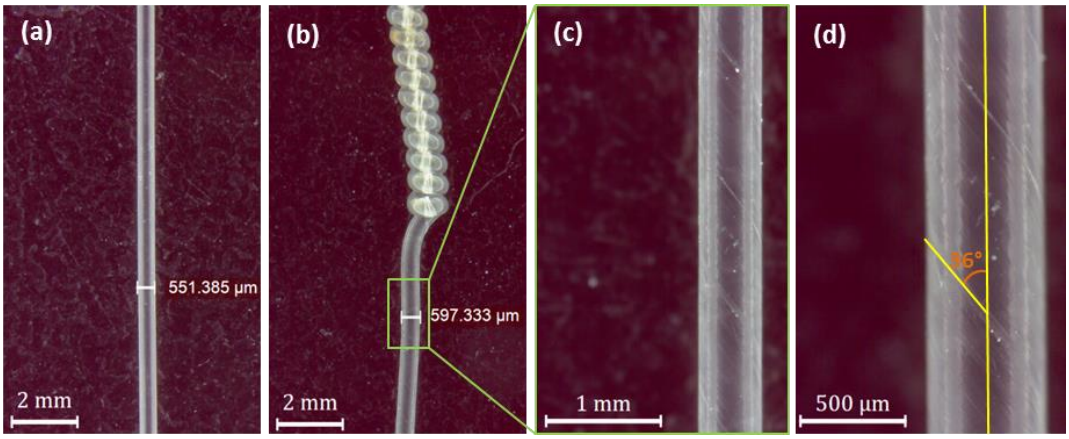

Figure 2 5. Optical micrographs of (a) precursor nylon 6 fibre, (b) twisted fibre with twist-induced coil section, (c) extracted twisted section, and (d) observed bias angle from higher magnification micrograph of twisted section. The diagonal markings

observed in (c) and (d) arise from extrusion marks originally oriented along the axis of the untwisted fibre.

The torsional stiffness and moduli of the twisted nylon 6 fibres were evaluated from inverse gradient of stroke/torque plots (Equation 2.2) and gradient of corresponding stiffness/inverse length plot (Equation 2.3). Figure 2.6(a) shows that shaft rotation linearly progresses as the amount of mechanically applied torque increases. Three different sample lengths (10, 35, and 70 mm) of identical twisted fibre were considered and showed a linear relationship between torsional stiffness and length [Figure 2.6(b)]. The resulting length independent torsional modulus was found to be 3.56×10^{-6} N·m^2 at room temperature.

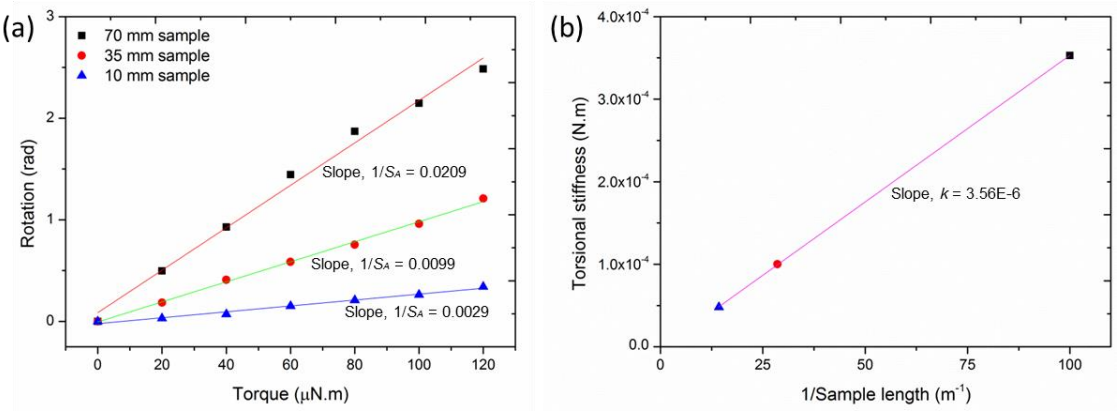

Figure 2.6. Torsional properties of twisted fibre prepared from 550 mm diameter nylon 6 and tested at room temperature: (a) shaft rotation against mechanical torque, and (b) torsional stiffness of different lengths of fibre with the slope giving the torsional modulus.

Torsional properties of nylon 6 fibre were also evaluated in terms of fibre diameter. Figure 2.7(a) shows the angular rotation of two fibres under increasing external torque: a twisted nylon 6 fibre of original length of 10 mm long and 550 μm diameter (d_2) and

an untwisted fishing line 10 mm long and 330 μm diameter (d_1) that was used as a return spring in some actuation experiments. The torsional moduli were 3.56×10^{-6} N·m^2 for the twisted fibre and 4.7×10^{-7} N·m^2 for the return spring.

$$\frac{k_1}{k_2} = \left(\frac{d_1}{d_2}\right)^4 \tag{2.10}$$

Here, k_1 and k_2 are the torsional moduli of the twisted fibre and the return spring fibre, respectively. Experimental results [Figure 2.7(b)] show the torsional modulus ratio to be 7.57, in reasonable agreement with the fourth power of the diameter ratio (7.72), as predicted by theory. The shear moduli of twisted nylon 6 fibre and untwisted return spring were very similar (0.40 GPa and 0.41 GPa, respectively) as is expected for fibres with the same composition and structure.

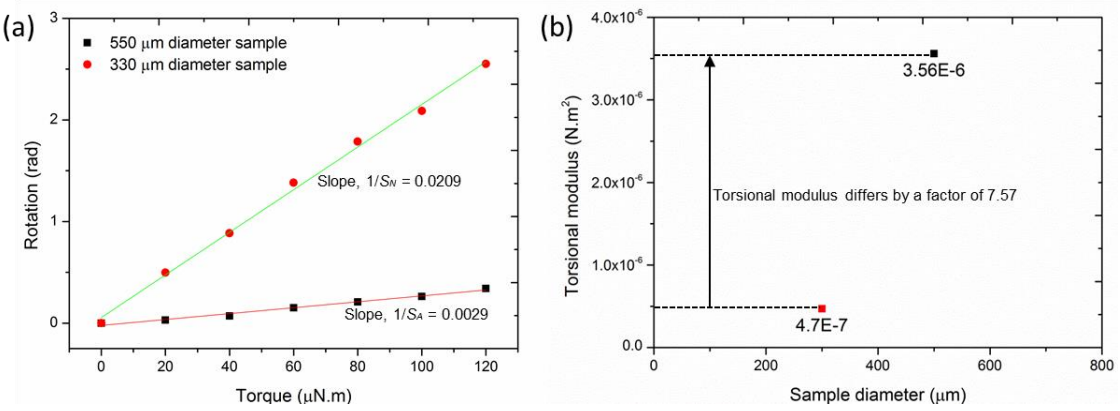

Figure 2.7. Torsional properties of nylon 6 fibres (a) shaft rotation against mechanical torque of different diameter fibre, and (b) torsional stiffness with resultant modulus.

Torsional properties of the 550 μm twisted fibre were also evaluated at the maximum temperature reported for actuation tests in this study. Figure 2.8 shows the angular movement of twisted fibres at 60ºC under increasing external torque. The torsional modulus was 3.19×10^{-6} N·m^2. Shear modulus of the twisted fibre at this particular temperature were calculated by considering the change in fibre diameter resulted from

applied heat and found to be ~0.24 GPa, which is significantly lower than the value obtained at room temperature, as expected [182].

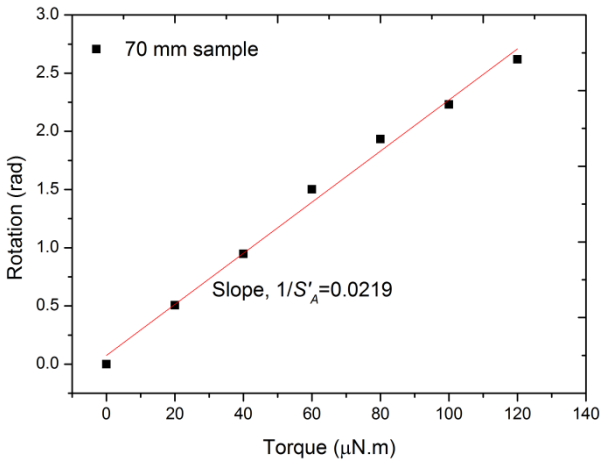

Figure 2.8. Fibre rotation at 60°C against applied mechanical torque. The inverse slope of the rotation/torque curve defines the torsional stiffness.

2.3.2 Torsional Actuation Test Results

2.3.2.1 Free Fibre Rotation

In free rotation tests, the twisted nylon 6 fibre was attached at one end to the air bearing shaft and the other end clamped. Heating allowed the non-clamped fibre end to rotate freely with negligible external resistance. Figure 2.9 shows optically measured torsional rotation of the air bearings. The fibre was observed to rotate in the untwist direction during heating and to retwist on cooling in the range 28-62ºC. The rate of rotation was higher above ~50ºC, which corresponds approximately to the T_g of nylon 6. A small hysteresis between heating and cooling was observed, especially above T_g. The final rotation angle after heating to 62ºC reached an approximately constant value of -171º, or -2.45º/mm based on fibre length, after several heating and cooling cycles.

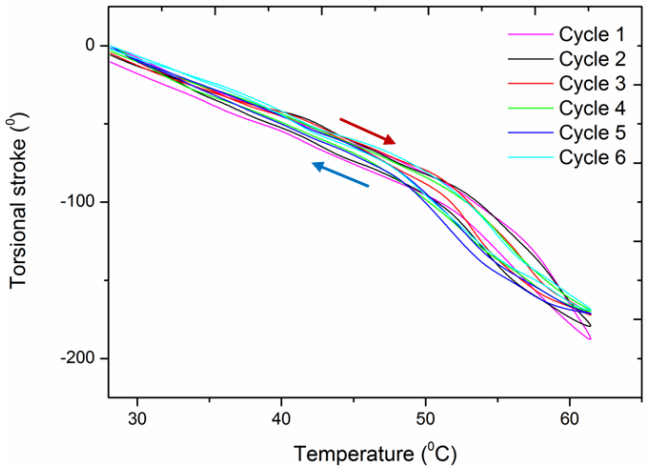

Figure 2.9. Optically measured torsional actuation of twisted nylon 6 during slow heating and cooling. The 70 mm long, 550 mm diameter fibre was attached to air bearings that allowed one end of the fibre to rotate freely with negligible friction. Negative values of torsional stroke represent untwisting. Arrows indicate the heating and cooling directions.

2.3.2.2 Constant Torque Torsional Actuation

The torsional actuation of the twisted fibre was also tested isotonically under constant torque. Figure 2.10 shows the thermally driven torsional stroke of twisted fibre acting against a constant opposing torque of ~68 μN·m applied to the bearing shaft surface when the sample was subjected to heat/cool cycles in the range of 28-62ºC. The torsional stroke was calculated from the lever arm deflection and was validated by optical measurements of the bearing rotation that demonstrated 99.5% accuracy. Hence, it was concluded that the lever arm provides immediate, convenient and continuous measurement of the fibre rotation without the need for off-line image analysis.

The thermally-induced isotonic torsional stroke of the nylon 6 was similar to that observed during free rotation. The 70 mm long and 550 μm diameter twisted nylon 6 generated a maximum -2.32°/mm fully reversible torsional rotation when heated slowly from 28 ºC to 62 ºC (Figure 2.10). The maximum rotation angle from cycle to cycle was more consistent than in free rotation tests. The original shape was regained after the

cooling cycle by retwisting the fibre with almost 100% reversibility. Again, a higher rate of rotation was observed above T_g of ~50ºC. A small hysteresis between heating and cooling cycles of unknown origin occurred at lower temperatures between 30 and 40ºC.

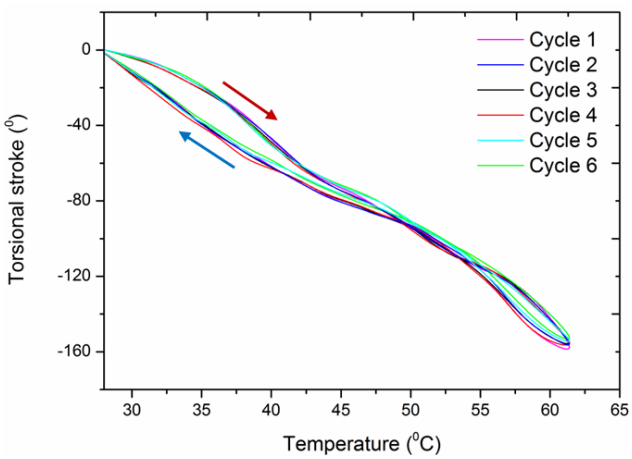

Figure 2.10. Isotonic constant torque (68 mN m) actuation stroke of twisted nylon 6 over 6 consecutive heat/cool cycles.

Similar tests were also conducted using several different constant applied torque values. In all cases, the torque was applied so as to oppose the fibre untwisting that occurred during heating. Figure 2.11 shows the torsional stroke during heating and cooling with increase of torque occurring in successive actuation cycles. The torque adjustment occurred isothermally at 26ºC and torsional stroke in each actuation cycle is reported after training the sample by several heating/cooling cycles at each new torque level. As shown, the actuation stroke after heating from 26-62ºC decreased as the opposing torque increased. The torque was increased by a factor of ~16 times resulting in a decrease in the torsional stroke of ~32%. A final heat/cool cycle was performed after resetting the torque to its initial value, and the results show that the torsional stroke followed the original curve very closely. It can be concluded that the higher torque

isotonic tests caused no degradation or other permanent effects on the torsional actuation behaviour of the twisted nylon 6 fibre.

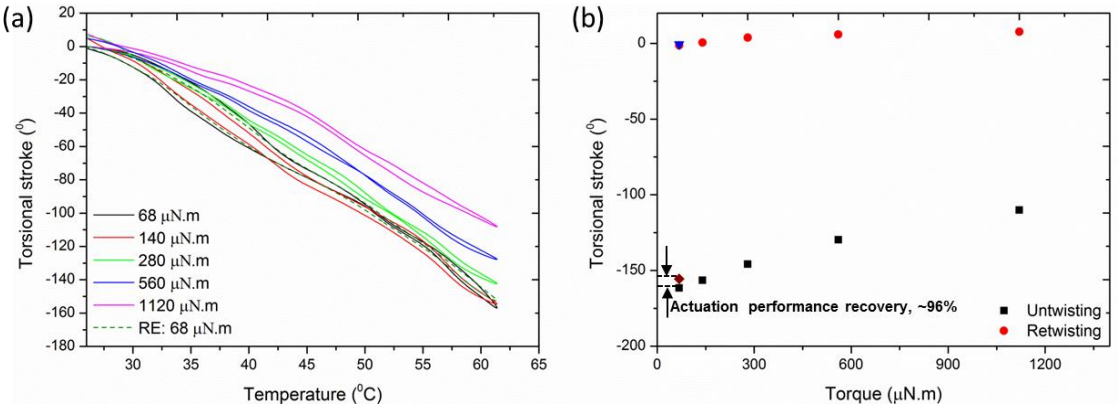

Figure 2.11. Cycle based constant torque actuation profile of twisted nylon 6. Mechanical torque at the levels indicated was increased step-by-step corresponding to successive actuation cycles. A final heat/cool cycle was also performed at the original torque value (denoted RE for repeat).

2.3.2.3 Torque generation and torque-stroke curves

The torque generated during heating and cooling of the twisted fibres was determined by isometric testing where the fibre rotation was completely blocked by the lever arm and the blocking force measured. The samples were first conditioned using the normal training cycles where the fibre was allowed to freely rotate until the untwist and retwist on heating and cooling became fully reversible. At this point, the blocked rotation test was performed and a 70 mm long and 550 μm diameter twisted fibre was able to produce ~225 μN·m torque when the sample was heated from 28 to 62ºC (Figure 2.12). On cooling, the torque returned to the starting value, demonstrating the reversibility of the torsional actuation. A noteworthy hysteresis was observed between the torque generated in the heating and cooling cycles. The hysteresis was mostly due to a small

force decay that occurred during the isothermal hold period at the maximum temperature and prior to cooling.

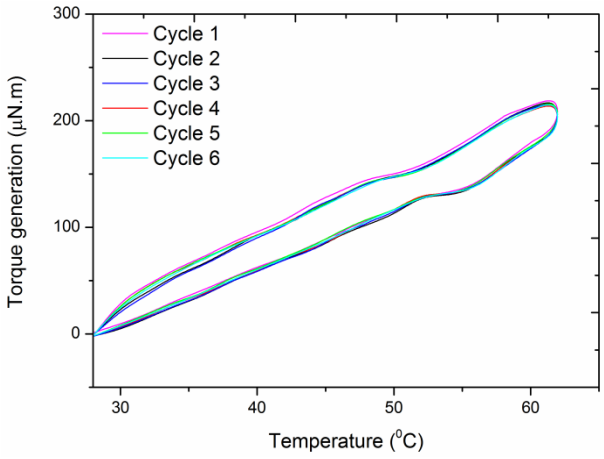

Figure 2.12. Thermally-induced torque generation by twisted nylon 6 after free rotating training cycles.

Torque-stroke curves were also generated by first measuring the blocked force during heating and then allowing the fibre to untwist isothermally until the torque was fully relaxed. The fibre was next retwisted isothermally to restore the measured blocked force and the sample cooled under isometric conditions. Figure 2.13(a) shows the testing sequence and Figure 2.13(b) shows the torque-stroke curves obtained during the isothermal period at 60ºC. The fibre was allowed to untwist as the torque was relaxed and the free rotation stroke could be estimated from the zero torque point on the curve. Here, the free torsional stroke was -204º or -2.91º/mm [Figure 2.13(b)]. Interestingly, this free stroke value was significantly higher than measured during the free rotation experiments (-2.45 º/mm). The slope of the torque-stroke curve also provides a measure of the fibre torsional modulus at 60ºC giving a value of 4.26×10^{-6} N·m^2 for the 70 mm long twisted fibre. Again, this value is higher than the torsional modulus reported above. Possible explanations for these differences are considered in the Discussion section.

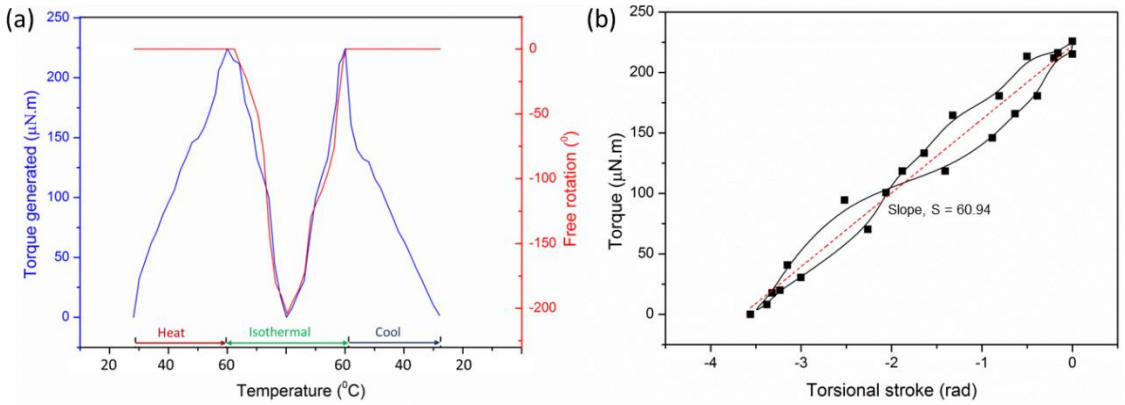

Figure 2.13. Torque stroke curves of nylon 6 fibre; (a) isometric force generation followed by free rotation on torque relaxation/regeneration, and (b) torque vs torsional stroke; trend extracted from isothermal section.

2.3.2.4 Variable torque torsional actuation using a return spring

This experiment was conducted by thermally actuating the twisted fibre against a return spring, as has been commonly used in previous studies [110]. The test system included a second nylon 6 fibre connected to the opposite end of the air bearing shaft and then tethered to the supporting frame. Here, rotation of the shaft resulted from torsional actuation of the actuating fibre twists the return spring fibre, thereby generating an increasing opposing torque as the sample rotation proceeds. In addition to the return spring torque, the lever arm was operated in isotonic mode and applied a small constant torque of 68 µN·m that also opposed the sample rotation. This small torque was necessary for accurate measurement of the shaft rotation using the lever arm displacement transducer. Figure 2.14 shows the thermally induced torsional stroke of a 70 mm long, 550 µm diameter twisted nylon 6 fibre acting against the variable torque applied by a 70 mm long and 330 µm diameter nylon 6 return spring. Fully reversible torsional actuation was observed during heating and cooling in the range of 28-62ºC with very little hysteresis. The maximum rotation angle decreased slightly during

successive cycles to a value of -2.04º/mm, which was considerably smaller than rotations observed in free rotation tests due to the restrictions imposed by the return spring. The quantitative evaluation of the return spring effects is considered in Section 2.4.

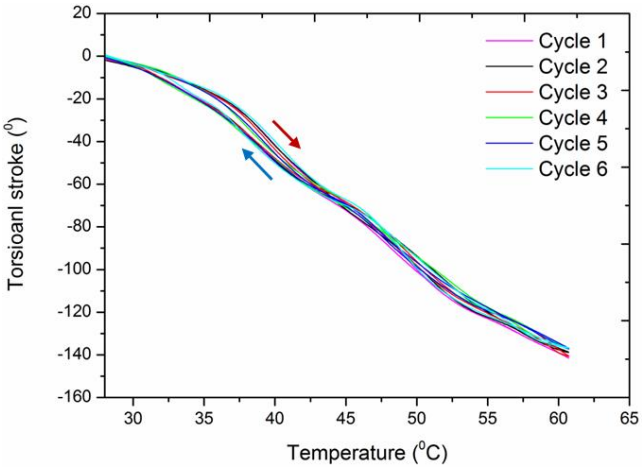

Figure 2.14. Variable torque actuation profile of nylon 6 with multi-cycle test validation.

The effect of spring stiffness on torsional stroke was also investigated by using different lengths of return spring fibres. Starting from 70 mm, the spring length was decreased by ~14 times in five stages (Figure 2.15). The corresponding torsional stroke of the same actuating fibre was decreased by ~61% when comparing the shortest return spring with the longest return spring fibre and using a constant 26-62ºC temperature range. A final heat/cool cycle was performed using the initial spring length and the actuation behaviour was almost identical to the first heat/cool cycle.

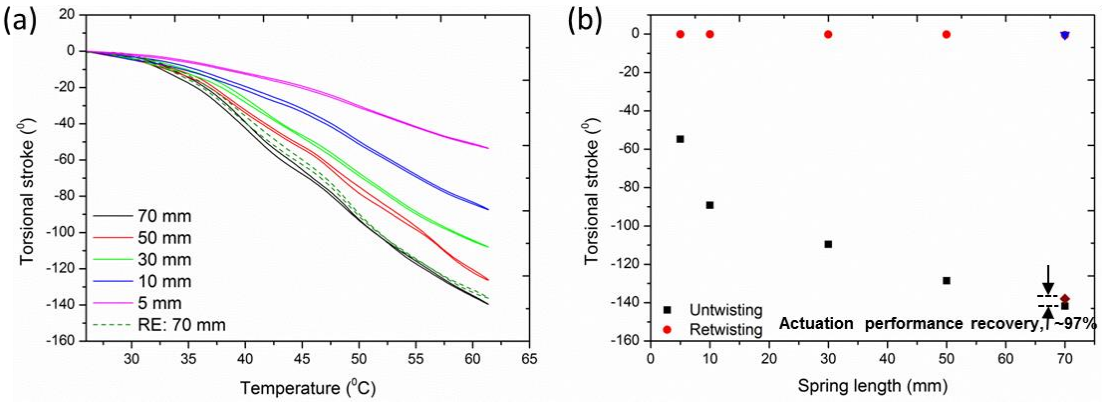

Figure 2.15. (a) Actuation profile of twisted Nylon 6 fibre during heating and cooling and operated with different return spring lengths. A small constant torque of 68 mN m was also applied by the lever arm measurement system. Tests were performed with progressively shorter return spring lengths and a final repeat test using the original return spring length (denoted RE for repeat). (b) Final torsional stroke at 60°C (untwisting) and when cooled to 26 C (retwisting) at different return spring lengths.

2.4. Discussion

The main aim of the present work was to establish a method for analysing torsional actuation obtained from different test methods. The analysis starts with the 'free' torsional stroke per fibre length of θ (deg/mm) obtained experimentally from actuating fibres tethered at only one end [110]. The effect of a return spring and/or an externally applied torque on the torsional stroke is theoretically shown in Equation (2.7). Finally, the expected torque generated is given by the product of torsional stroke and final torsional stiffness with the maximum torque predicted from Equation 2.2 (blocked torque). These analyses suggest that all torsional actuation parameters can be determined from knowledge of the free stroke (θ), actuating fibre stiffnesses (S_A and S'_A for initial and final temperatures, respectively), return spring stiffness (S_N) and actuating fibre length (L_A). A comparison of the experimentally obtained torsional stroke

parameters with the theoretical estimates are provided in Figure 2.16. The parameters used for calculating the theoretical values are given in Table 2.1.

Table 2.1. Measured parameters used in theoretical calculations of actuation stroke and torque for twisted nylon 6 fibre.

Temperature range	26 - 62ºC
Actuating fibre length (L_A)	70 mm
Free stroke per length (θ)	-2.45 º/mm
Initial torsional modulus of actuating fibre (k_A)	3.56×10^{-6} N·m^2
Final torsional modulus of actuating fibre (k'_A)	3.19×10^{-6} N·m^2
Torsional modulus of return spring fibre (k_N)	4.7×10^{-7} N·m^2

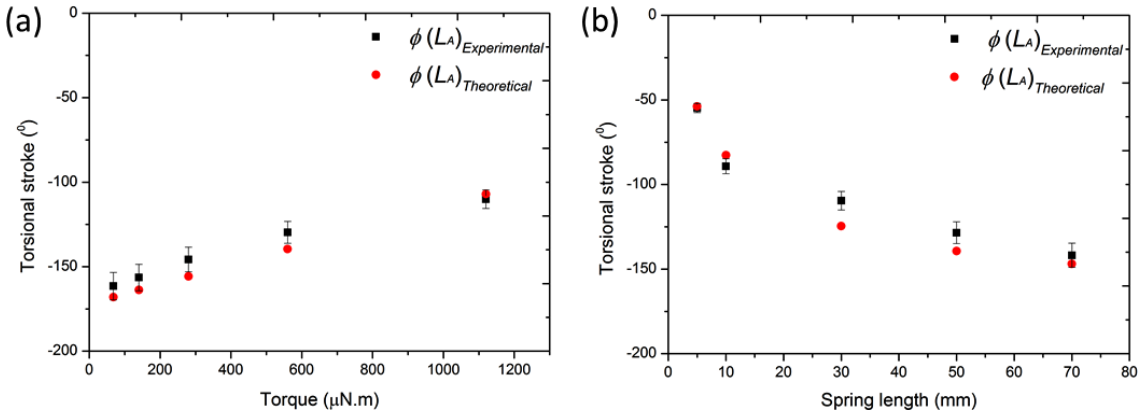

Figure 2.16. Comparison of experimentally measured and theoretically calculated torsional strokes [Equation (2.7)] for 70 mm long twisted nylon 6 fibre: (a) isotonic torsional stroke when operated against a constant external torque; (b) torsional stroke when using return springs of different lengths.

As seen for both the isotonic actuation tests [Figure 2.16(a)] and actuation tests against a return spring [Figure 2.16(b)], the agreement between measured and calculated values is very good. The close agreement indicates that the theoretical treatment based on

torsion mechanics is a suitable method for evaluating torsional actuation in twisted fibres. In some cases, however, discrepancies were found between the measured and calculated values. The expected blocked torque determined from the parameters given in Table 2.1 of 136 μN·m was significantly less than the measured value of 225 μN·m. Similarly, the free stroke and torsional stiffness determined from the torque-stroke curve measured following the blocked torque measurement were higher than obtained directly from free stroke tests. The reasons for these discrepancies are not yet known, however, changes in the internal structure of the twisted fibre during the training cycles may be involved. Further studies are underway to investigate the effect of training on the structure and properties of the twisted fibres.

2.5 Summary

This paper has investigated test methods for characterising torsional actuators using a twisted oriented semicrystalline polymer fibre as the test subject and temperature change to induce actuation. An experimental method was designed and developed which was able to continuously measure thermally-induced torsional actuation of fibrous materials. Various different testing modes were studied that replicate possible application conditions: free stroke in a one-end-tethered fibre, torsional actuation against an externally applied torque (isotonic), blocked rotation to determine torque generated, and torsional actuation against a return spring fibre when operated in the two-end-tethered state. Theoretical prediction of torsional stroke generation of twisted fibre was developed using torsion mechanics that gave good agreement between experimental measurement and calculated values for the isotonic and return-spring experiments. The analysis allows the prediction of torsional stroke based on the fundamental characteristics of the actuator: free stroke and stiffness. Some discrepancy was noted in the estimation of the blocked torque. Further studies are underway to

investigate whether ‘training’ cycles result in structural changes within the twisted fibres that may affect the torsional behaviour.

CHAPTER 3 Controlled and Scalable Torsional Actuation of Twisted Nylon 6 Fibre

This chapter has been adapted from the article "S. Aziz, S. Naficy, J. Foroughi, H. R. Brown and G.M. Spinks, *Journal of Polymer Science Part B: Polymer Physics* 54:1278-1286 (2016)".

The introduction and experimental sections in this chapter are shortened versions compared with the published article to avoid duplication with the previous chapters.

3.1 Introduction

Scalability of torsional actuation is an important practical issue that remains mostly unexplored. Important insights are provided by the study of Haines *et al.* [155] in which coils made by twisting nylon 6,6 monofilaments with diameters ranging from 0.15 mm to 2.45 mm and heated and cooled to induce tensile actuation showed tensile strokes and gravimetric work capacities that were essentially scale independent. The authors suggested that the scale invariance of the tensile stroke was due to the similar twisted structures produced in all fibres and was interpreted through the known direct link between fibre torsional stroke (ΔT in turns per fibre length) and fractional coil stroke (ΔL / L), which is the change in coiled fibre length (ΔL) normalized to its length at room temperature (L). A modified version from Equation 1.2 can now expressed as:

$$\frac{\Delta L}{L} = \frac{l^2.\Delta T}{N.L} \tag{3.1}$$

with l representing the twisted fibre length and N the number of turns in the coil. Observations of the coils made from the different diameter fibres showed all to have the same fibre twist bias angle (α_f) and identical coil bias angles (α_c) so that the reorganised Equation (3.1) is the product of three scale invariant terms:

$$\frac{\Delta L}{L} = \left(\frac{l}{L}\right)\left(\frac{l}{d.N}\right)(d.\Delta T) \tag{3.2}$$

The first term is simply the inverse of $cos\ \alpha_c$ (= L/l) and the second term is proportional to $sin\ \alpha_c$ (=$\pi ND/l$), since the coil diameter (D) is approximately double the fibre diameter (d). The final term is also scale invariant if it assumed that the degree of fibre untwist during actuation is proportional to the twist inserted per untwisted fibre length (T) during coil fabrication, since $\tan\alpha_f = \pi dT$. The untested assumption in this

analysis is that the fibre untwist during actuation depends only on the amount of inserted twist and is otherwise independent of fibre diameter.

Treating the twisted fibre as a simple single helix of equivalent diameter and bias angle provides some basis for the torsional stroke being dependent on the inserted twist. Partial untwist of the fibre or yarn is known to result from a volume expansion (Figure 3.1), as has been experimentally demonstrated thermally, electrochemically, photonically, and chemically [110, 117, 155].

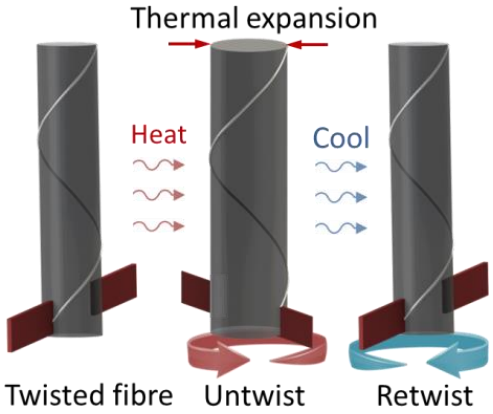

Figure 3.1. Schematic illustration of the thermally induced torsional actuation in a twisted fibre. Radial expansion results in untwist and rotation of the paddle attached to the fibre free end. The helically oriented polymer chains are assumed to be inextensible and are illustrated by a single helix at the fibre surface.

The volume (v) of the cylinder enclosed by a single helically wound string depends on the string length (l_s); the length (l) and diameter (d) of the cylinder; and the number of turns the string makes in forming the helix (n). A change in volume of the cylinder can be accommodated by changes in any of the above parameters so that the ratio of final to initial volume is described by the following expression, in which zero subscripts represent the initial values:

$$\frac{v}{v_o} = \left(\frac{n_o}{n}\right)^2 \left(\frac{l}{l_o}\right)^2 \left(\frac{{l_s}^2 - l^2}{{l_{s,o}}^2 - {l_o}^2}\right)^2 \tag{3.3}$$

Rearranging Equation (3.3) gives an expression representing the torsional actuation in terms of the ratio of final turns to initial turns:

$$\frac{n}{n_o} = \left(\frac{v_o}{v}\right)^{1/2} \left(\frac{l}{l_o} \cdot \frac{{l_s}^2 - l^2}{{l_{s,o}}^2 - {l_o}^2}\right) \tag{3.4}$$

Observations made by Haines *et al.*[155] of their twisted nylon 6,6 fibres indicated that the volumetric thermal expansion was mainly in the diameter direction with small axial contraction occurring upon heating. This asymmetry in thermal expansion has been long established in oriented, semi-crystalline polymer fibres [171]. Assuming that the cylinder length change is negligible and that the string length is constant, Equation (3.4) simplifies to:

$$\frac{n}{n_o} \approx \left(\frac{v_o}{v}\right)^{1/2} = \frac{d_o}{d} \tag{3.5}$$

Represented as the change in twist per cylinder length gives:

$$\Delta T = \frac{n}{l} - \frac{n_o}{l_o} \approx \frac{n_o}{l_o}\left(\frac{d_o}{d} - 1\right) \tag{3.6}$$

The above expression suggests that the torsional stroke (ΔT) indeed depends on the inserted twist ($T_o = n_o/l_o$) and the diameter change from volume expansion, such as occurs during heating. If fibre twist has negligible effect on the asymmetric volume expansion of the fibre, then the above analysis suggests that the torsional stroke depends only on inserted twist and is independent of fibre diameter.

We here report further investigations of the scale dependency of torsional stroke and generated torque in twisted nylon 6 monofilaments. Twisted fibres were prepared from

fibres with a two-fold difference in diameter and with different inserted twist. The key assumption that torsional stroke depends only on inserted twist is experimentally tested. Further, the single helix approximation of the twisted fibre structure is evaluated in terms of the quantitative prediction of the torsional stroke during fibre heating.

3.2 Experimental

3.2.1 Twist Insertion in Nylon 6 Fibre

Twist insertion into commercially available nylon 6 fibre (Sport Fisher monofilament fishing line) was conducted by an electrical DC motor (Figure 2.2) as described in Chapter two. Neat samples of different diameters, d (400, 500, 780, and 1000 μm) were chosen to be twisted under constant axial stress of 10 MPa (based on the cross-sectional area of the untwisted fibre). Initially, all the twisted samples were fabricated having similar twist directed bias angle (α_f, ~30°) by calculating the amount of needed twist (T) using Equation 2.9.

Next interest was the insertion of the same amount of twist (170 T.m^{-1}) in the different diameter fibres to give a range of different bias angles. Finally, different amounts of twist were inserted into a fibre of fixed diameter (780 μm). Overall fabrication variables are graphically illustrated in Figure 3.2.

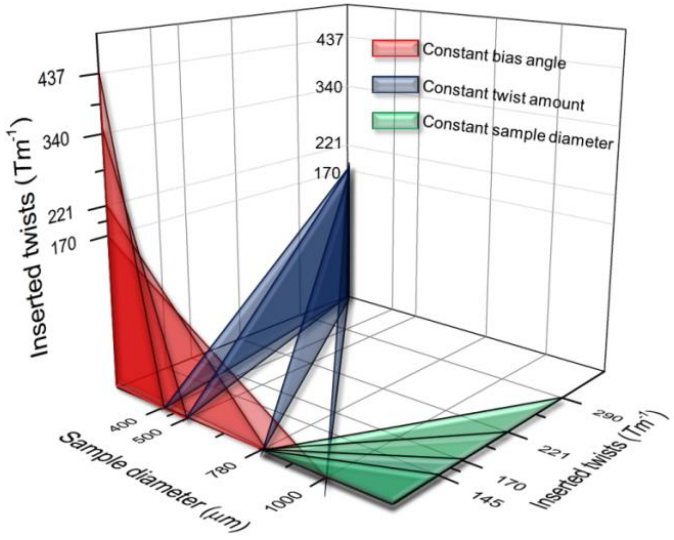

Figure 3.2. Accounted fabrication variables during twist insertion into nylon 6 fibre.

3.2.2 Thermo-Physical Change in Fibre Dimensions

Thermally induced dimensional changes of twisted nylon 6 fibre were investigated by heating the sample in a silicone oil filled capillary tube. Silicone oil has high thermal stability and is particularly suitable as a high temperature heat-transfer liquid [183]. Fibre samples twisted in all experimental conditions were used, hence provided the detailed understanding of thermal expansion or contraction. Figure 3.3 shows the illustration of tests used to measure changes in length, diameter and volume of twisted fibre before and after heating. An optical microscope (ISSCO-OPTEK) was used to accurately measure the change in liquid level and fibre length.

Starting with the same initial volume of oil, the volume changes for the oil-only (ΔV_1) and fibre-in-oil cases (ΔV) can be written as:

$$\Delta V_1 = \pi . R^2 . (L_1{}' - L_1) \tag{3.7}$$

$$\Delta V = \pi . R^2 (L' - L) \tag{3.8}$$

The negligible change in capillary diameter over the temperature range used is ignored. Subtracting Equation (3.7) from (3.8), gives the volume change of the twisted fibre (Δv):

$$\Delta v = \pi . R^2[(L' - L) - (L_1{}' - L_1)] \tag{3.9}$$

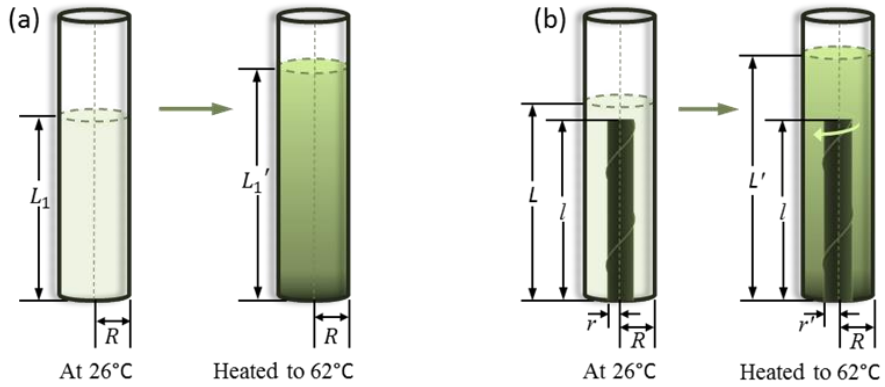

Figure 3.3. Experimental illustration of dimension change in twisted fibre operated in a silicone oil filled glass capillary (radius $\boldsymbol{R}$); (a) calibration of oil thermal expansion having liquid height $\boldsymbol{L_1}$ at 26°C, and $\boldsymbol{L_1}'$at 62°C, (b) Combined thermal expansion of oil with immersed fibre from initial liquid level $\boldsymbol{L}$ raised to $\boldsymbol{L}'$ at 62°C. Fibre length (l) remained almost constant while radius changed from $\boldsymbol{r}$ to $\boldsymbol{r}'$when heated.

Experimentally, it was observed that the fibre length change was negligible over the temperature range from 26°C to 62°C for all fibres, regardless of diameter and amount of inserted twist. The fibre volume change can be expressed solely as a change in radius (r):

$$\Delta v = \pi . l\left[r'^2 - r^2\right] \tag{3.10}$$

Combining Equations (3.9) and (3.10) gives a general expression of change in radius of twisted fibre which was used to calculate the thermal expansion/contraction coefficients for further theoretical analysis:

$$r' = \sqrt{\frac{R^2[(L'-L)-(L_1'-L_1)]}{l} + r^2} \quad (3.11)$$

3.2.3 Thermally-Induced Torsional Actuation Test

Torsional actuation tests were conducted in an in-house-built testing apparatus (Figure 2.3 and Figure 2.4) described in Chapter two. All the isotonic tests (constant torque) reported herein were conducted under a constant small external torque (68 μN·m) applied by the lever arm and opposing the fibre untwisting. The same apparatus was also used to evaluate the torque generated during heating/cooling of the twisted nylon fibre. In this case, the lever arm was operated in the isometric (constant length) mode to prevent fibre rotation and provided a measure of the blocked torque. Unless otherwise stated, a constant twisted sample length (70 mm) and a constant temperature range (26-62°C) at average heating and cooling rates of 3.6°C/min and 1.8°C/min, respectively, were programmed and used for all the actuation tests.

3.2.4 Torsional Stiffness Measurements

Fibre torsional stiffness was measured using the same apparatus. Controlled rotation of the shaft attached to the free end of the fibre using the lever arm generated the torque – rotation relation. Previous studies of the same nylon 6 fibres have established that their torsional behavior is linear elastic over the range of rotations used here [184]. The torsional stiffness (*S*) were obtained from the slopes of these lines, as described previously [184].

3.3 Results

3.3.1 Characterisation of Twisted Fibres

Several fabrication parameters were considered while preparing twisted nylon 6 fibres for actuation testing. Firstly, fibres from four different diameters (400, 500, 780, and

1000 µm) were twisted to 428, 340, 221, and 170 $T.m^{-1}$, respectively, producing the same surface bias angle of ~30° (Figure 3). In a second set of samples, the four different diameter fibres were twisted to a constant twist (170 $T.m^{-1}$). Finally, a third set of samples was prepared by twisting fibres of constant diameter (780 µm) to 145, 170, 221, and 290 $T.m^{-1}$. The prepared fibres were examined using optical microscopy after fabrication to measure the surface bias angle and final fibre diameter. When twisted to a constant bias angle of 30°, the diameter of each fibre was increased by approximately 8% compared to their initial diameters (Figure 3.4). Fibre bias angle measurements show good agreement to the diameter/twist/bias angle relationship of Equation (2.9).

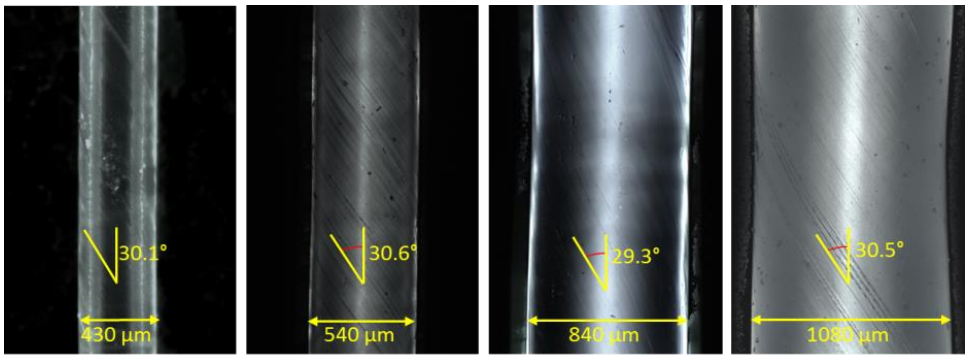

Figure 3.4. Photographs of different diameter fibres twisted to a constant bias angle by inserting twist of 428, 340, 221, and 170 $T.m^{-1}$ for fibres of starting diameters of 400, 500, 780, and 1000 µm and with a constant axial stress of 10 MPa applied during twist insertion. The obtained surface fibre twist bias angle and fibre diameter are as indicated.

3.3.2 Asymmetric Thermal Volume Expansion of Twisted Fibres

The twisted fibres were heated slowly in an oil-filled capillary to experimentally measure the length and volume change as described in Figure 3.3. In all cases, the fibre length change was negligible when heated from 26°C to 62°C and this observation is consistent with previously published results for the axial thermal expansion of oriented nylon 6 fibres over this temperature range [171]. In contrast, the thermal strain in the

radial direction was considerably larger and almost identical for all of the twisted fibres prepared with different fabrication parameters (Figure 3.5).

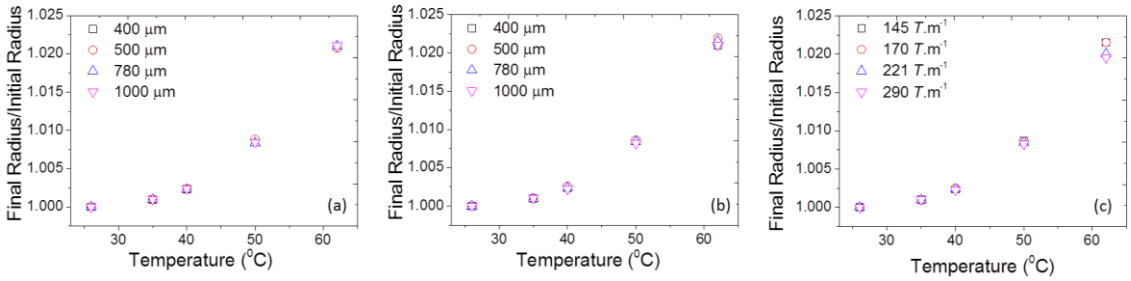

Figure 3.5. Thermally induced radial expansion of twisted nylon 6 fibres normalised to the diameter at 26°C: (a) different diameter fibres twisted to the same bias angle (30°); (b) different diameter fibres with the same amount of inserted twist (170 $T.m^{-1}$); and (c) different inserted twist in constant diameter fibres (780 µm).

3.3.3 Effect of Fibre Diameter and Inserted Twist on Torsional Actuation

3.3.3.1 Constant Bias Angle Fibres

The torsional stroke and torque generated from custom fabricated twisted fibres were found to be strongly influenced by the starting fibre diameter and amount of inserted twist. Figure 3.6(a) shows the thermally induced torsional stroke of different diameter nylon 6 fibres prepared with the same bias angle (~30°) achieved by inserting different amounts of twist.

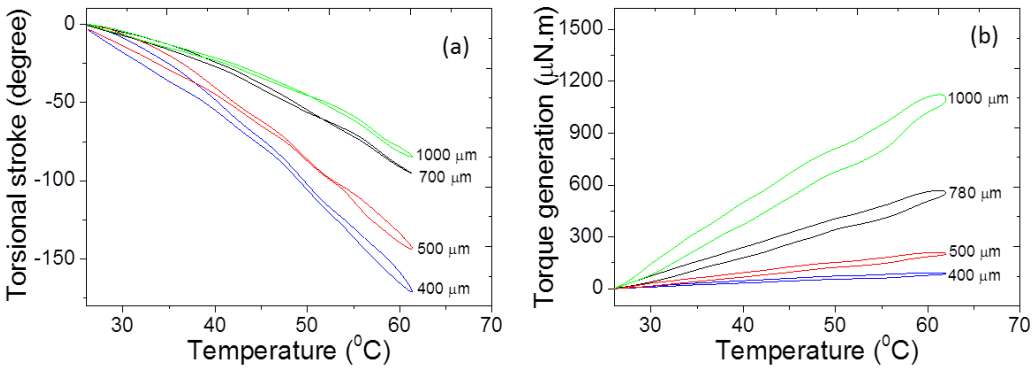

Figure 3.6. Torsional actuation test results of twisted nylon 6 fibres of different diameters and having the same bias angle (30^{o}): (a) isotonic torsional stroke; and (b) isometric torque generation.

The fibre rotation during both heating and cooling is shown to be fully reversible with a small hysteresis, which is at least partially related to the thermal lag between the recorded temperature of the furnace and the true fibre temperature. Slow heating and cooling rates minimized the magnitude of the observed hysteresis. It can be seen that the smallest considered diameter fibre has produced the largest stroke and the stroke at any given temperature decreased monotonically with increasing fibre diameter.

Figure 3.6(b) shows the isometric torque generation by these same different diameter fibres with constant bias angle. A steady increase of generated torque at any given temperature was noticed as fibre diameter increased. The torque generated during heating was fully relaxed during cooling with some hysteresis. In addition to the thermal lag, the hysteresis in torque was also increased by some stress relaxation that occurred during the short isothermal holding period between heating and cooling.

3.3.3.2 Constant Twist Insertion

Figure 3.7(a) shows the thermally induced torsional stroke of different diameter nylon 6 fibres prepared with the same amount of twist inserted per length of as-received fibre (~170 $T.m^{-1}$). All fibres generated remarkably similar torsional stroke-temperature curves during both heating and cooling. The results show that torsional stroke was clearly independent of the 2.5 fold difference in fibre diameter when fibres were prepared with the same inserted twist.

In contrast, the generated blocked torque of these same fibres increased significantly when larger diameter fibres were used [Figure 3.7(b)]. As described in more detail below, the generated torque is determined by the product of the torsional stroke and the fibre stiffness and the latter is strongly dependent on fibre diameter.

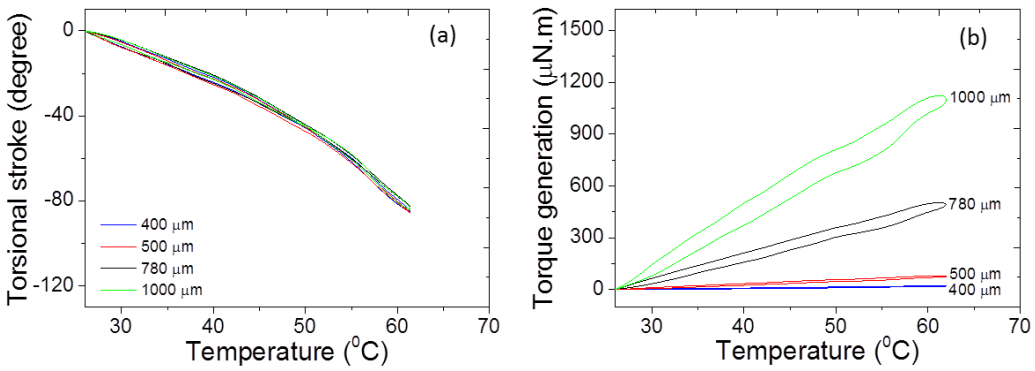

Figure 3.7. Torsional actuation test results of twisted nylon 6 fibre with different diameters and having the same twist inserted per initial fibre length (~170 $T.m^{-1}$): (a) isotonic torsional stroke; and (b) isometric torque generation.

3.3.3.3 Constant Fibre Diameter

The final experiment investigated the effect of inserted twist in fibres of constant diameter (780 µm). Figure 3.8(a) shows the torsional stroke increased monotonically

with the amount of twist inserted. Similarly, Figure 3.8(b) shows blocked torque and the torque generation during heating was also seen to be dependent on the amount of twist inserted and increased with increasing amount of twist.

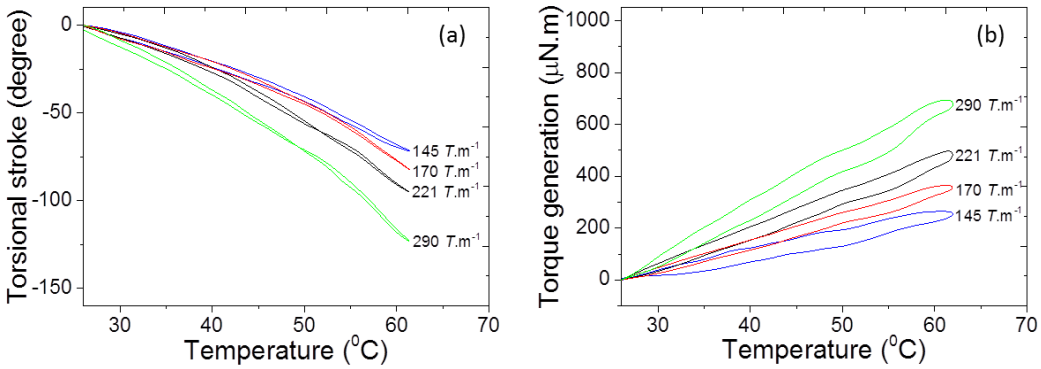

Figure 3.8. Torsional actuation test results of twisted nylon 6 fibre with a constant diameter and having variable twist inserted per initial fibre length: (a) isotonic torsional stroke; and (b) isometric torque generation.

3.4 Discussion

3.4.1 Theoretical Estimation of Torsional Rotation

Previous investigations of torsional actuation in twisted fibres and yarns have suggested that a single helix approximation can provide some insight into the actuation mechanism [110, 155]. Figure 3.9 illustrates two states of a helical string encompassing a cylinder of different volumes. The geometric analysis is facilitated by "opening up" the cylinder so that the string can be visualized as forming the hypotenuse of a right triangle. Derivation of Equation (3.3) then follows. The expression has previously been applied to explain the possibility of fibre untwist during a volume expansion, [110, 155] but has not been used to quantitatively predict the amount of untwist.

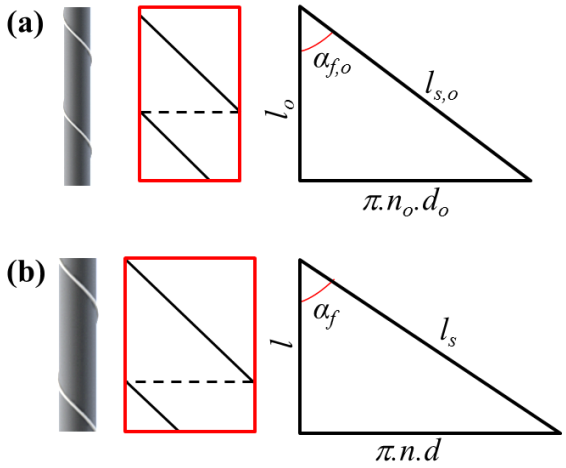

Figure 3.9. Illustration of a single helix fibre geometry, (a) before actuation, and (b) after actuation. l denotes fibre length, l_s is length of the helically wrapped string, d is fibre diameter, and $\boldsymbol{n}$ is the amount of twist, $\boldsymbol{\alpha_f}$ denotes the helix bias angle. Zero subscripts represent the initial state.

Combined torsional actuation measurements and volume expansion data allows the application of the single helix model to quantitatively predict the amount of torsional stroke. The starting assumption is that the "string length" in the single helix remains constant during the volume change. For the twisted nylon fibres the "string" can be thought of as the oriented polymer chains on the surface of the fibre. These molecules are likely highly extended and firmly connected through crystalline blocks. This topology exhibits a high axial stiffness and can be considered mechanically inextensible. However, previous work has shown a negative thermal expansion of oriented nylon fibres in the fibre direction[171]. In the present study, the temperature range for actuation tests has been chosen to minimise the axial length change and experiments confirm negligible changes in length of twisted fibre. This observation and the assumption that the string length is constant greatly simplifies Equation (3.4) to Equation (3.5) where the torsional actuation, in theory, depends only on the change in fibre diameter and the amount of twist inserted.

The torsional strokes have been calculated using Equation (3.6) and from the measured diameter change. The results are shown in Figure 3.10 for each of the 3 series of prepared fibres.

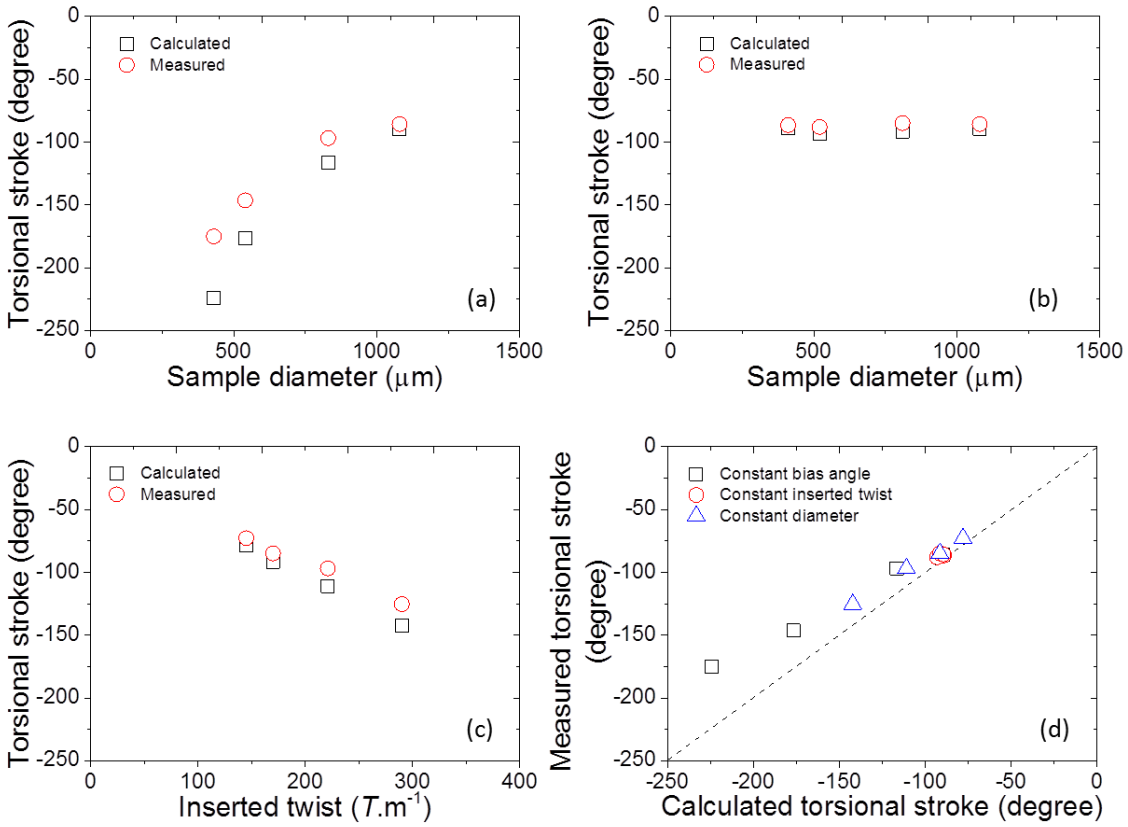

Figure 3.10. Comparison of experimentally measured and theoretically calculated torsional strokes for 70 mm long twisted nylon 6 fibre prepared with (a) similar bias angle (30^{o} to the fibre axis); (b) similar amount of twist (170 T.m^{-1}); (c) similar fibre diameter (780 μm). All calculated and measured torsional strokes are compared in part (d).

The measured torsional strokes are included for comparison and in all cases there is a very good agreement between the measured and calculated values. The single helix theory correctly predicts the dependence of torsional stroke on the diameter change and the amount of inserted twist. The theory also predicts the quantitative torsional strokes with high accuracy, giving support to the underlying assumption that the string length

remains unchanged during heating. It is noted that the theory is slightly less accurate in quantitatively predicting torsional stroke for the most highly twisted fibres, for reasons that are not yet known. The overall degree of agreement between calculated and measured torsional strokes is especially good considering that the twisted fibres are not single helices encompassing a hollow cylindrical core as assumed in the model. A closer approximation to the actual fibre structure is described by a series of nested helices of different diameter and the same number of turns per length (and, hence, different bias angles). If all these helices displayed the same diameter expansion ratio and no change in length, then they would all produce equivalent torsional stroke.

The real fibre structure, however, likely involves entangled helices of oriented polymer chains joined by the crystalline blocks. The structure of the fibre, including crystal block size, defects and chain orientation, may be altered by the twist insertion and with possible variations in structure occurring along the radial direction. These molecular differences may affect the degree of "co-operation" between inner and outer layers in generating the torsional actuation. The data of the present study suggest that at smaller amounts of twist insertion the "co-operation" is good and all layers generate the predicted torsional stroke. However, at higher twist insertion some process slightly impedes the untwisting mechanism and further studies are needed to identify the cause(s).

3.4.2 Theoretical Estimation of Torque Generated

A quantitative analysis of torque generation from differently twisted fibres was also conducted. It has been shown previously that the maximum torque generated when the twisted fibres are heated occurs when the fibres ends are securely clamped [184]. This

"blocked torque" ($\tau_{blocked}$) can be calculated using standard torsion mechanics and as verified previously [184]:

$$\tau_{blocked} = \Delta n.\frac{JG}{l} \tag{3.12}$$

Here, Δn represents the free rotation (in radians) of a fibre of length l that is clamped at one end and whose other end is free to rotate. G is the fibre shear modulus in the final state and J is the polar moment of inertia of fibre and formulated in terms of sample diameter (d) for a fibre of circular cross-section:

$$J = \frac{\pi d^4}{32} \tag{3.13}$$

Therefore, the general quantitative expression when combined with equation (3.5) can be written as:

$$\tau_{blocked} = \Delta n.\frac{\pi.d^4.G}{32.l} = \frac{\pi.d^4.G.n_o}{32.l}\left(\frac{d_o}{d} - 1\right) \tag{3.14}$$

Fibre shear moduli were determined from torsion tests at both the starting and finishing temperatures used in the actuation tests. The torsional stiffness ($S = \frac{JG}{l}$) of a 500 µm diameter nylon 6 fibre was experimentally evaluated and the stiffness of the other diameter fibres were calculated theoretically from equation (3.15) and verified previously [184]:

$$\frac{S_1.l}{S_2.l} = \left(\frac{d_1}{d_2}\right)^4 \tag{3.15}$$

Here, S_1 and S_2 are torsional stiffness of two different diameter fibres d_1 and d_2 of length l. Table 3.1 shows the torsional stiffness of different diameter fibres at two experimental conditions of 26°C and 62°C. The shear moduli are also included in Table

3.1 and it is seen that all fibres have nearly equivalent moduli of ~0.43 GPa and ~0.39 GPa at 26°C and 62°C, respectively.

Table 3.1. Torsional properties of twisted nylon 6 fibres having different diameter.

Fibre diameter (μm)	Torsional stiffness (N·m)		Shear modulus (GPa)	
	26°C	62°C	26°C	62°C
400	1.46×10^{-4}	1.31×10^{-4}	0.43	0.39
500	3.56×10^{-4}	3.19×10^{-4}	0.42	0.38
780	2.11×10^{-3}	1.89×10^{-3}	0.44	0.41
1000	5.70×10^{-3}	5.10×10^{-3}	0.43	0.38

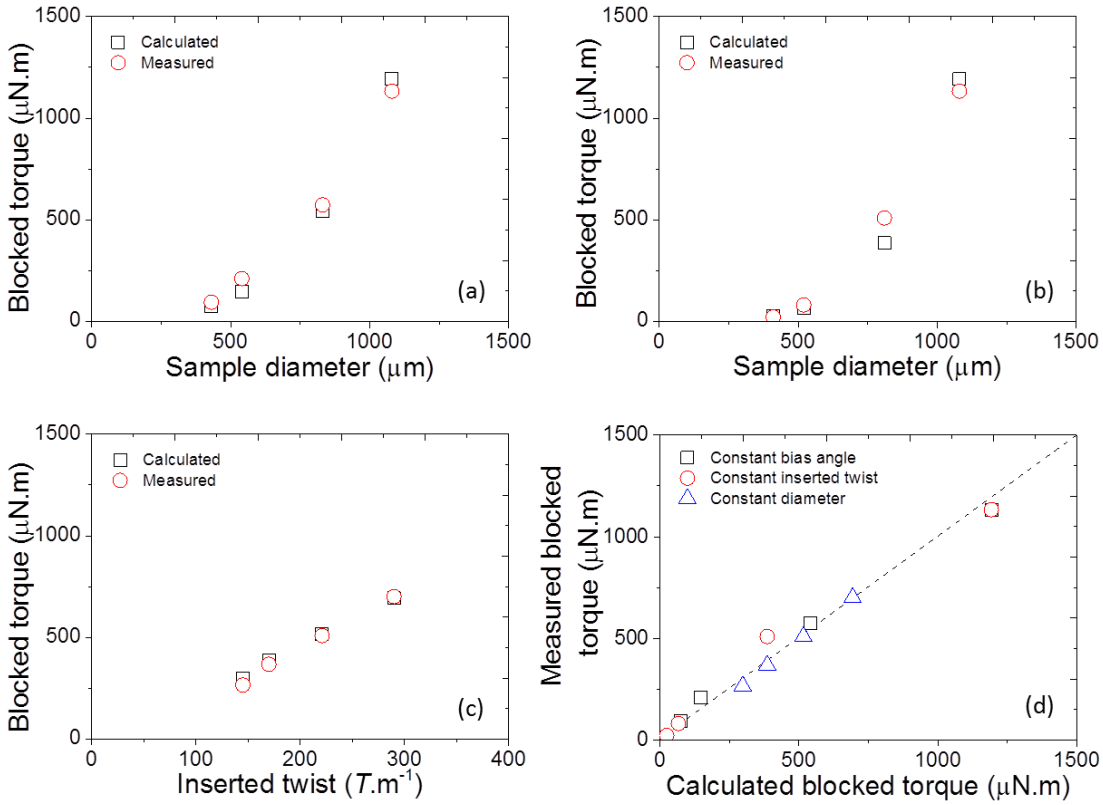

Figure 3.11. Comparison of experimentally measured and theoretically calculated blocked torque generated from 70 mm long twisted nylon 6 fibre of different fabrication

parameters: (a) similar bias angle (30^o to the fibre axis); (b) similar amount of twist (170 $T.m^{-1}$); (c) similar fibre diameter (780 μm). All calculated and measured torsional strokes are compared in part (d).

Figure 3.11 shows the calculated blocked torques obtained from equation (3.14) and includes the measured torques for comparison. In all cases, there is an excellent agreement between the measured and calculated values, further supporting the analytical approach based on a single helix. Unlike the results of torsional stroke, the torque generation from the twisted fibres is strongly dependent on fibre diameter as indicated by the fourth power dependency of torque on fibre diameter in equation (3.14). Thus, for fibres having a constant amount of inserted twist [Figure 3.11(b)], the torque generated increases by a factor of 40 times for a 2.5 times increase in diameter. The generated torque also depends linearly on the amount of inserted twist, as shown in Figure 3.11(c) for fibres of constant diameter.

3.5 Summary

The aim of this study was to further investigate the scalability of torsional actuation in twisted monofilament fibres and to evaluate the single helix model for quantitatively predicting torsional stroke and torque. Nylon 6 monofilaments were prepared with different fibre diameters, amount of inserted twist and twist bias angle. Heating and cooling the samples over a ~30^oC range provided a measure of both torsional stroke and generated torque. The torsional stroke was dependent only on the amount of twist inserted into the fibre and was independent of fibre diameter and fibre bias angle. The single helix model accurately predicted the torsional stroke based on the measured fibre diameter change during heating. Generated torques were also accurately predicted by the single helix model when combined with the measured fibre torsional stiffness.

Torque was strongly dependent on fibre diameter, along with the amount of inserted twist. A summary of the dependencies of stroke and torque on diameter for each of the three types of fibres prepared is given in Table 3.2.

Table 3.2. Prediction of torque generation from induced twisted fibre.

Parameters			Theoretical prediction of blocked torque ($\boldsymbol{\tau_{blocked}}$)
Bias angle	Number of twist	Fibre diameter	
Constant	Variable	Variable	$\tau_{blocked} \sim D^3$
Variable	*Constant*	Variable	$\tau_{blocked} \sim D^4$
Variable	Variable	*Constant*	$\tau_{blocked} \sim \tan\alpha$ or, $\tau_{blocked} \sim T$

The degree of agreement between the measured torsional actuation parameters and those calculated from the single helix model was impressive. There were some small discrepancies between the calculated and measured torsional strokes obtained from the most highly twisted fibres, and possible causes for these differences are the subject of future work. The success of the single helix model indicates that the solid twisted fibre behaves co-operatively, with the mechanism of fibre untwist operating consistently throughout the fibre thickness. In the example studied, it was found that the fibre length change was negligible and this observation greatly simplified the application of the single helix model. Further work will consider fibres in which significant fibre length changes occur during heating and then evaluate whether the single helix approximation remains valid.

CHAPTER 4 Comparison of Torsional Actuation in Twisted Polymer Fibres: Polyethylene, Polypropylene and Polyamide-6

This chapter has been submitted for publication as "S. Aziz, S. Naficy, J. Foroughi, H. R. Brown and G.M. Spinks, *Polymer*, Awaiting Revision (2017)".

The introduction and experimental sections in this chapter are shortened versions compared with the submitted article to avoid duplication with the previous chapters.

4.1 Introduction

Torsional actuation occurs during volume change of systems that contain a helically oriented and mechanically stiff element in their structure. Macroscopic examples include elastomeric bladders wrapped with reinforcing fibres. Pneumatic inflation of the bladder causes rotation of the unclamped end, however, reported torsional strokes are small (0.002 turns/mm) [109] since the number of turns made by the reinforcing fibre is limited. For a given wrap angle (α_f), the number of turns (N) the reinforcing fibre makes per length of bladder (L) is inversely related to the bladder diameter (D):

$$\tan \alpha_f = \frac{\pi N D}{L} \tag{4.1}$$

This same relation describes the helix angle at the surface of a twisted fibre or yarn with a diameter of D, length of L, and N number of twist. As described in Chapter 3, the torsional stroke is proportional to the amount of twist inserted into the fibre [119, 185], therefore high stroke torsional actuators are favoured by small diameter fibres as maximum N that can be inserted into a fibre before destabilization is controlled by fibre diameter.

Further insight into the torsional actuation behaviour has been provided by treating the twisted fibre or yarn as a single helix [185]. The ratios of final to initial turns (λ_n), fibre length (λ_l), fibre diameter (λ_d) and string length (λ_s) are geometrically related by:

$$\lambda_n = \left[\frac{1}{\tan^2 \alpha_f}\left(\frac{\lambda_s^2 - \lambda_l^2}{\lambda_d^2}\right) + \frac{\lambda_s^2}{\lambda_d^2}\right]^{1/2} \tag{4.2}$$

where α_f is the initial wrap angle at the fibre surface, relative to the long axis of the fibre. This simple approximation provided remarkably accurate predictions of the measured torsional stroke occurring in polyamide-6 fibres (commercial nylon 6 fibre) of different diameters and prepared with different number of twists [185]. The fibres were torsionally actuated by heating and the dimensional changes measured over the same temperature range. Experimentally, it was observed that the length change in all tested fibres was negligible (*i.e.* $\lambda_l \sim 1$). Also the assumption was made that the string length, corresponding to the helically oriented extended polymer chains and crystal blocks, was unchanged by heating (*i.e.* $\lambda_s \sim 1$). Under these circumstances, equation (4.2) simplified to:

$$\lambda_n = \frac{1}{\lambda_d} \tag{4.3}$$

The aim of the present study was to extend this analysis to explore twisted fibre systems where both length and diameter changes occurred on heating. Oriented fibres of polyethylene and polypropylene were chosen to compare with polyamide-6. Choy *et al.* [171] have shown that these three polymers show different thermal expansion anisotropies over the temperature range of interest. Comparison of torsional strokes from these different fibres is reported and the differences are explained in terms of thermo-physical properties of fibre materials. Torque generated during heating of similarly fabricated actuators is also measured and theoretically validated by using torsion mechanics.

4.2 Experimental

4.2.1 Twist Insertion and Sample Characterization

Commercially received ultra-high molecular weight oriented polyethylene braided fibre (DYNEEMA braided fishing line) and polypropylene monofilament (textile thread - Tengzhou Tuoliduo Industrial & Trade Co. Ltd.) were twisted by attaching their top end to a rotating motor and the bottom end to a suspended mass that retains the fibre tensioned at constant stress (10 MPa). The bottom end of the fibre is restricted from rotation around the vertical axis, thus every turn of the motor produces one turn of twist in the fibre. After a certain amount of twist was inserted, the fibres started to buckle and formed a coiled loop. The motor was stopped at the onset of coiling and the twisted section of fibre was utilized in further experiments. This fabrication method produces a temporary twisted configuration on the fibre surface and requires an additional annealing process to set the newly formed helical structure. Previous studies on twisted polyamide fibres have shown that annealing at temperatures approaching the melting point are most effective. Differential scanning calorimetry (DSC) was used to determine melting points and suitable heat-setting temperature of twisted fibres for both polyethylene and polypropylene samples. The twisted samples were held at the predetermined temperatures for 30 minutes with ends firmly clamped to prevent them from untwisting during heat setting. Then, the samples were cooled to ambient temperature over 2 hours while still kept tethered at both ends to prevent twist loss during cooling.

Surface morphology of fabricated samples was evaluated by using an optical microscope (Leica Z-16). The number of twists per initial fibre length was calculated

from equation (1) by using the observed twist bias angle and twisted fibre diameter [110, 184].

4.2.2 Thermally-Induced Physical Characterization

The test set-up shown in Figure 4.1 was used to observe the axial and radial thermal expansion of twisted polyethylene and polypropylene fibres. One end of the twisted sample was attached to a lever arm force / distance transducer with micrometre length resolution (Aurora Scientific 305B). A metal hook was used to attach the fibre to the lever arm which allowed horizontal movement of the fibre at the tethering point but fully restricted the torsional movement. The other end of the fibre was connected to a rigid support through an ultra-low stiffness commercial thread (30 μm diameter polyamide-6 monofilament). This thread applied negligible opposing torque to the twisted fibre and allowed free rotation of the actuated fibre during heating. A thermal imaging camera was used to measure the temperature on the fibre surface, and in-parallel, an optical microscope was placed radially to the fibre to observe the change in diameter. Length changes in the sample were recorded from the lever arm signal as a function of temperature increase when exposed to an infrared heating source (IXL 275W infrared heat lamp held at ~10 mm from sample).

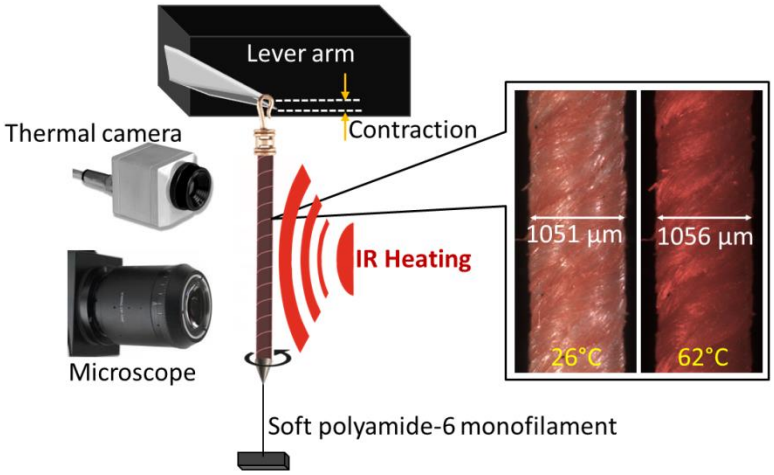

Figure 4.1. Schematic illustration of thermally induced test for measuring dimensional changes in twisted fibre (inset shows the example of radial thermal expansion of twisted polyethylene fibre heated in between 26 – 62°C).

The radial expansion measurement of polypropylene was found difficult because of small dimensional changes that occurred during heating and cooling. Therefore, our previously developed oil bath method to evaluate thermal expansion of an immersed filament was used [185]. Initially, thermal volume expansion of silicon oil in a glass tube was measured over the 26 – 62°C temperature range. Afterwards, seven units of identical twisted polypropylene fibre were immersed in the oil filled glass tube and the thermal volume expansion of the whole unit was then determined. The following equation describes how both radial and axial length changes occurring in the fibres upon heating are related with each other:

$$r' = \sqrt{\frac{R^2[(L'-L)-(L_1'-L_1)]}{l'-l} + r^2} \tag{4.4}$$

Here, silicon oil height poured in glass tube is L_1 at 26°C, combined oil with immersed fibre liquid level is L at 26°C, fibre length is l at 26°C and fibre radius is r at 26°C. The notation ($'$) denotes the same parameters at 62°C.

4.2.3 Torsional Actuation Tests and Torsional Property Evaluation

Thermally induced torsional actuation tests were performed in a torsion testing apparatus developed in-house [184]. The apparatus includes an electrically heated chamber, a DC power supply, programmable temperature controller (Electro Chemical Engineering Pty Ltd) and the lever arm force/distance transducer system (Aurora Scientific 305B). One end of the fibre end was firmly clamped and the other end attached to a shaft supported by two near frictionless air bearings. A high modulus fibre wrapped around the bearing was connected to the lever arm transducer. Isotonic torsional stroke (ϕ_{isotonic}) was determined from the lever arm displacement under an opposing and constant normal force (F_N) applied to the surface of the shaft to give a constant torque (τ_{ext}) acting on the twisted fibre. The same torsion tester was also used to measure the torque generated during heating/cooling of the twisted fibre. In this case, the lever arm was operated in the isometric mode (constant length) to prevent fibre rotation and provide a measure of the blocked torque (τ_{blocked}).

The torsional stiffness [180] of the twisted fibres was evaluated at the two temperature extremes representing the actuated (high temperature) and non-actuated (low-temperature) states. The lever arm system was used to rotate the shaft, twist the fibre, and measure the applied force. As in previous studies [185], the fibres were found to be linearly elastic in torsion and the torsional stiffness was calculated from the slope of the torque vs degree of rotation. The free rotation (ϕ_{free}) expected during the heating of the twisted fibre could be then be predicted from the measured isotonic torsional stroke using:

$$\phi_{\text{isotonic}} = \phi_{\text{free}} + \tau_{\text{ext}}\left(\frac{1}{S'_A} - \frac{1}{S_A}\right) \tag{4.5}$$

by inserting the measured torsional stiffnesses in the non-actuated (S_A) and actuated (S_A') states.

4.3 Results

4.3.1 Surface Morphology and Thermo-Physical Properties

Twisting a single ply polyethylene braided structure (606 μm diameter) produced a complex and non-uniform helical structure [Figure 4.2(a)]. The phenomenon happens due to the frustration of inter-filament spacing which leads to identical shapes of self-twisting bundles that break the symmetries of packing and of the inter-filament forces, paralleling a morphological instability throughout the fibre [186]. In contrast, when two plies of the same structure were twisted together the result was a compact fibre of uniform diameter [Figure 4.2(b)] since the identical helical instabilities twisted and wrapped over each other. The reduced diameter of 1050 μm (instead of 1212 μm) after twisting highlights the considerable compaction in the twisted fibre made of individual micro-filaments that form the braided fibres. From equation (4.1), the number of twists was calculated as ~680 turns per meter which closely compares with manually counted ~648 turns per meter during twist insertion.

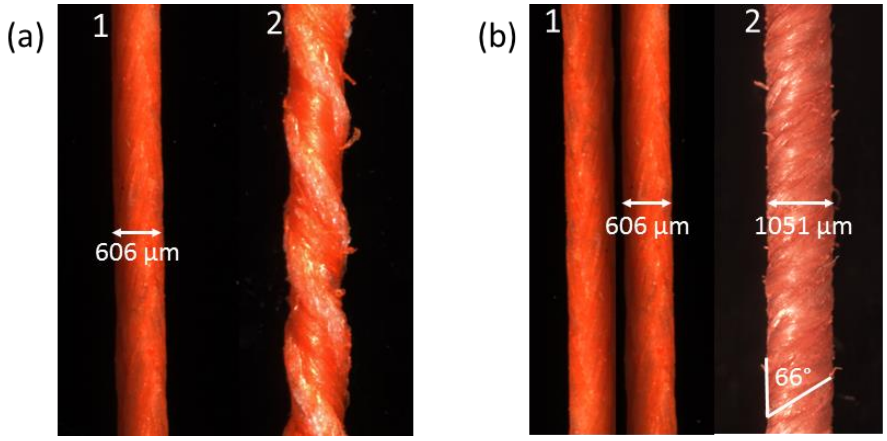

Figure 4.2. Polyethylene braided structures. (a) Single ply braid (a1) as-received and (a2) after twisting. (b) Two ply of same structure (b1) as-received and (b2) after twists were inserted.

A polypropylene fibre of ~350 µm diameter was also twisted to the point of coil formation. Figure 3 shows optical micrographs at different stages of the twisting process. Figure 4.3(a) represents the precursor fibre and Figure 4.3(b) shows the fibre after maximum twist insertion. However, significant 'necking' or plastic deformation was observed after twist insertion. The average fibre diameter was found to have increased during twisting by ~10% from ~350 µm to ~384 µm. The bias angle of the inserted twist was measured microscopically and found to be ~32°. The amount of twist inserted was calculated using equation (4.1) and found to be ~514 turns per meter of initial fibre length. Twist count during twisting was ~492 turns per meter of precursor fibre length which closely approximates the calculated value.

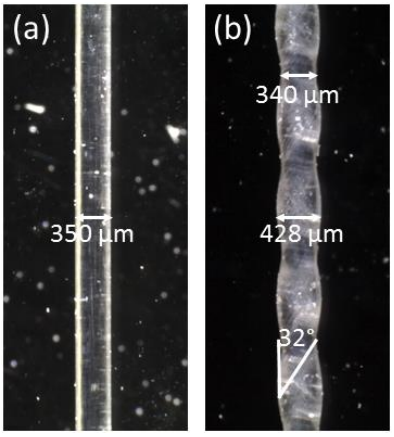

Figure 4.3. Micrographs of polypropylene monofilament structures; (a) as-received, and (b) highly twisted.

DSC tests were conducted to evaluate the melting point of twisted samples and then the heat-setting temperature was determined. Figure 4.4(a) shows the DSC result for twisted polyethylene where a first melting peak was observed at ~145°C and a second melting peak at ~154°C which lies in the range of reported melting temperature of commercial product of their types. Double melting peaks in a DSC experiment have been previously ascribed to melting of less stable crystalline structures followed by recrystallization and remelting of more stable crystals [187, 188]. An acceptable heat-setting temperature of 120°C was chosen for the twisted polyethylene braids so that any melting of the crystal structures was avoided. Figure 4.4(b) shows the DSC results for twisted polypropylene monofilaments where the melting temperature was observed at ~167°C. From DSC results, 120°C was selected as the heat-setting temperature of the polypropylene and polyethylene fibres. This temperature was sufficiently below the melting temperatures of both polymeric fibres, ensuring the crystalline structure of the fibres to remain intact.

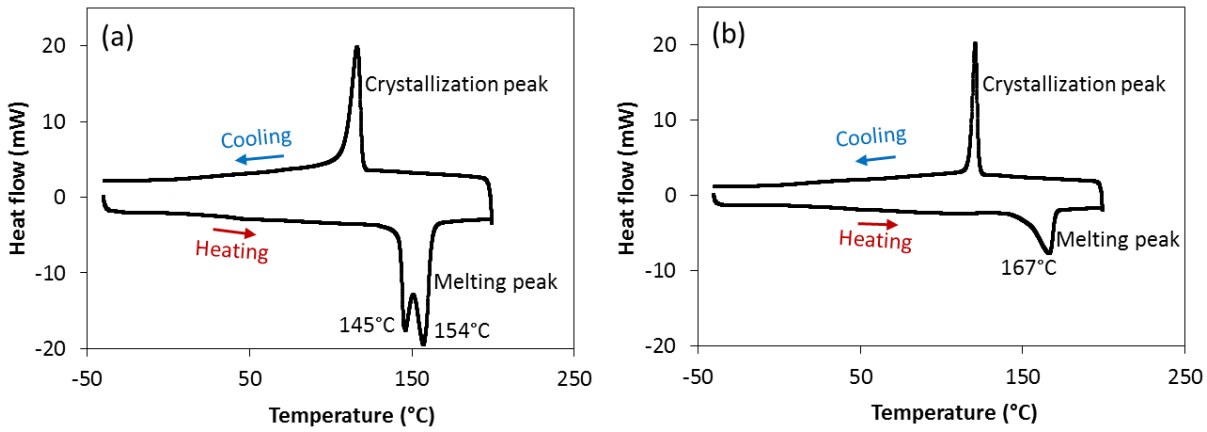

Figure 4.4. DSC results of twisted fibres; (a) polyethylene, and (b) polypropylene.

Torsional stiffness of both polyethylene and polypropylene fibres was measured from torque-stroke curves at 26°C (non-actuated state) and 62°C (actuated state). Figure 4.5 shows the relationship of applied torque and torsional stroke where the inverse slope of the lines denotes torsional stiffness. Torsional stiffness of a 70 mm long twisted polyethylene fibre (~ 606 µm diameter) was found to be ~667 and ~400 µN·m at 25 and 62°C, respectively. Significant drop of torsional stiffness in this temperature region is probably due to the rapid decrease in density of ultra-high molecular weight polyethylene fibres on heating [189]. The twisted polypropylene fibre (350 µm in diameter and 70 mm in length) had a considerably smaller torsional stiffness of ~54 and ~52 µN·m at 25 and 62°C, respectively.

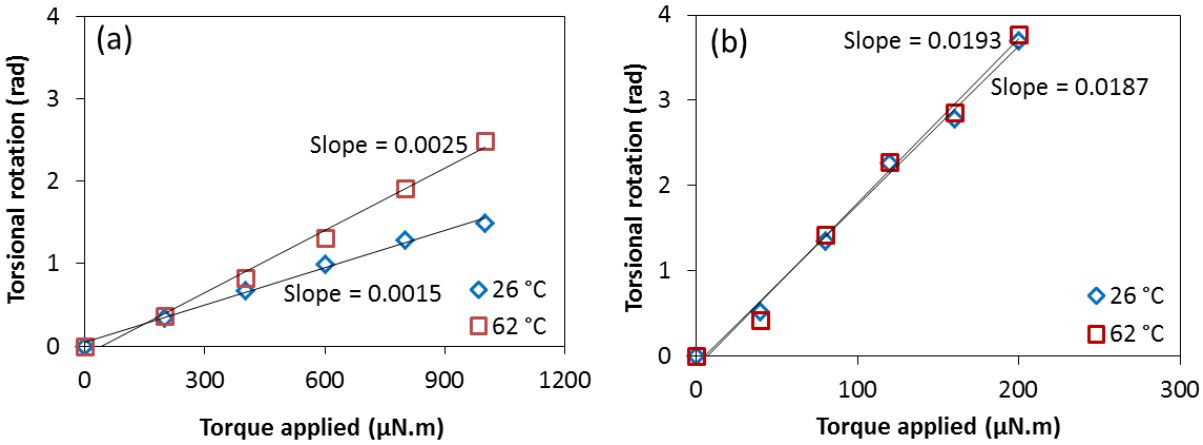

Figure 4.5. Torsional rotation of twisted fibres under applied torque; (a) polyethylene braided fibre, and (b) polypropylene fibre. (Inverse of slope of each curve denotes the torsional stiffness of that fibre).

To aid detailed theoretical calculation of free stroke over the 25 – 62°C temperature range, torsional stiffness of both fibres were also measured at 30, 40, and 50°C. Table 4.1 shows the torsional stiffness results at different temperatures.

Table 4.1. Torsional stiffness of twisted fibres in several temperatures.

Temperature (°C)	Torsional stiffness (µN·m)	
	Twisted polyethylene fibre	Twisted polypropylene fibre
26	667	54
30	556	53
40	500	53
50	435	52
62	400	52

4.3.2 Anisotropic Thermal Volume Expansion of Twisted Fibres

The twisted fibres were heated slowly using an infrared heating source while fibres were imaged with a microscope and the diameter change was recorded. The lever arm transducer system provided a measurement of the fibre length change under a constant external tensile stress. Within the 26°C to 62°C temperature range, the twisted polyethylene fibre showed radial thermal expansion of ~0.48% with an axial thermal contraction of ~0.06% (Figure 4.6).

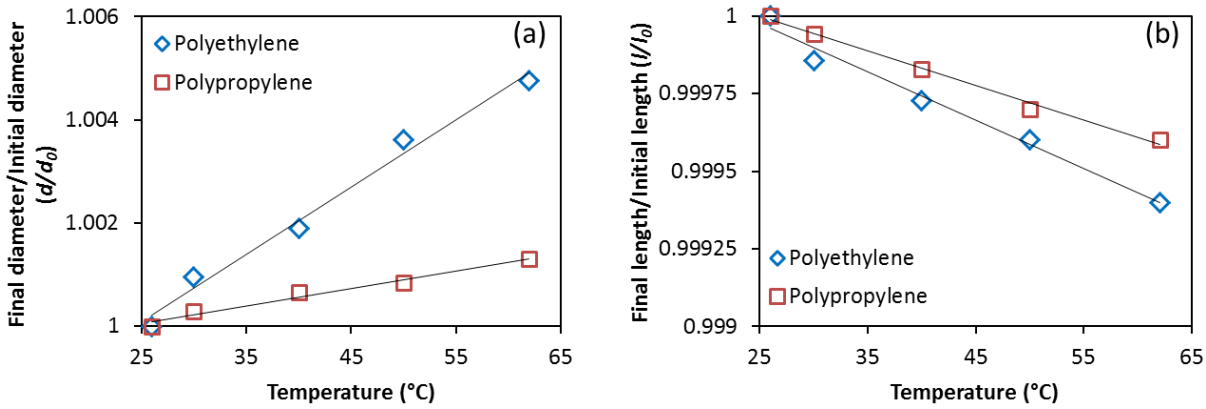

Figure 4.6. Thermal expansion and contraction of twisted polyethylene and polypropylene fibres; (a) diameter expansion, and (b) axial contraction with increasing temperature.

These observations are similar to previously published results for the anisotropic thermal expansion of oriented high density polyethylene fibre over this temperature range [171]. However, there is no such report for thermal expansion in ultra-high molecular weight oriented polyethylene fibres, such as the one used in the present study. Thermally-induced dimension change of polypropylene fibre was also measured within the same temperature range of 26°C to 62°C. A radial thermal expansion of ~0.12% was obtained along with axial thermal contraction of ~0.04% (Figure 4.6). Compared to the thermal expansion across the fibre, both polyethylene and polypropylene showed little

axial thermal contraction which also supports the previous studies regarding thermal properties of oriented polymers [171, 190].

4.3.3 Torsional Stroke and Torque Generation

Isotonic torsional stroke was measured at a small fixed applied torque and then converted to an equivalent free rotation at zero external torque by using torsional stiffness values (Table 4.1) in equation (4.5). Figure 4.7 shows the torsional stroke of twisted polyethylene fibres (opposed by 72 μN·m torque) and polypropylene fibres (opposed by 40 μN·m torque). The calculated free rotations are also plotted to demonstrate the comparison in the torsional actuation of twisted fibres: one under small external torque (experimental, broken lines) and the other calculated from equation (4.5) under zero torque (solid lines). The differences in the isotonic and free strokes are small because of the small external torques used and the small change in torsional stiffness of the fibres over the temperature range used. Free rotation of twisted polyethylene and polypropylene fibre was found to be -1.21 and -0.22 °/mm, respectively, over the 26 – 62°C temperature range. Torsional stroke of polyethylene fibre in higher temperature region got larger due to the rapid decrease in torsional stiffness as discussed previously. However, torsional stiffness of polypropylene drops only a small extent in this temperature range; hence, exhibited less torsional stroke. Both of the fibres have shown good reversibility and the results were reproducible for several actuation heating and cooling cycles. In comparison, the torsional stroke of polyamide-6 twisted fibres over the same temperature range was -3.14 °/mm [184].

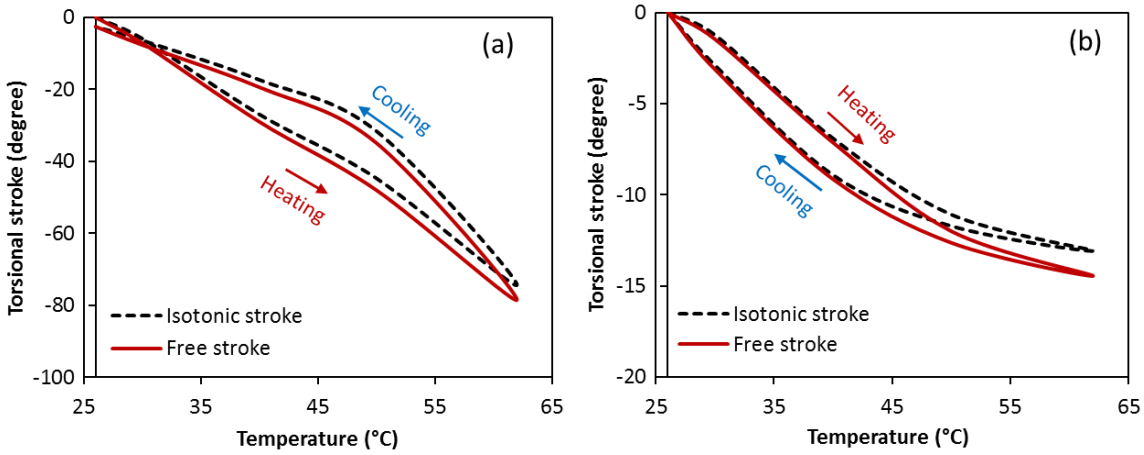

Figure 4.7. Torsional stroke of twisted fibres; (a) polyethylene, and (b) polypropylene. (Note that different Y-axis ranges are used for two figures).

Figure 4.8 shows the blocked torque generated from twisted polyethylene and polypropylene fibres. The maximum blocked torque of the twisted polyethylene and polypropylene fibres were 614 and 13 µN·m, respectively, when heated from 26°C to 62°C. The large difference in torques reflects the significant variation in torsional stiffnesses of the two fibres. A large hysteresis in blocked torque was shown by the polypropylene fibre during continuous heating and cooling. The hysteresis was smaller in the polyethylene fibres in comparison to the polypropylene fibred and may demonstrate a difference in the degree of viscoelasticity in these materials. A detailed investigation of the molecular processes of viscoelasticity was considered beyond the scope of the present thesis. However, both the of fibres showed high reversibility in torque generation when cooled, and the actuation pattern was quite reproducible for several heating / cooling cycles.

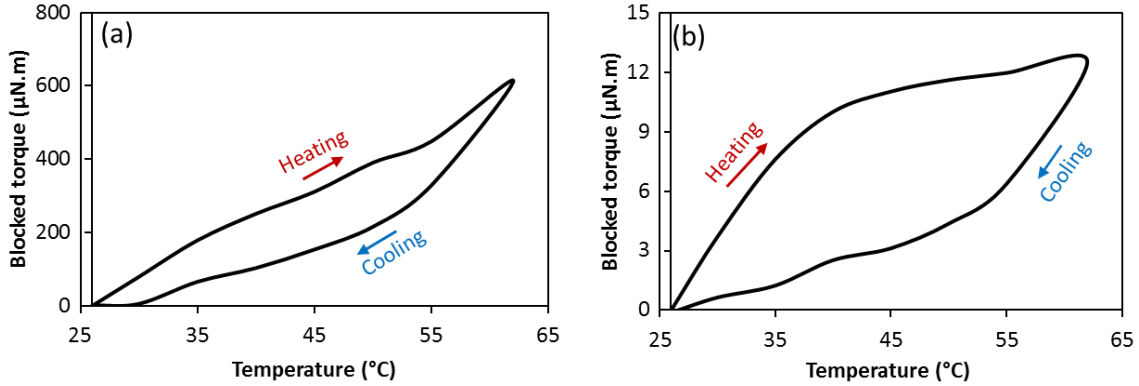

Figure 4.8. Blocked torque generated from twisted fibres; (a) polyethylene, and (b) polypropylene. (Note that different Y-axis ranges are used for the two figures).

4.4 Discussion

4.4.1 Theoretical Prediction of Torsional Actuation

Previous work has demonstrated that the single-helix approximation was able to predict the torsional stroke of twisted polyamide-6 monofilament. This material represented a special case since the length of the twisted fibre did not change during heating. Under these conditions, the single helix model can be greatly simplified from equation (4.2) to equation (4.3). The twisted polyethylene and polypropylene fibres used here displayed considerable length changes during heating. Therefore, to predict the torsional stroke of these fibres equation (4.2) must be validated and used. The expected torsional stroke was calculated at any given temperature using the measured fibre diameter and length expansion ratios (Figure 4.6). In Figure 4.9, the predicted torsional actuations are plotted as a function of temperature, together with previously reported torsional stroke of twisted polyamide-6 fibre (840 µm diameter). In Figure 4.9, the torsional actuation is presented as the final twist to initial twist numbers ratio (n/n_0). This expression is independent of the fabrication parameters used during twisting of the fibres, such as the number of inserted twist, bias angle, and fibre diameter. The n/n_0 only depends on the

thermally induced volumetric changes that occur during heating of the samples. In addition to the calculated torsional stroke of polyethylene and polypropylene by considering both length and diameter expansion coefficients, it was also evaluated by assuming negligible length change. In such cases the calculated torsional strokes deviate by ~3% for thermal expansions due to a small temperature change (26-62°C). However, the main aim of this work is to evaluate the scalability of actuator performance which can be extended to a broader temperature range to induce a larger torsional stroke. Therefore, equation (4.2) is recommended to be used which considers both λ_l and λ_d for more accurate prediction of torsional stroke. Experimentally measured torsional strokes are also included in Figure 9 for comparison with calculated values. There is a very good agreement between the measured and calculated values for all three samples. The single-helix theory is capable of correctly predicting the dependence of torsional stroke on the volume change and the amount of inserted twist. This theory also predicts the quantitative torsional strokes with high accuracy, meaning that our assumption in which the string length was considered constant is valid for oriented polyamide-6, polyethylene and polypropylene.

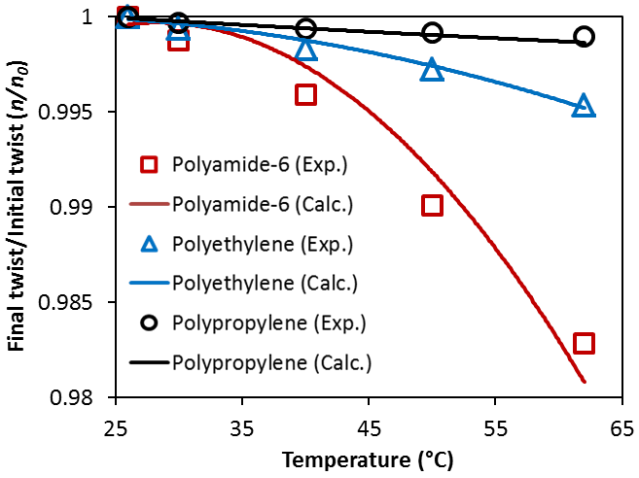

Figure 4.9. Torsional stroke of twisted fibres comparing experimentally measured values (symbols) with predictions from the single helix model (solid lines).

It is noted that the amount of torsional rotation varied significantly between twisted polyamide-6, polyethylene, and polypropylene fibres under the same experimental condition. The predictive single helix model allows exploring the possible reasons for the observed differences in torsional actuation of these three polymers.

Figure 4.10 shows calculated torsional strokes expressed as a fractional of twist bias angle. Of note, these three polymers were prepared with different initial twist bias angles. The analysis used the measured diameter and length expansion ratios, and assumed that these parameters were unaffected by the inserted twist. The calculated torsional actuation shows a slightly change over a wide range of initial bias angle for all three polymeric fibres. Figure 4.10 suggests that the bias angle has negligible effect on the actuation of fibres. Then, it can be concluded that the different torsional actuations that were observed between polymer fibres was mainly the result of their different thermal expansion. The thermal expansion of polyamide-6 is significantly higher than that of polypropylene monofilament and ultra-high molecular weight polyethylene braided fibres, hence resulting in much larger actuations. Higher thermal expansion can be due to the lower crystallinity or high friction between polymer chains in the amorphous phase. Amorphous polymers are known to show higher thermal expansion coefficients than crystalline polymers [191].

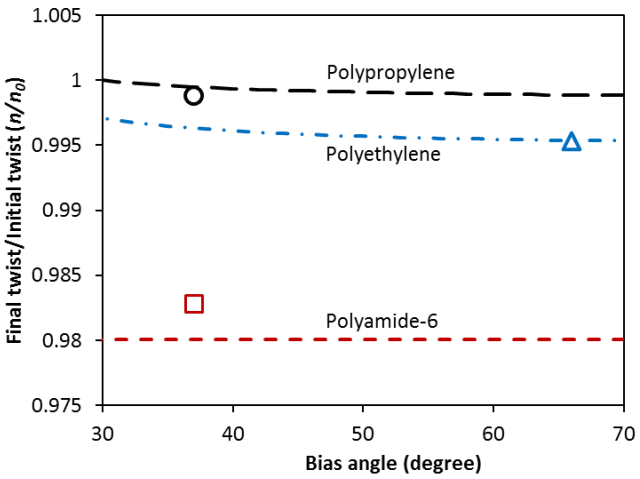

Figure 4.10. Torsional stroke of twisted fibres as a function of initial twist angles (dotted lines represent theoretically calculated values and the symbols denote experimentally measured values for the corresponding bias angles).

4.4.2. Theoretical Prediction of Generated Torque

Experimental results of the torque generated by heating twisted polyethylene and polypropylene fibre were significantly different. Theoretical analysis of the torque generated from these fibres was conducted using torsion mechanics [184] which is summarized in equation (4.6), and the results are plotted together with experimental results in Figure 4.11. Previously measured torque generation by twisted polyamide-6 fibre (840 µm diameter) is also included in the plot for comparison.

$$\tau_{\text{blocked}} = \Delta n . S'_A \qquad (4.6)$$

Here, τ_{blocked} is the torque generated from twisted fibre, Δn represents the calculated free rotation (in radians) for a certain length (l) of twisted fibre and S'_A is the fibre torsional stiffness in the actuated condition. In all cases, there is an excellent agreement between the measured and calculated values, which further supports the analytical approach based on a single-helix model. The higher torsional stiffness of the polyethylene fibre results in a generated torque that is similar to that produced by the

polyamide-6 twisted fibre, despite of showing almost three times smaller torsional stroke. The generated torque for polypropylene fibre is considerably small which is due to its small torsional actuation and low stiffness.

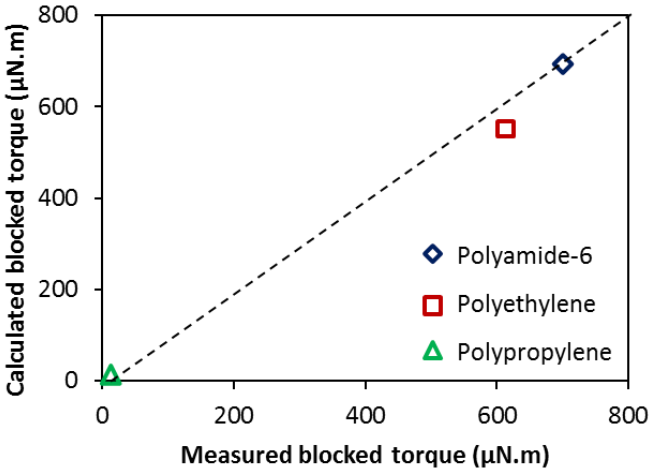

Figure 4.11. Measured and calculated blocked torque generated by twisted fibres when heated from 26^{o}C to 62^{o}C.

4.5 Summary

The objective of this work was to investigate the torsional actuation in twisted polymer fibres of different nature and to further evaluate the validity of the previously developed single-helix model for quantitative prediction of torsional stroke and torque. Highly twisted fibres were prepared by using a rotary motor and the torsional actuation tests were conducted over a temperature range of 26 – 62°C. As reported in our previous work, twisted polyamide-6 fibre showed negligible length change with significant diameter expansion when heated from 26 to 62°C. In comparison, both polyethylene and polypropylene fibres used here exhibited length contractions over this temperature range. Excellent agreement was found between the experimentally measured and theoretically calculated results for torsional actuation and generated force proving the validation of the single-helix model. The analysis also demonstrated that the torsional

actuation observed in twisted polymer fibres was mainly governed by the thermal expansion of fibres. The thermal expansion of fibres, in turn, is influenced by the degree of crystallinity.

CHAPTER 5 Thermo-Mechanical Effects in the Torsional Actuation of Twisted Nylon 6 Fibre

This chapter has been submitted for publication as "S. Aziz, S. Naficy, J. Foroughi, H. R. Brown and G.M. Spinks, *Journal of Applied Polymer Science,* DOI: 10.1002/app.45529 (2017)".

The introduction and experimental sections in this chapter are shortened versions compared with the published article to avoid duplication with the previous chapters.

5.1 Introduction

One practical issue raised in early work on both twisted and coiled polymer fibre torsional and tensile actuators was the need for several 'training cycles' of heating and cooling to achieve fully reversible actuation [155, 184]. In the first few cycles, the degree of fibre untwist during heating exceeded the fibre re-twist that occurred during cooling [184, 185]. The magnitude of this effect has not previously been reported, nor has the molecular origin been described. Fibre twisting and coiling of oriented semicrystalline polymer fibres is an elasto-plastic mechanism where much of the inserted twist is lost due to elastic recovery unless the twisted fibre is thermally annealed while maintaining an external torque. Annealing or heat-setting is also commonly used to improve the mechanical properties of drawn polymer fibres by altering the fibre microstructure [192-194]. Here, we apply these annealing techniques to modify the structure of twisted nylon-6 fibres and investigate the effects on the torsional actuation behaviour.

In addition, the effect on its torsional actuation response of the applied external load acting on the fibre on its torsional actuation response is investigated. Tensile creep is known in drawn, semicrystalline polymer fibres and is likely to also occur during the thermally-induced torsional actuation of twisted polymer fibres. The magnitude of this effect has yet to be established, and here we investigate torsional creep in twisted nylon 6 fibres when subjected to small temperature changes.

5.2 Experimental

5.2.1 Sample Fabrication

To fabricate the samples twist was inserted to the commercially available polymer fibres using a variable speed DC rotary motor [184] while keeping the fibres well stressed at

10 MPa axial stress. 500 μm diameter monofilaments of nylon 6 (Sport Fisher monofilament fishing line) were twisted (~445 turns per meter) just before the first coil was due to form as a result of overtwisting (saturation). In this saturated state, the twist angle on the surface of fibres remained consistent (~35° from the fibre axis) amongst all samples. Heat-setting of the twisted samples were conducted at acceptable temperatures which were held well below of the melting temperature of nylon 6. Differential scanning calorimetry (DSC) tests (TA Instrument DSC Q100) were conducted on as-received and twisted nylon 6 fibres, confirming their actual melting point. Heating rate was set at 10°C/min and cooling rate was at 20°C/min by using a 50 ml/min compressed nitrogen flow as the purging gas.

To study the effect of heat-setting on the actuation performance of twisted fibres, two different annealing approaches were conducted to permanently set the number of twists inserted and the helical structure introduced. In our previous studies, the heat-setting process used after the twist insertion was thoroughly described [184]. Following this process, four different samples of similarly twisted fibres were heat-set at 120, 150, 175, and 200°C for 2 hours followed by a 2 hours cooling period at room temperature (will be denoted 'Set A' hereafter). In the second approach (denoted 'Set B' hereafter), heat setting of twisted fibres was performed *in situ* and during the twist insertion process. Figure 5.1 shows the schematic illustration of this simultaneous twisting/heat-setting process. A two-end open electric heating furnace was used through which the fibre was suspended. A programmable temperature controller (Electro Chemical Engineering Pty Ltd, Australia) was used to sense and control the temperature throughout the furnace. Temperature was maintained at 120, 150, 175, and 200°C depending on the parameter chosen for fabrication process. Heating the sample during twist insertion causes a decrease in torsional stiffness of the fibre [184]; hence, the number of twists required to

form the first coil become higher compared to the twists needed in ambient temperature. Therefore, we inserted the similar number of twists (~445 turns per meter) in 'set B' fibres as has been inserted in 'Set A' fibres. After twisting the fibres were then left for 2 hours to cool down at atmospheric conditions. The sample was then taken out from the furnace and was directly used for actuation tests.

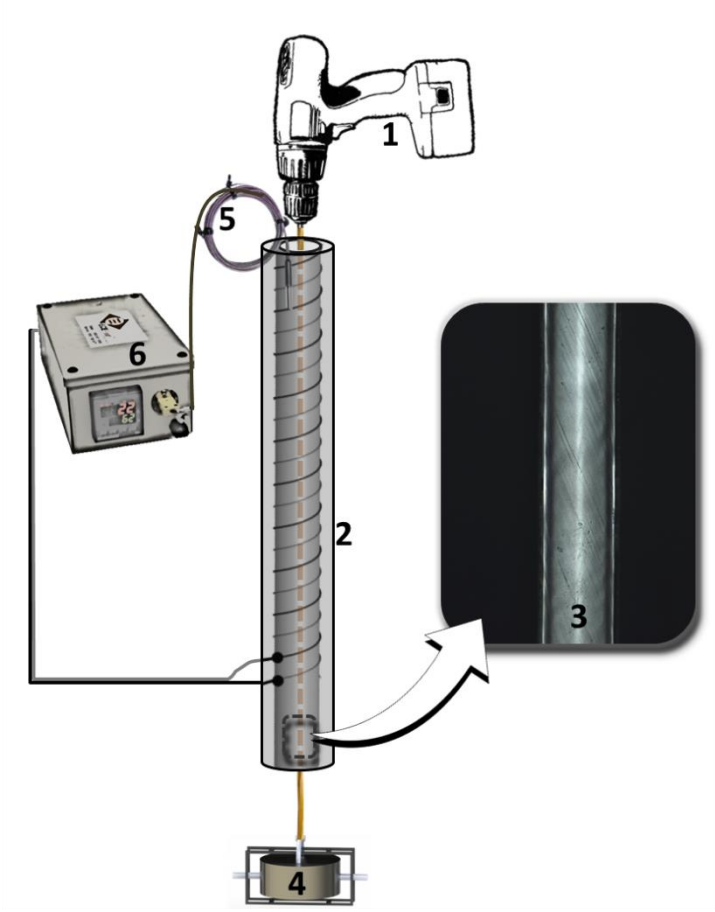

Figure 5.1. Experimental set up for simultaneous fibre twisting/heat-setting process: (1) DC rotary drill; (2) electrically driven heating furnace with proper insulation; (3) fibre under twist; (4) weight stone to apply stress to the fibre with rotation blocker to prevent untwist; (5) thermocouple for sensing inside temperature of the furnace; (6) programmable temperature controller maintaining the required power delivered to the furnace.

5.2.2 Thermogravimetric (TGA) Tests

To study the effect of water content on the actuation performance of twisted fibres exposed to moisture, thermal gravimetric analysis TGA (METTLER TOLEDO DSC/TGA) was employed. Initially, annealed samples were environmentally dried for ~24 hours and then, taken to the TGA chamber to be thermo-gravimetrically tested. The amount of water loss was analysed by heating the samples to 150°C. For comparison, other samples taken after annealing process were desiccator-dried (with anhydrous calcium chloride desiccant) for 24 hours to remove possible moisture. The dried samples were also tested with TGA and the results were compared with non-desiccated samples.

5.2.3 Torsional Actuation Tests

An in-house-built testing apparatus was used to perform thermally induced torsional actuation tests [184]. The test assembly was equipped with a DC power supply, programmable temperature controller and a dual mode lever arm force/distance transducer system (Aurora Scientific 305B). Twisted nylon 6 fibres were thermally actuated by electrical heating of the furnace. The fibres were fixed at one end and the other end was attached to a shaft supported by two near frictionless air bearings. Free rotation of actuated fibres was measured optically by placing an optical microscope (ISSCO-OPTEK) focused axially to the bearing shaft.

The rotation of the shaft caused by the isotonic (constant torque) torsional response of the twisted fibres was measured continuously from the lever arm that was connected to the shaft by a fibre held at constant tension. Different isotonic tests reported herein were conducted under a range of constant small external torques (68, 140, 280, and 560 μN·m) applied by the lever arm and opposing the fibre untwisting. Applied torque

values were chosen well below of the torsional yield stress at which the fibre starts to deform permanently to the twisting / untwisting direction. Unless otherwise stated, a constant twisted sample length (70 mm) and a constant temperature range (26-62°C) at average heating and cooling rates of 3.6°C/min and 1.8°C/min, respectively, were programmed and used for all the actuation tests.

5.3 Results and Discussion

5.3.1 Differential Scanning Calorimetry

The mechanical and physical properties of semicrystalline polymers are strongly related to their microstructure, which is here investigated by DSC. Figure 5.2(a) shows the DSC curves obtained from a 500 μm diameter as-received nylon 6 fibre when heated from 10°C to 300°C and then cooled. The melting temperature was ~223°C and the area of melting peak was 85.23 J/g from which a degree of crystallinity of 36% was calculated by comparison to the heat of fusion reported for a perfectly crystallized nylon 6 sample (239 J/g) [195, 196]. Figure 5.2(b) and 5.2(c) shows the DSC results for highly twisted fibres annealed at 120°C (Set A) and 120°C (Set B), respectively. Both materials show similar DSC thermograms with a slight increase in the melting temperature of 1-2°C and a small decrease in the degree of crystallinity by 1-2% when compared with the as-received fibre. The similar phenomenon was observed from the recrystallization peaks (on cooling) of different samples while recrystallization enthalpies decreased for twisted fibres compared to the as-received one. Tsujimoto *et al.* and co-workers have previously investigated the effect of twist and annealing on the microstructure of nylon 6 monofilaments [197]. They observed that twisting slightly decreases the degree of crystallinity by partial destruction of lamellae. The lamellae are initially oriented perpendicular to the fibre long axis and remain perpendicular to the

twist angle for low to medium levels of twist insertion. Twist strain is accommodated by distortion of the amorphous regions and be re-orientation and partial destruction of the lamellae. It was further observed that annealing of the twisted fibres at 170°C for 15 minutes when held at constant length did not alter the degree of crystallinity, but stabilised the structure possibly due to better packing within the amorphous regions [197].

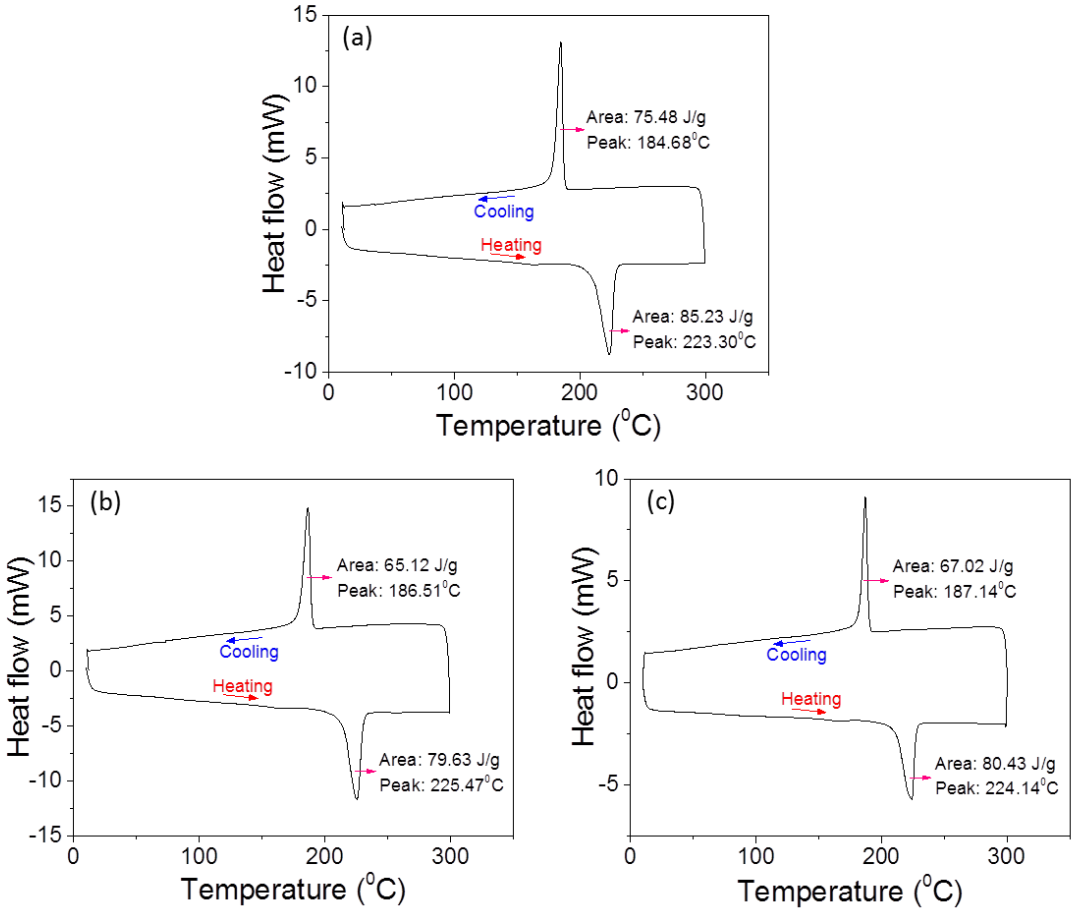

Figure 5.2. Differential scanning calorimetry result nylon 6: (a) as-received fibre; (b) highly twisted fibre annealed after twist insertion; (c) highly twisted fibre annealed during twist insertion.

5.3.2 Moisture Content in the Twisted Samples

Due to the presence of hydrogen bonds, nylon 6 absorbs considerable amount of water when left in natural condition [198, 199]. In particular, amorphous phase water sorption of nylon 6 is largely recognized [199-201] which acts as a plasticiser to reduce the glass transition temperature [202]. This process may influence the actuation performance, since the thermal expansion coefficient of polymers increases above Tg and thermal expansion drives the torsional actuation in twisted polymer fibres. TGA was performed to evaluate the amount of water present in the twisted fibres.

Figure 5.3 shows the TGA results for the twisted and annealed (200°C) nylon 6 samples when heated from 30°C to 150°C. Figure 5.3(a) shows gradual but continuous weight loss of up to 2.7 wt% for the non-desiccated sample, whereas the desiccated sample had a significantly lower water loss of 0.8 wt% when heated over the same temperature range [Figure 5.3(b)]. In both cases, successive heating cycles have shown almost negligible sample weight changes in that particular temperature region. These results indicate that the non-desiccated sample retained a small amount of atmospheric water. The reduction in mass due to water loss for both samples during their first heating cycle over the temperature range of 30-62°C was small. Since torsional actuation tests were conducted over this temperature range, it was concluded that the effect of moisture loss during actuation tests could be ignored in this study.

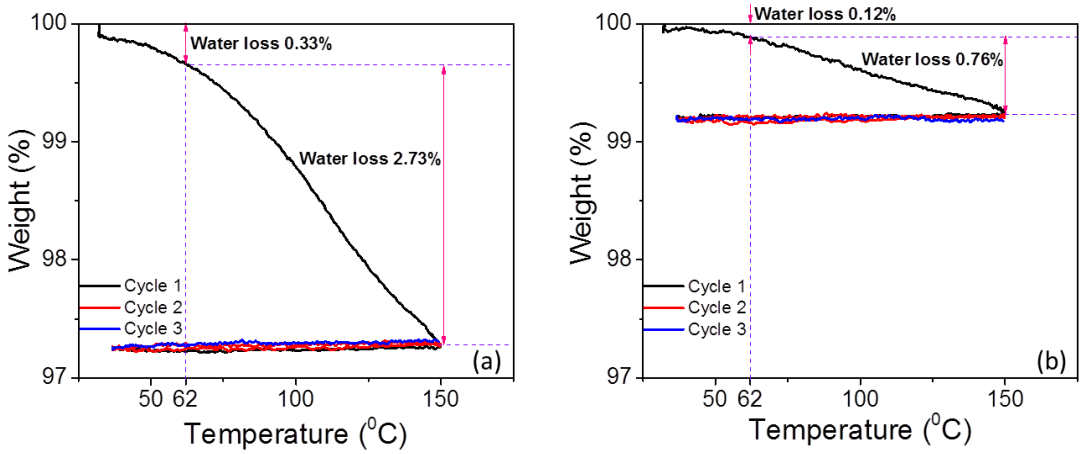

Figure 5.3. Thermogravimetric test results of twisted nylon 6 fibre: (a) as-twisted non-desiccated sample; (b) 24 hours desiccator dried sample.

5.3.3 Effect of Annealing Conditions on Torsional Actuation

Figure 5.4 shows the torsional stroke recorded during the first heat/cool cycle for twisted fibre samples prepared by both annealing methods. Almost identical torsional strokes were obtained for samples prepared by both methods when the annealing temperature was consistent. Regardless of the annealing method used, those fibres annealed at 120°C and 150°C showed large untwisting rotations of up to -7°/mm during heating, but with a smaller re-twisting recovery during cooling (+2°/mm). As the annealing temperature increased the fibres exhibited less untwisting on first heating but with considerably higher degrees of reversibility. Samples annealed at 200°C provided the smallest rotation of -1.7°/mm on heating and almost the same re-twisting on cooling. This result is the same as reported previously [184] for identical 500 um diameter nylon 6 twisted fibre that had been annealed at 120°C but had been further 'trained' for several heat / cool cycles to achieve full torsional reversibility.

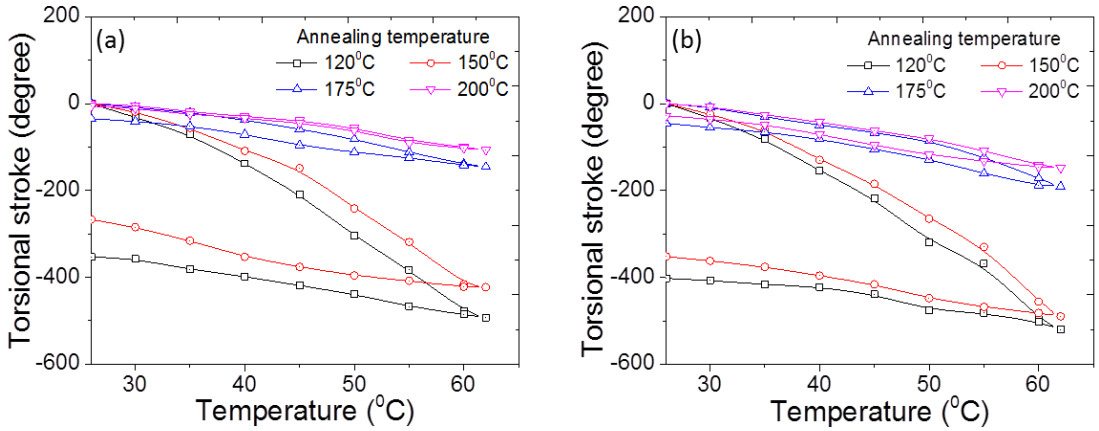

Figure 5.4. Torsional actuation test results of 70 mm long twisted nylon 6 fibre samples prepared at different annealing temperatures: (a) samples annealed after twisting (Set A); (b) samples annealed during twisting (Set B). (Each heating process is shown to start at '0' torsional stroke for all cases).

The effect of annealing temperature on the reversibility of torsional actuation of these twisted nylon 6 fibres may be understood from previous studies of heat-treatment induced microstructural changes in axially drawn nylon 6 fibres. Prior work has shown that important microstructural differences occur when fibres were annealed under tension or when slack [203]. Considerable shrinkage occurs in the length direction in slack fibres as a result of molecular refolding processes, but these mechanisms are significantly inhibited by applied tension. In the present study, annealing was conducted at constant fibre length thereby potentially limiting molecular reorganization. First heating during torsional actuation testing of incompletely annealed twisted fibres may allow sufficient molecular mobility for some reorganization to occur. Shrinkage along in the chain orientation direction, which forms helically paths in these twisted fibres, would then promote fibre untwisting. The result is a large untwisting during first heating due to both irreversible molecular reorganization and reversible thermal expansion effects. Twisted fibre samples annealed at 200°C appear to be immune from

these irreversible processes, suggesting that the higher annealing temperature allows a stable molecular structure to form even when the fibre was held at constant length during heat treatment. Indeed, Tsujimoto *et al.* have shown that annealing of twisted nylon 6 fibres at 170°C at constant length stabilises the molecular structure, possibly by increased molecular packing in amorphous regions [197].

5.3.4 Effect of External Torque on Torsional Actuation

The effect of an external torque applied in the twist direction on the torsional stroke during the first heating and cooling cycle was next investigated for samples prepared by annealing at 200°C (Figure 5.5). With increasing applied external torque, the untwisting rotation on heating diminished in magnitude and the retwisting on cooling increased. The net result was an increase in sample twist after the first heat / cool cycle for samples tested at high external torque.

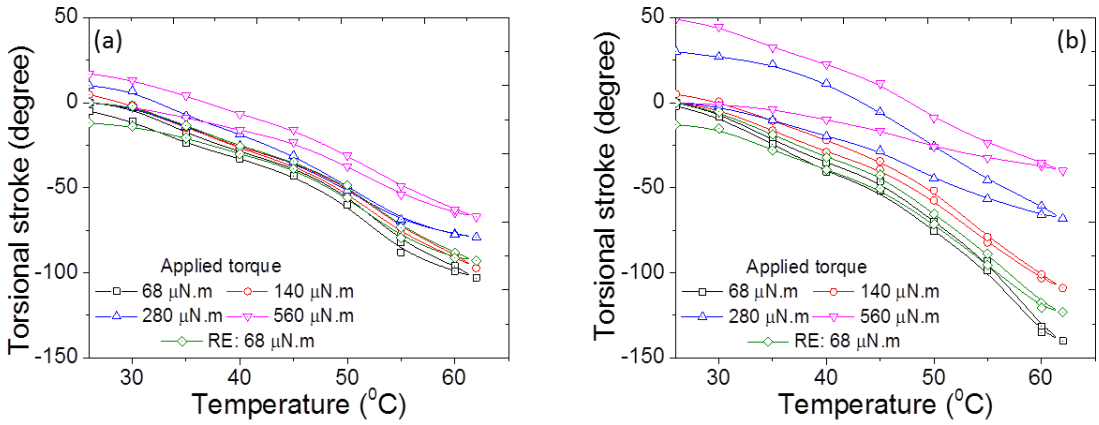

Figure 5.5. Torsional actuation test results of 70 mm long twisted nylon 6 fibre samples tested with different externally applied torque. (a) samples annealed after twisting (Set A); (b) samples annealed during twisting (Set B).

The effect of the applied torque was particularly noticeable for samples that were annealed during twisting and was smaller for samples that were annealed post twisting. It was found that two heat / cool 'training cycles' were required at a fixed external

torque before the sample showed equivalent untwist / retwist magnitudes during heating and cooling. Fibre samples tested at the maximum torque for three heat / cool cycles were then re-tested at the minimum torque. The first heat / cool cycle at the low torque condition showed a reversibility of 80-95% with some unrecovered untwist.

Torsional creep tests were conducted to further investigate the effect of applied torque on the torsional actuation response. Longer time exposure to an external torque applied in the twist direction resulted in a gradual increase in fibre twist with the effect more pronounced at higher torques and higher temperatures (Figure 5.6). The observed increase in twist due to this torsional creep correlates approximately with the results of Figure 5.5 when the temperature and timescale of the heat / cool cycles are considered. In addition, the sample tested initially at the maximum torque and then re-tested at the minimum torque showed some recovery of the torsional creep. Again, this observation is in qualitative agreement with the assumption that there was some net untwisting during the heating / cooling of the sample tested at the minimum torque immediately following testing at the maximum torque.

Tensile creep is well documented in polymers, and studies of nylon 6,6 demonstrate appreciable increases in compliance, even at room temperature and at the timescales of the experiments described here [204, 205]. This torsional creep can be explained as gradual deformation of oriented polymer chains. Thermal annealing treatment has been shown to aid creep deceleration in semicrystalline polyester and polyamide materials [206]. The reduced creep rate was reportedly due to the formation of undeveloped crystallites in the amorphous phase during annealing which serve as obstacles for sliding of chain ends between polymer chains [206]. In the present study, however, the high temperature annealing was unable to completely eliminate the torsional creep

process when high external torques were involved. Modelling approaches, such as proposed recently by Fancey [207], may allow the prediction of time-dependent torsional strokes at different loads and temperatures. Preferably, the creep in torsional actuators should be negligible and techniques used to reduce tensile creep in polymers, such as fibre reinforcement, or crosslinking are beyond the scope of the current thesis, but are worthy of further investigation.

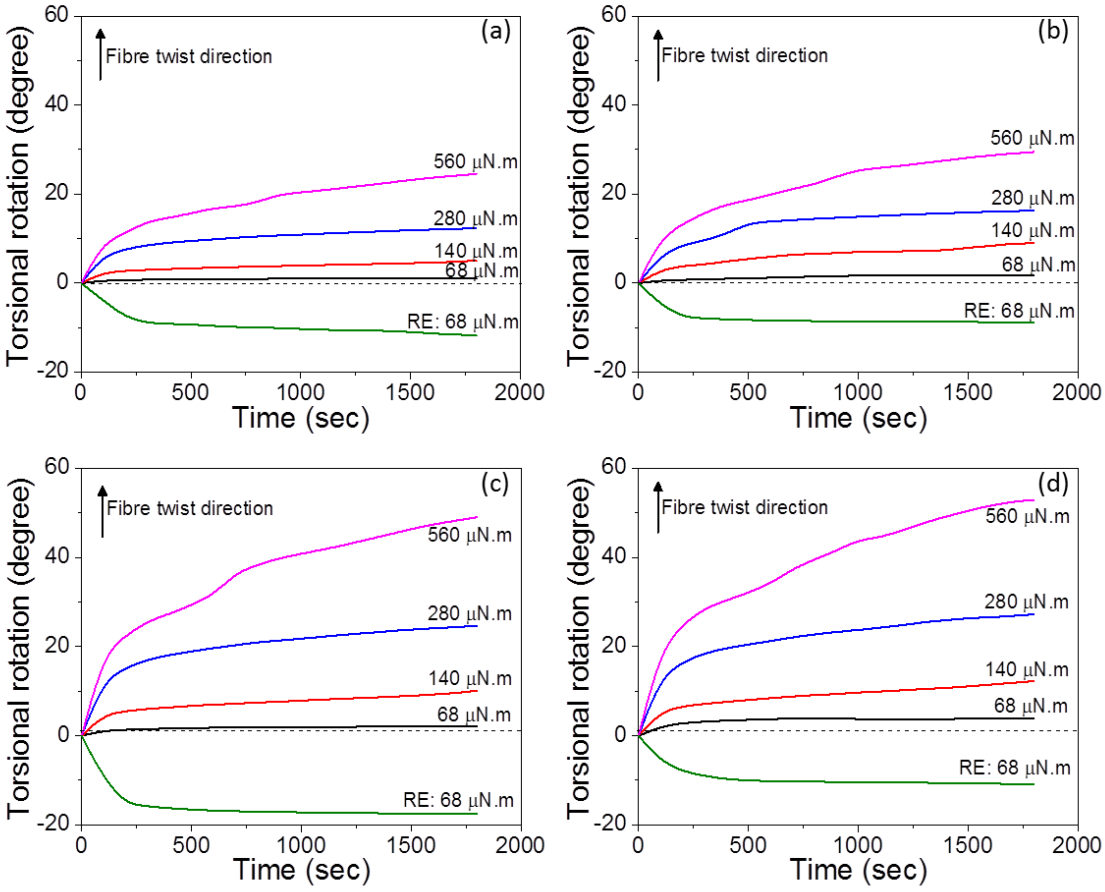

Figure 5.6. Time based torsional creep of twisted nylon 6 fibres under different isotonic torques. Tests were conducted at 26°C: (a) annealed at 200°C after twisting (Set A), (b) annealed at 200°C *in situ* twisting (Set B). Tests conducted at 62°C: (c) annealed at 200°C after twisting (Set A), (d) annealed at 200°C *in situ* twisting (Set B).

5.4 Summary

The purpose of this study was to further explore the torsional actuation of twisted nylon 6 monofilament and to optimise their fabrication conditions to achieve a more stable actuation performance under varying isotonic torques. Nylon 6 monofilaments were twisted and annealed at several temperatures below their melting point. One set of samples was prepared by heat-setting during twisting, whereas another sample set was annealed after twist insertion. Heating and cooling of the samples over a 36°C range resulted in cyclic torsional stroke due to untwisting (heating) and retwisting (cooling) of the fibres. As in prior studies, samples annealed at low temperature (< 175°C) showed a larger untwisting and smaller retwisting during the first heat / cool cycle. In contrast, samples annealed at 200°C showed complete reversibility in the first cycle, without the need for any 'training'. The application of an external torque caused torsional creep that was accelerated by increases in temperature and torque. The baseline twist in the fibre readjusts to a new level during the first two heat/cool cycles when the external torque is changed. Thereafter, the torsional untwist and retwist remain consistent in subsequent heat / cool cycles at constant torque. Heat setting can, therefore, be used as an effective means for fixing a consistent torsional actuation response.

CHAPTER 6 Twist–Coil Coupling for High Stroke Contractile Artificial Muscles

6.1 Introduction

Torsional artificial muscles made from twisted polymer fibres and yarns have created much interest lately mainly because they are the basis for high performance tensile actuation in twisted and coiled fibres and yarns [154, 155, 157, 161, 165, 208]. In these systems, the torsion that occurs when the twisted fibre is stimulated translates into a length change in the coil. Tensile strokes as high as 50% have been observed. Here we report a new mechanism of torsional driven tensile actuation. A torsionally active fibre is coupled in series with a second fibre that has a low critical torque for twist-induced coil formation. Significant length contraction occurs as coils form and this effect is optimised by consideration of the relative lengths of the two fibre materials.

The actuation process was first modelled to guide experimental design. The change in actuator length was considered based on the helix geometry and the number of turns expected to form was estimated based on torsion mechanics and the criterion of Ross [209] that predicts the torque needed to initiate coiling in a fibre, wire or slender rod:

$$\tau_c = \sqrt{2EIF} \tag{6.1}$$

where E is the tensile modulus and I is the fibre second moment of area, which is $\pi D_y^4/64$ for fibres of circular cross-section and diameter D_y. Fibres of low elastic modulus favour coil formation, so elastomeric fibres (commercially-available Spandex yarn) was used in the current work. The torsion was induced by heating a twisted and annealed nylon 6 fibre, as described in Chapter 3 [184]. The free torsional stroke per fibre length (Δn_{free}) and generated blocked torque (τ_{blocked}) have been shown in Chapter 3 to be given by [184]:

$$\Delta n_{\text{free}} = \frac{n_o}{l_A}\left(\frac{d_o}{d} - 1\right) \tag{6.2}$$

$$\tau_{\text{blocked}} = \Delta n_{\text{free}} \times J_{\text{A}} G_{\text{A}} \tag{6.3}$$

where n_o is the initially inserted twist (turns) per initial fibre length l_A, d_o and d are the fibre diameters before and after heating, and $J_A G_A$ is the torsional modulus of the twisted fibre after heating; G_A is the fibre shear modulus after heating and J_A is the polar moment of area which is $\pi d^4/32$ for fibres of circular cross-section. The above relation predicts the 'free', or unimpeded, torsional stroke. However, the attached spandex yarn acts as a return spring (torsional modulus, $J_N G_N$; length, l_N) as described in Chapter 2 [110, 184] and reduces the torsional stroke of the twisted fibre:

$$\Delta n = \Delta n_{\text{free}} \left(\frac{J_A G_A}{J_A G_A + \frac{l_A}{l_N}(J_N G_N)} \right) \tag{6.4}$$

The full range of generated torsional strokes and torques can be represented by the torque – stroke curve as shown schematically as line A in Figure 6.1. The effect of the return spring fibre is illustrated by the dashed line B having a slope equivalent to the torsional stiffness of the return spring. The intersection of lines A and B represent the final torsional stroke and residual torque applied by the torsional actuator on the return spring. The case of a return spring fibre that forms a coil when connected in series to a torsional actuator is represented by line C. Here, the torsional stiffness of the return spring changes when each coil turn forms. First coil turn forms when the torque acting on the return spring reaches the critical torque (τ_c) or equivalently the critical twist ($l_N n_c$) inserted in the return spring fibre. The number of turns formed in the coil (N_c) depends on the remaining torsional stroke after the initiation of first coil formation so that:

$$N_{\text{c}} = (l_A \Delta n - l_N n_{\text{c}}) \tag{6.5}$$

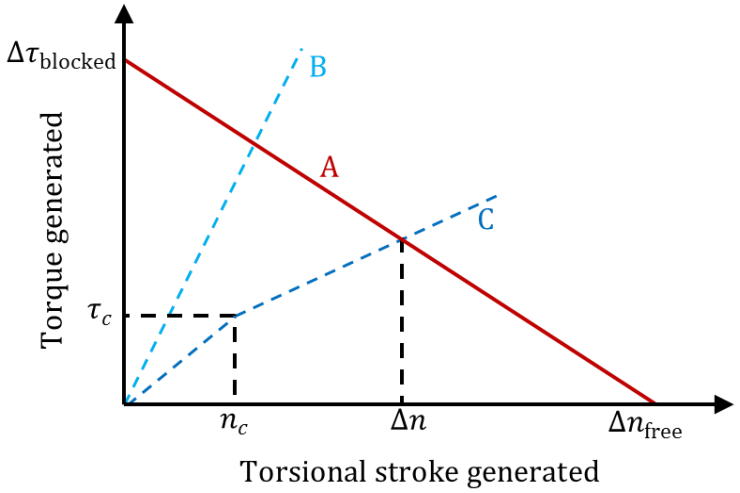

Figure 6.1. Schematic illustration of the mix of torque generated and torsional stroke generated by a torsional actuator when activated (line A). The final torque and stroke generated depends on the external loading conditions. Free rotation generates the largest torsional stroke ($\Delta\boldsymbol{n}_{\mathbf{free}}$) and blocked rotation generates the largest torque ($\boldsymbol{\tau}_{\mathbf{blocked}}$). The torsional properties of non-coiling and coiling return spring fibres are represented by lines B and C, respectively.

The overall length contraction (ΔL_{total}) of the series actuator by the formation of coil turns can be predicted using the geometry of a single helix. Figure 6.2 shows the schematic illustration of the series actuator arrangement. The total length before stimulation (L_{total}) comprised the elastomer yarn length (L) and the length of the torsionally-active twisted polymer fibre (l_A). For each coil turn that forms, a straight segment of elastomeric fibre of length L_{S} is converted to a coil of length L_{c}. Assuming that the overall length of both the elastomeric fibre and the twisted polymer fibre remain unchanged, then the formation of N_{c} turns in the elastomeric fibre causes an overall length change given by:

$$\Delta L_{\text{total}} = N_{\text{c}}\left(L_{\text{c}} - L_{\text{s}}\right) = N_{\text{c}}\left(\pi D_{\text{c}} \tan\alpha_{\text{c}} - \frac{\pi D_{\text{c}}}{\cos\alpha_{\text{c}}}\right) = \pi N_{\text{c}} D_{\text{c}} \frac{\left(\sin\alpha_{\text{c}} - 1\right)}{\cos\alpha_{\text{c}}} \qquad (6.6)$$

where D_c is the coil diameter and α_c is the coil bias angle taken against the perpendicular direction to the long axis of the elastomeric return spring yarn. Here, ΔL_{total} is the contraction of the elastomeric yarn which also represents the overall tensile stroke of the series muscle since the length change during torsional actuation of the twisted fibre has been found to be negligible in previous studies [185]. Combining equations (6.5) and (6.6) gives the final predicted tensile stroke for the series actuator:

$$\Delta L_{total} = \pi D_c (l_A \Delta n - l_N n_c) \frac{(\sin\alpha_c - 1)}{\cos\alpha_c} \quad (6.7)$$

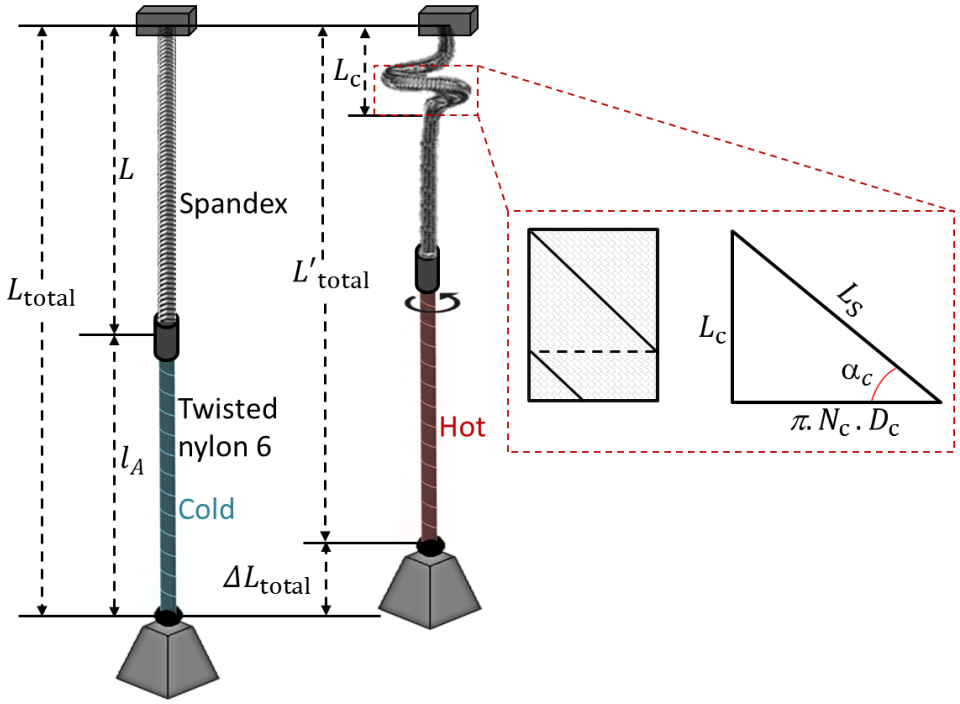

Figure 6.2. Schematic illustration of single-helix approximation for coiled spandex yarn formed due to torsional actuation of twisted nylon fibre.

A series of experiments were conducted using different lengths of spandex yarn return spring and nylon 6 torsionally active fibres to evaluate equation (6.7). The lengths of each fibre affects the expected torsional stroke as described in equation (6.4) since torsional stiffness depend inversely on fibre length and the torsional free stroke of the

actuating fibre is proportional to actuating fibre length. The tensile stroke is expressed as a percentage of the initial unloaded length of the series actuator to effectively compare the performance of different length combinations. The effect of the applied external load on coil formation and tensile stroke is also considered.

6.2 Experimental

6.2.1 Materials

Commercially sourced nylon 6 fibre (0.54 mm diameter, Sport Fisher monofilament fishing line), silver coated nylon multifilament yarn (0.50 mm diameter, Sheildex Shieldex silver plated polyamide yarns) and spandex yarns (0.6, 1.2, and 1.7 mm diameter, Spandex Co. Ltd., China) were used. The torsional actuating samples were made by co-twisting the nylon 6 fibre with a slightly longer length of silver coated nylon multifilament yarn. A total of 428 twists per meter of fibre length were inserted with a constant axial stress of 10 MPa applied to the nylon 6 monofilament. The twisted fibres were heat set at 120 °C for 30 minutes [184]. The desired lengths of twisted nylon fibre and spandex yarn were joined using a metallic crimp to prepare series actuator samples.

Tensile properties of the spandex yarn samples were measured using a tensile tester (Shimadzu EZ-L Tester) and elastic moduli (E) were calculated by fitting engineering stress (σ) and extension ratio (λ) data to the rubber elasticity theory [210]:

$$\sigma = \frac{E}{3}\left(\lambda - \frac{1}{\lambda^2}\right) \tag{6.8}$$

Torque-torsional stroke curves were generated experimentally by using the custom built torsion tester described in Chapter 2 [184] for different diameter yarns where the slope

of the curves denote torsional stiffness. Figure 6.3 shows the test apparatus along with the inset showing the functional parts. Yarns of different length were tested, since torsional stiffness proportionally depends on the yarn length. A force / distance transducer (Aurora Scientific lever arm model 305B) was utilised to apply certain torques to the yarn connected to the shaft of a frictionless air bearing. During the test, the yarn was also subjected to a constant axial force from a second horizontally placed lever arm (Aurora Scientific model 300B) that allows contraction/expansion of the yarn length. Gradually increasing torque applied by the lever arm to the shaft caused twisting of the yarn at one end and therefore provided a measure of torque-torsional stroke relationship. Torsion testing of spandex yarns in this manner was continued until coils formed and the torsional stiffnesses before and after coil formation could be determined.

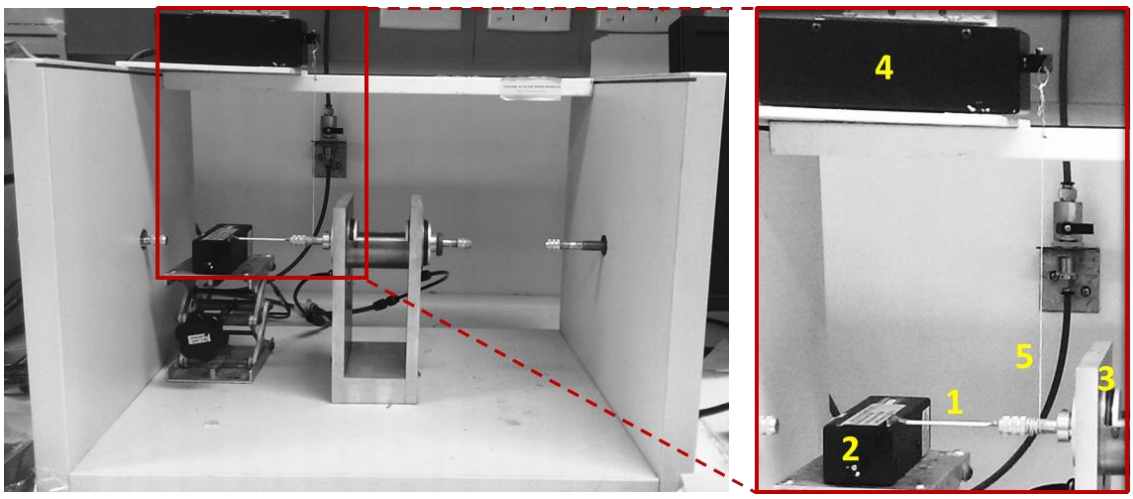

Figure 6.3. Test apparatus for generating torque-torsional stroke curve (components are shown in right panel): (1) spandex yarn, (2) first lever arm applying axial tension to the yarn, (3) air bearing for frictionless yarn rotation, (4) second lever arm applying torque to the yarn, and (5) connecting fibre transferring torque from a second lever arm to the bearing shaft connected with yarn.

6.2.2 Actuation Tests

The overall length change of the series actuator during electrical heating (over 26-125°C temperature range) of the nylon 6 torsional element was measured under isotonic conditions (Figure 6.4). One end of the spandex fibre was tethered to a force / distance transducer (Aurora Scientific lever arm 305B). The other end of the nylon fibre was firmly clamped and a small constant tension was applied using the lever arm to keep the muscle straight. A DC power supply (TMS® Precision Variable 30V 5A DC Power Supply) was connected to the twisted fibre and an infrared thermal imaging camera (Micro-Epsilon TIM 160, supplied by Bestech Australia Pty Ltd) was used to measure the temperature of the fibre surface. Five different lengths of spandex yarn were considered for each of the three yarn diameters and twisted fibre lengths were varied according to the rotation requirements. As-made samples were used for the tests without changing geometrical configurations.

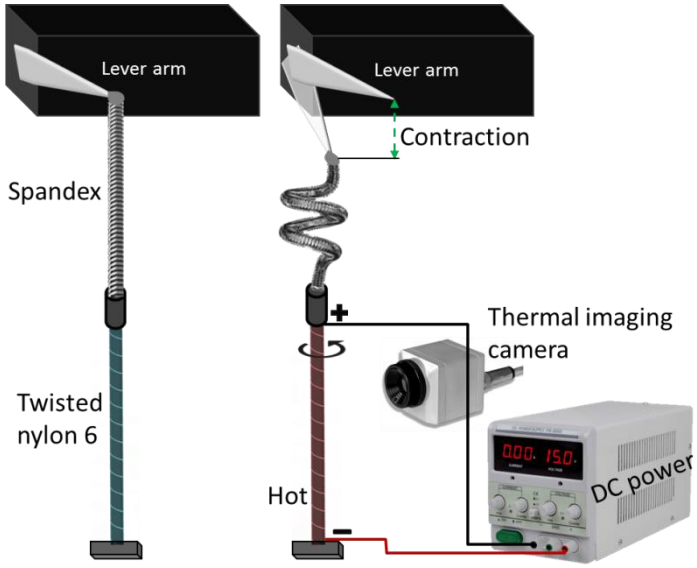

Figure 6.4. Schematic illustration of actuation test set-up used for torsional actuation driven contractile artificial muscle.

In a separate experiment, the nylon 6 fibre volume was measured optically over the experimental temperature range (26-125°C) by heating with an infrared light. The diameter and bias angle of coils formed in the spandex yarn were observed and measured microscopically (ISSCO-OPTEK microscopic camera).

6.3 Results

6.3.1 Characteristic Properties of Actuator Segments

The critical torque to initiate coil formation in the spandex yarns were measured. Figure 6.5(a) shows torque-torsional rotation curves for three different diameter yarns each of 10 mm length. The axially applied force was kept constant at 0.02 N while the yarn was rotated at one end and fixed at the other end. All three samples showed a linear increase in torque with increasing rotation angle and with a distinct change in slope that corresponded to the initial formation of the first coil turn. The axial displacement of the yarn during twisting and with a constant axial force was also measured [Figure 6.5(b)]. The yarn contraction during twisting and before coil formation was less than 3% of the yarn length. The rate of length contraction with twist insertion increased significantly as the first coil turn formed. The larger diameter spandex yarns generated the largest length contractions of up to 30% from the formation of one coil turn.

The critical torque required to initiate coiling increased with spandex yarn diameter. The predicted critical torques were calculated using the Ross criterion and the measured spandex elastic modulus of 0.24 MPa. As shown in Figure 6.5(c) the calculated critical torques increased with both spandex yarn diameter and applied tensile force. The measured critical torques were slightly higher than the calculated values for all three yarns, but the results agree within 5% in all cases. Based on this comparison, it is

concluded that the Ross criterion can be used as a reasonable estimate for coiling torque in the further analysis of the series actuator.

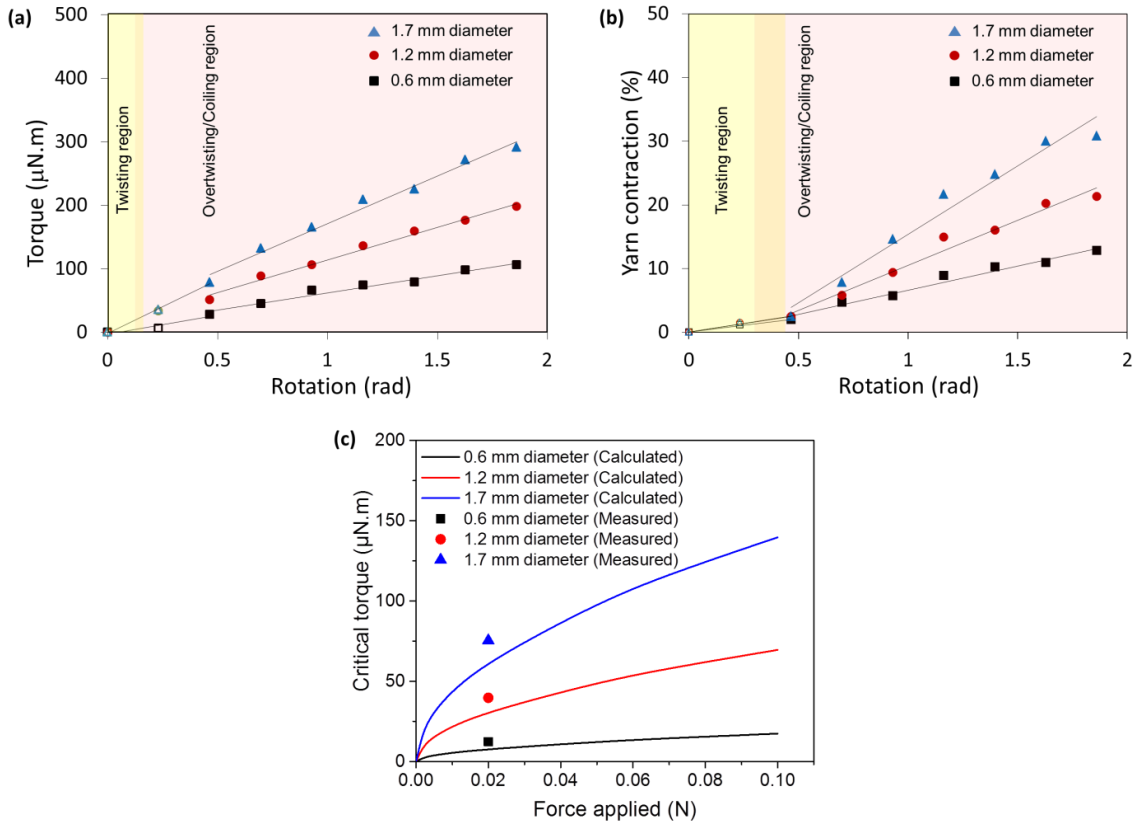

Figure 6.5. Torque requirement for 10 mm long spandex yarn; (a) torque-torsional rotation curves showing change in stiffness of different diameter yarns, (b) yarn contraction during twisting and coiling, and (c) critical torques for differently loaded yarns.

Table 6.1 shows the parameters of the coil forming spandex yarn that will be used for the theoretical calculation of actuator contraction. The amount of rotation needed prior to form the first coil turn (critical twist, n_c) was calculated from the critical torque and the measured yarn stiffness, as given in equation (6.3).

Table 6.1. Spandex yarn (10 mm long) parameters for theoretical calculation of actuator contraction under 0.02 N axial force.

Spandex yarn diameter (D, m)	Torsional modulus before critical point (S_N, μN·m^2)	Calculated critical torque (τ_c, μN·m)	Calculated critical twist (turns)
0.0006	0.60	7.8	0.021
0.0012	1.10	31.1	0.045
0.0017	1.68	62.4	0.059

The torsional rotation produced by thermally actuating a 0.54 mm diameter twisted nylon 6 fibres was calculated as previously described [185] using measured values of the radial thermal expansion and torsional stiffness. As described in Chapter 3, free torsional rotation of twisted nylon 6 depends only on the amount of twist inserted into the fibre and the diameter expansion caused by the heating process [185]. The torsional stiffness of the heated nylon 6 fibre was calculated from the previously reported shear modulus (G_A) value at the maximum temperature of 125°C [182, 184]. Radial thermal expansion was measured microscopically over the same temperature range of 26-125°C that was used for actuation test (Figure 6.6). These measurements were used to calculate the expected free rotation of the nylon 6 fibre, as given by equation (6.2). Since the diameter of the twisted nylon 6 fibre was kept constant for all experiments, the blocked torque was also independent of fibre length. Table 6.2 summarises the torsional and thermal properties of the twisted nylon fibre used for theoretical calculation of muscle contraction.

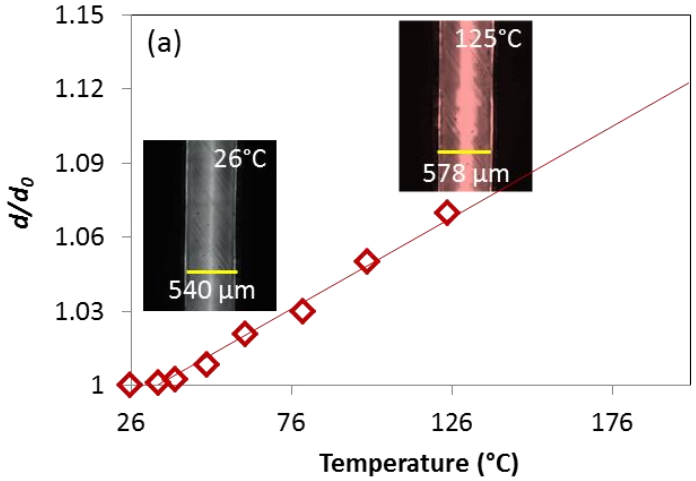

Figure 6.6. Thermal expansivity of twisted nylon 6 fibre diameter ($\boldsymbol{d/d_0}$) over 26-125°C temperature range.

Table 6.2. Torsional and thermal properties of 0.54 mm diameter twisted nylon fibre.

Temperature	Shear modulus (G_A, GPa)	Radial thermal expansion (%)	Blocked torque ($\tau_{blocked}$, µN·m)	Free rotation (Δn_{free}, turns/m)
26°C	0.40	-	-	
125°C	0.30	7%	440	30

6.3.2 Spandex Coil Geometry

The theoretical calculation of the muscle contraction requires the measurement of the diameter and bias angle of the coils that form in the spandex yarn. Figure 6.7(a) shows images of three different diameter spandex yarns when the first coil is formed at a constant 0.02 N axial force. For all spandex yarns investigated, a similar coil bias angle was produced at this lowest applied force. The coil bias angles were negative as defined in Figure 6.2. The single coil model is illustrated from the top [Figure 6.7(b)] to show the active diameter (D_c) of yarn coil was considered to be calculated by subtracting yarn

diameter (D_y) from coil outer diameter (D). Figure 6.7(c) shows coils formed in the 1.7 mm diameter spandex yarn and when the axial force applied during coil formation varied from 0.02 N to 0.1 N. When higher axial forces were applied, the formed coils were deformed and stretched out so that the coil bias angles increased.

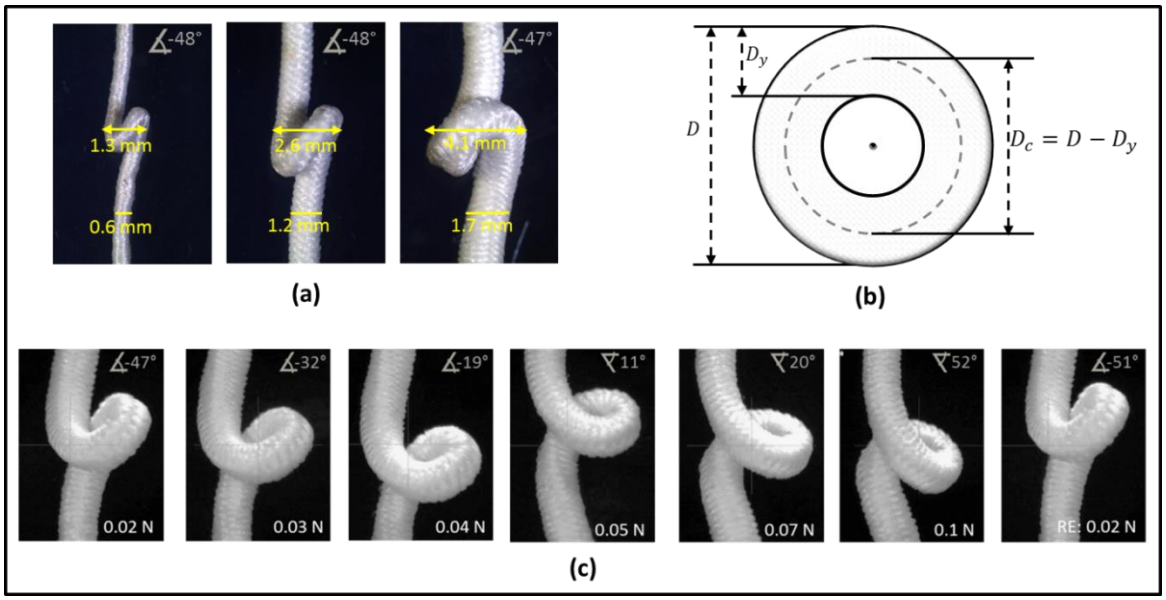

Figure 6.7. Dimension and geometry of spandex yarn coils; (a) three different diameter yarns showed similar coil bias angle when twisted under 0.02 N axial force, (b) coils formed in 1.7 mm diameter yarn when actuated under different axial forces increasing from 0.02 N to 0.1 N and then repeated at 0.02 N; and (c) top view of yarn coil showing active diameter ($\boldsymbol{D_c}$) to be used in theoretical calculation of muscle contraction.

The proof of active diameter concept was experimentally evaluated by using a solid rubber cylinder. A portion of the solid rubber cylinder (length, L_S = 264 mm and diameter, D_y = 10 mm) was wrapped around a 10 mm diameter cylindrical mandrel which forms 4 full coil turns [Figure 6.8(a)]. The outer diameter (D) of the coil was measured to be 30.5 mm; therefore, the active coil diameter was calculated as 20.5 mm. From Figure 6.8(b), the expression for length of coil diameter can be expressed as:

$$L_c = \sqrt{{L_S}^2 - (\pi . N_c . D_c)^2} \tag{6.9}$$

The calculated coil length was found to be ~58 mm which agrees quite accurately with the measured coil length of ~61 mm. These results confirm that the active coil diameter is the most appropriate dimension in using the single coil model to evaluate the overall contraction of the series muscle.

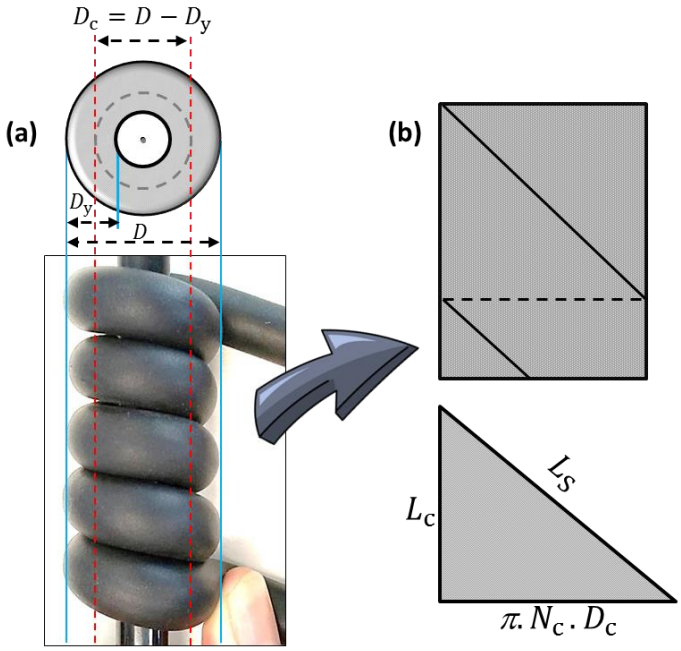

Figure 6.8. Experimental validation of the use of active coil diameter ($\boldsymbol{D_c}$) to calculate overall series muscle contraction; (a) coil dimensions, (and (b) single helix model for calculation.

6.3.3 Tensile Actuation Results

First experiments used five different lengths of 1.7 mm diameter spandex yarn with a constant 2:1 ratio of nylon fibre to spandex yarn length. Reproducible results with fully reversible actuation were obtained for all samples when heated and cooled over the 26-125°C temperature range [Figure 6.9(a)]. The actuation stroke increased with increasing overall combined sample length, but actuation strains remained at ~10% since strains

are independent of starting length. This actuation strain is similar to that obtained from fully twisted and coiled nylon 6,6 fibres when heated over the same temperature range [155]. The rate of contraction of the series nylon-spandex actuators was higher when the samples were heated above 60°C which accords with larger torsional rotation described in Chapter 2 for nylon 6 above its glass transition temperature (T_g~ 50°C) [211]. Actuation tests were also conducted for a 10 mm long spandex yarn attached with 20 mm twisted nylon 6 fibre under different isotonic loading conditions [Figure 6.9(b)]. Since the critical torque and rotation were shown to be larger for muscles subjected to higher axial force, a lower fraction of the overall twisted fibre rotation is then available for coiling the spandex yarn. Consequently, the overall muscle contraction decreased significantly at higher applied tensile forces. Notably, reversible actuation was observed even at the higher loading conditions.

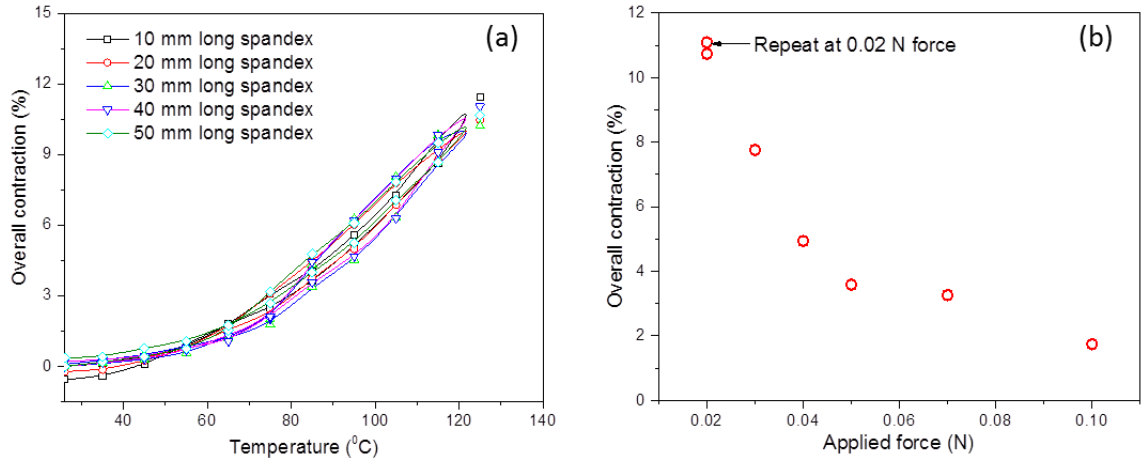

Figure 6.9. Experimentally obtained muscle contraction for 0.54 mm twisted nylon 6 fibre attached to 1.7 mm diameter spandex yarn; (a) in terms of different spandex lengths where the spandex yarn length was always double the twisted nylon 6 lengths, and (b) in terms of externally applied tensile force acting on a sample of 10 mm long spandex yarn and 20 mm long twisted nylon 6 fibre.

6.4 Discussion

Calculated tensile strokes occurring as a result of torsion-induced coil formation in the spandex yarn were obtained using equations (6.1), (6.2), (6.4) and (6.7). The free torsional stroke expected from the nylon fibre was first calculated using equation (6.2) from the measured nylon fibre diameter at various temperatures over the experimental range. Measured fibre torsional stiffnesses were then used with equation (6.4) to determine the torsional stroke available when the nylon fibre was connected in series with the spandex yarn. This calculated torsional stroke (Δn) was experimentally verified by observing the junction rotation during the heating of a 180 mm long nylon 6 fibre attached in series to a 30 mm long, 0.6 mm diameter spandex yarn [Figure 6.10(a)]. At the maximum actuation temperature (125°C), a measured rotation of 2 turns was observed which agreed within 2% of the calculated result. The critical torsional stroke needed for first coil turn formation was calculated using equations (6.1) and (6.3) and the measured spandex yarn torsional modulus. The analysis of coiling can be expressed graphically by plotting the torque-stroke curve of the twisted nylon fibre super-imposed with the torsional stiffness curve of the coiling spandex yarns. Figure 6.10(b) shows the torque-stroke curve in which free rotation and blocked torque of a 20 mm long twisted nylon fibre is plotted and connected (green dotted line). The green shaded region now shows the rotation available ($\Delta n - n_c$) for spandex coil formation.

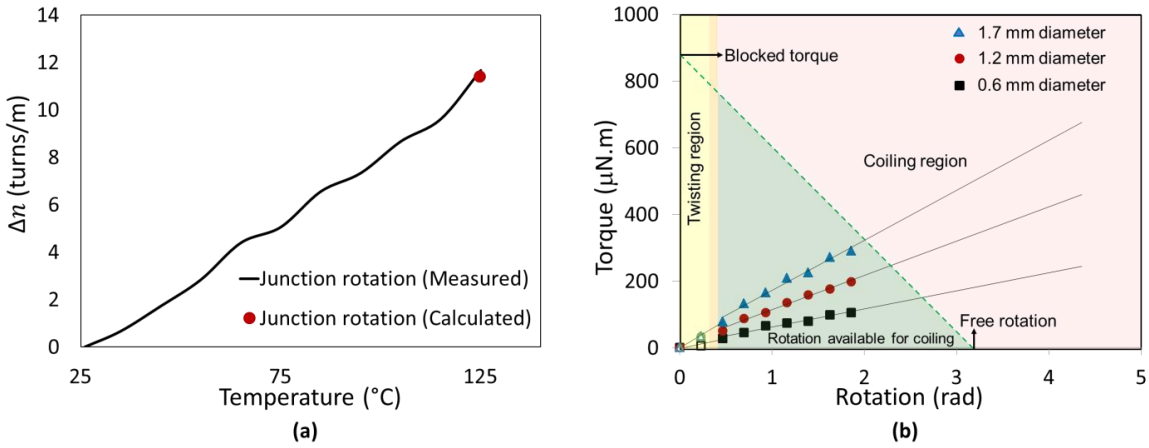

Figure 6. 10. (a) Thermally induced torsional rotation at the junction of a 180 mm long nylon 6 fibre and 30 mm long, 0.6 mm diameter spandex yarn. (b) Graphical representation of effective torsional rotation of a 20 mm long 540 μm twisted nylon 6 fibre when heated from 26°C to 125°C and the formation of coils in serially attached 10 mm long spandex yarns of three different diameters.

Finally, the tensile stroke was calculated from equation (6.7) using the measured coil diameter and bias angles. Figure 6.11 shows plots for calculated muscle contraction using three different spandex diameters and each with five different lengths. Tensile contractions are expressed as a percentage compared to the total initial length. All spandex yarns showed a peak contraction as the twisted nylon yarn length increased. The torsional stroke generated by the twisted nylon fibre initially increased and then decreased as the fibre length increased due to the competition between increasing free stroke and decreasing torsional stiffness. The maximum contraction strain was consistent regardless of the spandex yarn lengths and occurred at a consistent ratio of ~2 of spandex yarn to twisted nylon fibre length (inset Figure 6.11(d)). The maximum peak contraction was found to depend on the spandex yarn diameter. The largest diameter yarn (1.7 mm diameter) had a maximum peak contraction of ~12% compared to ~9.7% (1.2 mm diameter) and ~7% (0.6 mm diameter). This effect reflects the dominance of the larger coil diameter formed from larger diameter spandex yarns (Figure 6.11(d)).

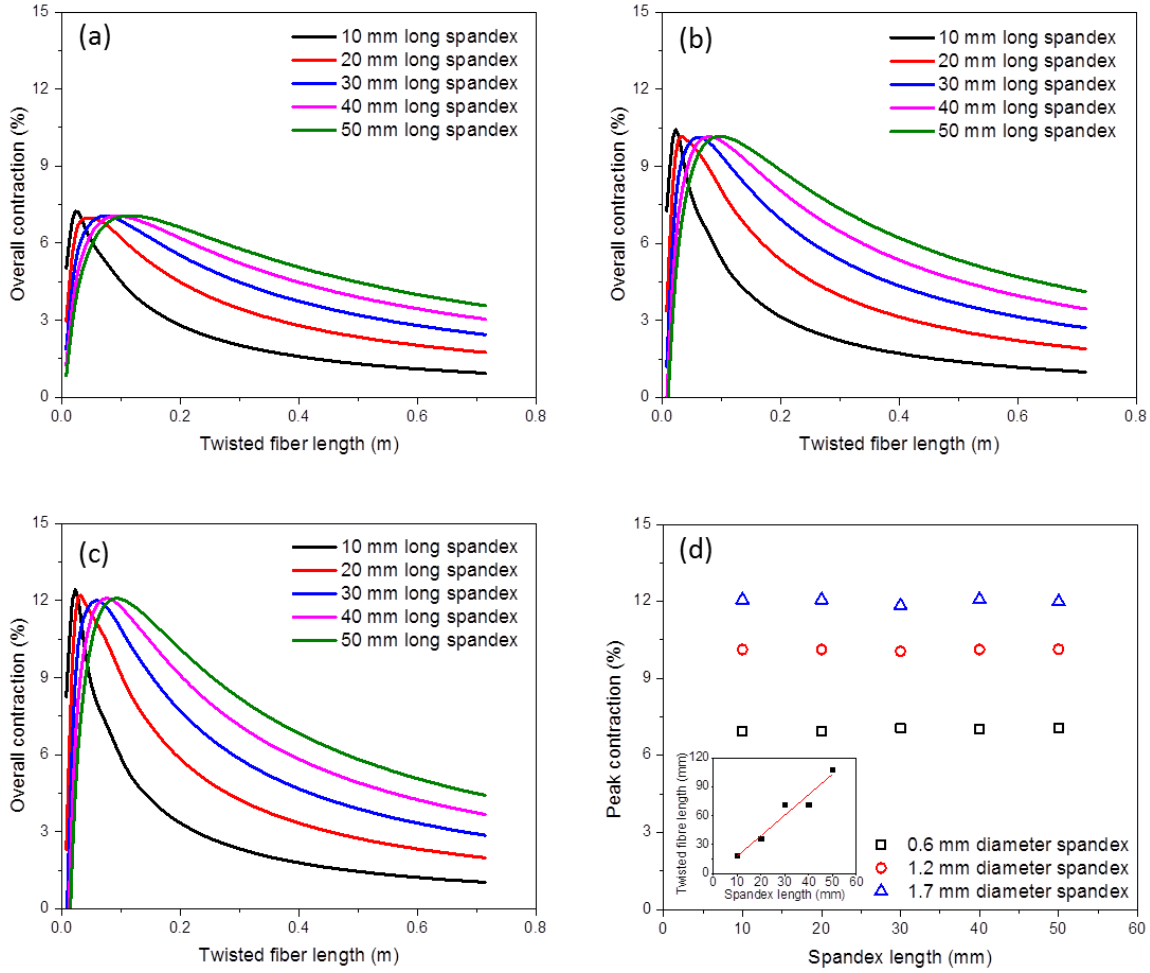

Figure 6.11. Theoretically predicted contraction of spandex yarn attached to a twisted nylon 6 fibre artificial muscles in terms of different muscle lengths for; (a) 0.6 mm diameter yarn, (b) 1.2 mm diameter yarn, (c) 1.7 mm diameter yarn, and (4) peak contraction comparison (inset shows the ratio of twisted fibre to spandex yarn that provides the peak contraction).

The theoretically calculated results were then compared to the measured muscle contraction. Figure 6.12(a) shows the comparative peak contraction between calculated and measured values of the actuators having 2:1 length ratios of twisted nylon 6 fibre to attached spandex yarn. Figure 6.12(b) shows the actuator contraction of a 10 mm long spandex yarn connected to a 20 mm long nylon 6 fibre when subjected to different axial

loads. For all of the experimental conditions, experimental results agree with the theoretical calculations within the limit of ~10% standard deviations. .

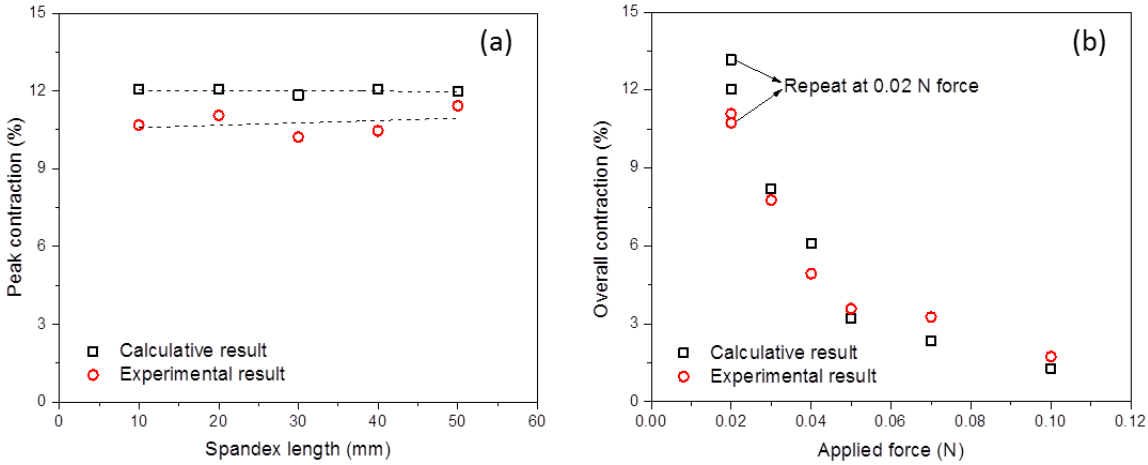

Figure 6.12. Comparison of theoretically calculated muscle contraction to that measured ones; (a) in terms of different muscle length, (b) under different axial force condition.

Additionally, a well-desired characteristic was achieved from the concept of a series actuator. Previous studies have shown that polymer fibres when modified to twisted structure, exhibit low structural stability during the first few actuation cycles [184, 185], therefore training of the fibres is necessary before a consistent result is achieved. This criterion also exists when the actuation experiments are conducted under different loading conditions i.e. torque applied [185]. In this work, due to the presence of significant rubber-elasticity spandex return spring highly reversible actuation obtained from the very first cycle. Coils of spandex yarn store a significant amount of torque while formed, and released the torque acted to the direction of retwisting during the cooling process of twisted fibre. Hence, both of these torques enhances the reversibility of overall muscle contraction which is practically demanding to use this systems as a feasible real world artificial muscle.

6.5 Summary

A new type of contractile artificial muscle is demonstrated herein with a combination of torsional and tensile actuation. Preliminary aim was to make the muscle functional and then to optimise the contraction ability. Another interest was to investigate the reversibility of actuation and practical usability under different mechanical conditions. A set of identical twisted nylon 6 fibre was fabricated having 540 μm diameter and ~428 twists per meter of fibre length. Spandex yarn was attached to the twisted fibre in series under certain tension blocking the end torsional drive but allowing tensile movement. Thermally induced torsional rotation of twisted fibre caused formation of coils in spandex yarn which resulted in overall muscle contraction. Torsional rotation of twisted fibre and resultant spandex coil geometry are utilized to theoretically predict the amount of muscle contraction by means of a modified single helix theory. Experimental tests were conducted considering similar muscle parameters as used in theoretical calculations and a good agreement was found in between measured and calculated results. Practical applicability of this muscle was evaluated by using different mechanical conditions. It was found that this multifunctional muscle could be useful as a real world actuator system without prior preconditioning which is considered as a significant drawback among other polymer artificial muscles.

CHAPTER 7 Conclusions and Recommendations

7.1 Conclusions

Highly twisted oriented polymer fibres or yarns show large scale torsional actuation from volume expansion that can be induced, for example, thermally or by electrochemical charging. When formed into spring-like coils, the torsional actuation within the fibre or yarn generates powerful tensile actuation per muscle weight. For further development of these coil actuators and for the practical application of torsional actuators, this Ph.D. project aimed to investigate the fundamental mechanism that determines the response of twisted actuators. The aims of the thesis were achieved in a progression of four steps. Initially, a test method with an in-house built apparatus was developed to characterize the torsional actuation and related torsional properties of twisted fibre or yarn structures. Next, torsional actuation was measured from differently twisted fibre and quantitative prediction of such results was successfully made by using a single-helix based model. After that, thermo-mechanical investigation was conducted to evaluate a path in reducing the unwanted torsion based properties (torsional creep, stress relaxation, stroke irreversibility) of twisted oriented polymer fibres. Finally, an integrated contractile artificial muscle system was proposed by utilizing torsion actuation of twisted polymer fibre, and a modified single-helix model was presented to predict the overall muscle contraction.

The research project demonstrated a new test method to measure torsional actuation of twisted fibre or yarn in terms of free stroke and blocked torque in a one-end-tethered system. In addition, it was also shown that the actuation can be measured when operating against an externally applied torque (isotonic) and actuation against a return spring fibre (variable torque). These analyses suggested that all torsional actuation parameters can be determined from knowledge of the free stroke, actuating fibre stiffnesses, return spring stiffness and actuating fibre length. Theoretical prediction of

torsional stroke generation of twisted fibre was developed using torsion mechanics that gave good agreement between experimental measurement and calculated values for the isotonic and return-spring experiments.

Previous investigations of torsional actuation in twisted fibres and yarns have suggested that a single-helix approximation can provide some insight into the actuation mechanism [110, 155]. This project further investigated the scalability of torsional actuation in twisted fibres and yarns and to evaluate the single-helix model for quantitatively predicting torsional stroke and torque. Combined torsional actuation measurements and volume expansion data allows the application of the single-helix model to quantitatively predict the amount of torsional stroke. The starting assumption is that the "string length" in the single helix remains constant during the volume change. For the twisted nylon fibres the "string" can be thought of as the oriented polymer chains helically wrapped around the surface of the fibre. These molecules are likely highly extended and firmly connected through crystalline blocks. This topology exhibits a high axial stiffness and can be considered mechanically inextensible. The single-helix model accurately predicted the torsional stroke based on the measured fibre diameter and length changes occurring during heating of twisted nylon 6, polyethylene and polypropylene fibres. Generated torques were also accurately predicted by the single-helix model when combined with the measured fibre torsional stiffness. Torque was strongly dependent on fibre diameter, along with the amount of inserted twist.

The degree of agreement between the measured torsional actuation parameters and those calculated from the single-helix model was remarkable considering that the model greatly simplifies the complex internal structure of the twisted fibres and yarns to a single helix. In contrast, the real twisted fibre is a solid where the twist angle (α_f)

increases from zero at fibre centre to a maximum at the fibre surface. Treating the twisted fibre as a series of concentric cylinders of increasing diameter and with the same inserted twist provides some insight into why the single helix model is appropriate. Each cylinder in the concentric cylinder model can be described by equation 4.2:

$$\lambda_n = \left[\frac{1}{\tan^2\alpha_f}\left(\frac{\lambda_s^2-\lambda_i^2}{\lambda_d^2}\right)+\frac{\lambda_s^2}{\lambda_d^2}\right]^{1/2} \tag{4.2}$$

where the parameters are defined in Chapter 4. In the case where the string length and twisted fibre length do not change during fibre volume expansion, equation 4.2 reduces to equation 4.3:

$$\lambda_n = \frac{1}{\lambda_d} \tag{4.3}$$

So that all cylinders would show the same torsional rotation. All cylinders would rotate in sychronicity. However, if the fibre length did change appreciably during fibre volume expansion, then equation 4.2 indicates that the torsional rotation of each cylinder would be different and the connection between cylinders would result in a constraining effect. This situation is still to be tested experimentally.

One practical issue raised in early work on both twisted and coiled polymer fibre torsional and tensile actuators was the need for several ‘training cycles’ of heating and cooling to achieve fully reversible actuation. In this project, the effect of annealing conditions applied to twisted nylon 6 monofilament is investigated to overcome the aforementioned issue and it was found that annealing at 200°C eliminates the need for the training cycles. Furthermore, the effect of an applied external torque on the torsional actuation is also investigated and torsional creep is shown to be affected by the temperature and load. The baseline twist in the fibre readjusts to a new level during the

first two heat/cool cycles when the external torque is changed. Thereafter, the torsional untwist and retwist remain consistent in subsequent heat / cool cycles at constant torque.

This thesis also introduced a concept of integrated artificial muscle which shows contractile behaviour originated from torsional actuation of a twisted polymer fibre. The core idea was adapted from the torsional muscle with a return spring fibre connected in series. A spandex yarn is attached to the twisted nylon 6 fibre in series under certain tension blocking the end torsional drive but allowing tensile movement. Thermally induced torsional rotation of twisted fibre caused formation of coils in spandex yarn which resulted in overall muscle contraction. Torsional rotation of twisted fibre and resultant spandex coil geometry are utilized to theoretically predict the amount of muscle contraction by means of a modified single-helix theory. Experimental tests are conducted considering similar muscle parameters as used in theoretical calculations and a good agreement is found in between measured and calculated results. Practical applicability of this muscle is evaluated by using different mechanical conditions. It is found that this multifunctional muscle could be useful as a real world actuator system without prior preconditioning (training cycles) which is considered as a significant drawback among other polymer artificial muscles.

7.2 Future Recommendations

With the development of twisted CNT yarn, graphene oxide yarns, and polymer fibres torsional artificial muscles find more potential applications, such as soft robotics, microfluidic mixing, microsensors, photonic displays, and even energy-harvesting devices. In this thesis, we highlighted the recent advances of polymer fibre based torsional actuators, their actuating mechanism and potential applications, and featured limitations. A detailed actuating mechanism, characterization methods as well as

scalability of these actuators were investigated in this thesis. Several areas of direct extension of this work include:

- The further investigation of the single helix model and the suggested concentric cylinder model to evaluate the torsional actuation in fibres where appreciable length changes occur during actuation.
- Helix model studies can be approximated for twist induced hierarchically helical coiled structures. Further work can also extend the modelling to study the untwisting of co-twisted fibres and their effect on linear actuation of hierarchical coiled structures.
- Investigation of the origin of the thermal expansion anisotropy in oriented fibres. The present thesis has shown that the measured length and diameter expansions can be used to predict the torsional actuation. However, there is no accurate prediction of the thermal expansion based on first principles.
- Creep has been shown to influence the load-dependency and time-dependency of the torsional actuation. Methods for mitigating creep in oriented polymers could be investigated for twisted polymer fibre torsional actuators.
- Further optimisation of the series connected torsional actuator with a coiling fibre could be considered and guided by an extension of the theory presented in Chapter 6.

Despite the developments highlighted in this thesis, it should also be understood that the gap between the lab bench and real world application is still massive. More efforts are required to narrow the gap and the future development of practical applications for torsional actuators needs to address many challenges, including:

- High-speed torsional actuators based on small diameter twisted fibre/yarn still lack acceptable torque generation compared to that of low-speed actuators such as SMAs. Practical methods for increasing the speed of fibre expansion and contraction in twisted polymer fibres need to be developed.
- Attention should also be paid to the biocompatibility of the torsional actuators as such systems could be useful for several biomedical aspects such as microscopic surgery tool, and drug delivery devices.
- Bulk and continuous production of twisted fibre/yarn actuators are needed. Small lengths of twisted fibre are easy to make, but mass production techniques will be needed for commercial application of torsional actuators.

As a final point, exciting progress has been made in recent decade in the field of torsional actuators. Extraordinary performances, novel and integral functionalities and convenient fabrication procedures have been exploited. However, investigations on the protocols for the massive production of controllable torsional actuators are needed to translate these promising systems into designer artificial muscles for human welfare.

References

[1] J.D.W. Madden, N.A. Vandesteeg, P.A. Anquetil, P.G.A. Madden, A. Takshi, R.Z. Pytel, S.R. Lafontaine, P.A. Wieringa, I.W. Hunter, Artificial muscle technology: physical principles and naval prospects, IEEE Journal of Oceanic Engineering 29(3) (2004) 706-728.

[2] M. Shahinpoor, M. Mojarrad, Soft actuators and artificial muscles, US6109852 A, Google Patents, U.S.A., 2000.

[3] Q. Pei, R. Pelrine, M.A. Rosenthal, S. Stanford, H. Prahlad, R.D. Kornbluh, Recent progress on electroelastomer artificial muscles and their application for biomimetic robots, 2004, pp. 41-50.

[4] Y. Bar-Cohen, Electroactive Polymers as Artificial Muscles: A Review, Journal of Spacecraft and Rockets 39(6) (2002) 822-827.

[5] K. Dai, C.Q. Ning, Shape Memory Alloys and their Medical Application, in: D.G. Poitout (Ed.), Biomechanics and Biomaterials in Orthopedics, Springer London, London, 2004, pp. 179-184.

[6] Z. Guo, H. Yu, L.B. Wee, Design of a novel compliant differential Shape Memory Alloy actuator, 2013 IEEE/RSJ International Conference on Intelligent Robots and Systems, 2013, pp. 4925-4930.

[7] D.J. Hartl, D.C. Lagoudas, Aerospace applications of shape memory alloys, Proceedings of the Institution of Mechanical Engineers, Part G: Journal of Aerospace Engineering 221(4) (2007) 535-552.

[8] S. Jae-Eul, Q. Ying-Jun, W. Wei, R. Hugo, S. Sung-Hyuk, A. Sung-Hoon, A smart soft actuator using a single shape memory alloy for twisting actuation, Smart Materials and Structures 24(12) (2015) 125033.

[9] K.P. Jamie, H. Elliot, J.W. Robert, A novel low-profile shape memory alloy torsional actuator, Smart Materials and Structures 19(12) (2010) 125014.

[10] K.P. Jamie, J.W. Robert, A bidirectional shape memory alloy folding actuator, Smart Materials and Structures 21(6) (2012) 065013.

[11] A.P. Jardine, J.N. Kudva, C.A. Martin, K. Appa, Shape memory alloy TiNi actuators for twist control of smart wing designs, 1996, pp. 160-165.

[12] J.E. Jeanette, C. Inderjit, In-flight tracking of helicopter rotor blades using shape memory alloy actuators, Smart Materials and Structures 10(1) (2001) 104.

[13] D.C. Lagoudas, Shape Memory Alloys: Modeling and Engineering Applications, Springer US2008.

[14] L. Lecce, A. Concilio, Shape Memory Alloy Engineering: For Aerospace, Structural and Biomedical Applications, Elsevier Science2014.

[15] M. Elahinia, Shape Memory Alloy Actuators: Design, Fabrication and Experimental Evaluation, First ed., Wiley, U.S.A., 2016.

[16] S. Chiba, S. Stanford, R. Pelrine, R. Kornbluh, H. Prahlad, Electroactive Polymer Artificial Muscle, Journal of the Robotics Society of Japan 24(4) (2006) 466-470.

[17] J.W. Paquette, K.J. Kim, Ionomeric electroactive polymer artificial muscle for naval applications, IEEE Journal of Oceanic Engineering 29(3) (2004) 729-737.

[18] K.J. Kim, S. Tadokoro, Electroactive Polymers for Robotic Applications: Artificial Muscles and Sensors, Springer London2010.

[19] C. Federico, K. Roy, S.-L. Peter, A. Gursel, Electroactive polymer actuators as artificial muscles: are they ready for bioinspired applications?, Bioinspiration & Biomimetics 6(4) (2011) 045006.

[20] S.G. Wax, R.R. Sands, Electroactive polymer actuators and devices, SPIE, U.S.A., 1999, pp. 2-10.

[21] Y. Bar-Cohen, Q. Zhang, Electroactive Polymer Actuators and Sensors, MRS Bulletin 33(3) (2008) 173-181.

[22] R. Kornbluh, R. Pelrine, J. Eckerle, J. Joseph, Electrostrictive polymer artificial muscle actuators, Proceedings. 1998 IEEE International Conference on Robotics and Automation (Cat. No.98CH36146), 1998, pp. 2147-2154 vol.3.

[23] S. Chiba, M. Waki, R. Kornbluh, R. Pelrine, Innovative power generators for energy harvesting using electroactive polymer artificial muscles, 2008, pp. 692715-692715-9.

[24] K. Kishi, Piezoelectric vibrating elements and piezoelectric electroacoustic transducers, Google Patents, 1987.

[25] R. Pelrine, R. Kornbluh, Q. Pei, J. Joseph, High-Speed Electrically Actuated Elastomers with Strain Greater Than 100%, Science 287(5454) (2000) 836-839.

[26] C. Lemonon, F. Micheron, P. Wang, Polymeric piezoelectric transducer with thermoformed protuberances, US4284921 A, Google Patents, U.S.A, 1981.

[27] G.K. Klute, J.M. Czerniecki, B. Hannaford, Artificial Muscles: Actuators for Biorobotic Systems, The International Journal of Robotics Research 21(4) (2002) 295-309.
[28] R.H. Baughman, Conducting polymer artificial muscles, Synthetic Metals 78(3) (1996) 339-353.
[29] R.K. Josephson, Contraction Dynamics and Power Output of Skeletal Muscle, Annual Review of Physiology 55(1) (1993) 527-546.
[30] J.D.W. Madden, N.A. Vandesteeg, P.A. Anquetil, P.G.A. Madden, A. Takshi, R.Z. Pytel, S.R. Lafontaine, P.A. Wieringa, I.W. Hunter, Artificial muscle technology: physical principles and naval prospects, Oceanic Engineering, IEEE Journal of 29(3) (2004) 706-728.
[31] M. Kohl, Shape Memory Microactuators, Springer2004.
[32] M. Elahinia, Shape Memory Alloy Actuators: Design, Fabrication and Experimental Evaluation, Wiley, U.S.A., 2015.
[33] C.K. Andrew, P.C. Gregory, Thermo-mechanical characterization of shape memory alloy torque tube actuators, Smart Materials and Structures 9(5) (2000) 665.
[34] C. Liang, F.M. Davidson, L.M. Schetky, F.K. Straub, Applications of torsional shape memory alloy actuators for active rotor blade control: opportunities and limitations, 1996, pp. 91-100.
[35] H. Prahlad, I. Chopra, Modeling and Experimental Characterization of SMA Torsional Actuators, Journal of Intelligent Material Systems and Structures 18(1) (2007) 29-38.
[36] K. Gilpin, E. Torres-Jara, D. Rus, Controlling Closed-Chain Robots with Compliant SMA Actuators: Algorithms and Experiments, in: O. Khatib, V. Kumar, G. Sukhatme (Eds.), Experimental Robotics: The 12th International Symposium on Experimental Robotics, Springer Berlin Heidelberg, Berlin, Heidelberg, 2014, pp. 149-163.
[37] H. Tobushi, T. Sakuragi, Y. Sugimoto, Deformation and Rotary Driving Characteristics of a Shape-Memory Alloy Thin Strip Element, MATERIALS TRANSACTIONS 49(1) (2008) 151-157.
[38] B.H. Shin, T. Jang, B.-J. Ryu, Y. Kim, A modular torsional actuator using shape memory alloy wires, Journal of Intelligent Material Systems and Structures 27(12) (2016) 1658-1665.

[39] J.-s. Koh, S.-r. Kim, K.-j. Cho, Self-Folding Origami Using Torsion Shape Memory Alloy Wire Actuators, (46377) (2014) V05BT08A043.

[40] Z. Zhakypov, J.L. Huang, J. Paik, A Novel Torsional Shape Memory Alloy Actuator: Modeling, Characterization, and Control, IEEE Robotics & Automation Magazine 23(3) (2016) 65-74.

[41] S. Jun, P.D. Jaydev, Design, modeling and characterization of a novel meso-scale SMA-actuated torsion actuator, Smart Materials and Structures 24(10) (2015) 105005.

[42] M. Salerno, S. Tognarelli, C. Quaglia, P. Dario, A. Menciassi, Anchoring frame for intra-abdominal surgery, The International Journal of Robotics Research 32(3) (2013) 360-370.

[43] H. Tobushi, T. Sakuragi, Y. Sugimoto, Deformation and Rotary Driving Characteristics of a Shape-Memory Alloy Thin Strip Element, Materials Transactions 49(1) (2007) 151-157.

[44] H. Tobushi, E. Pieczyska, K. Miyamoto, K. Mitsui, Torsional deformation characteristics of TiNi SMA tape and application to rotary actuator, Journal of Alloys and Compounds 577, Supplement 1 (2013) S745-S748.

[45] K.J. Gabriel, W.S.N. Trimmer, J.A. Walker, A micro rotary actuator using shape memory alloys, Sensors and Actuators 15(1) (1988) 95-102.

[46] H. Rodrigue, B. Bhandari, M.-W. Han, S.-H. Ahn, A shape memory alloy–based soft morphing actuator capable of pure twisting motion, Journal of Intelligent Material Systems and Structures 26(9) (2015) 1071-1078.

[47] Z. Zhakypov, J.-L. Huang, J. Paik, Modeling, Characterization and Control of a Novel Torsional Shape Memory Alloy (SMA) Actuator, IEEE Robotics and Automation Magazine 23(3) (2016) 65-74.

[48] J.G. Drobny, Polymers for Electricity and Electronics: Materials, Properties, and Applications, Wiley, U.S.A., 2012.

[49] W.H. Duan, Q. Wang, S.T. Quek, Applications of Piezoelectric Materials in Structural Health Monitoring and Repair: Selected Research Examples, Materials 3(12) (2010) 5169.

[50] D. Damjanovic, R.E. Newnham, Electrostrictive and Piezoelectric Materials for Actuator Applications, Journal of Intelligent Material Systems and Structures 3(2) (1992) 190-208.

[51] T. Morita, R. Yoshida, Y. Okamoto, M.K. Kurosawa, T. Higuchi, A smooth impact rotation motor using a multi-layered torsional piezoelectric actuator, IEEE Transactions on Ultrasonics, Ferroelectrics, and Frequency Control 46(6) (1999) 1439-1445.
[52] K. Jaehwan, K. Byungwoo, Performance test and improvement of piezoelectric torsional actuators, Smart Materials and Structures 10(4) (2001) 750.
[53] A.E. Glazounov, Q.M. Zhang, C. Kim, Torsional Actuator and Stepper Motor Based on Piezoelectric d15 Shear Response, Journal of Intelligent Material Systems and Structures 11(6) (2000) 456-468.
[54] C.L. Pan, Z.H. Feng, Y.T. Ma, Y.B. Liu, Small torsional piezoelectric fiber actuators with helical electrodes, Applied Physics Letters 92(1) (2008) 012923.
[55] D. Brei, B.J. Cannon, Piezoceramic hollow fiber active composites, Composites Science and Technology 64(2) (2004) 245-261.
[56] B.M. Finio, R.J. Wood, Optimal energy density piezoelectric twisting actuators, 2011 IEEE/RSJ International Conference on Intelligent Robots and Systems, 2011, pp. 384-389.
[57] J.G. Webster, The Measurement, Instrumentation, and Sensors: Handbook, CRC Press1999.
[58] T.R. Gururaja, Piezoelectric transducers for medical ultrasonic imaging, Applications of Ferroelectrics, 1992. ISAF '92., Proceedings of the Eighth IEEE International Symposium on, 1992, pp. 259-265.
[59] D.H. Pearce, A. Hooley, T.W. Button, On piezoelectric super-helix actuators, Sensors and Actuators A: Physical 100(2–3) (2002) 281-286.
[60] J.F. Tressler, S. Alkoy, R.E. Newnham, Piezoelectric Sensors and Sensor Materials, Journal of Electroceramics 2(4) (1998) 257-272.
[61] D.H. Pearce, K.A. Seffen, T.W. Button, Net shape formed spiral and helical piezoelectric actuators, Journal of Materials Science 37(15) (2002) 3117-3122.
[62] F. Mohammadi, A.L. Kholkin, B. Jadidian, A. Safari, High-displacement spiral piezoelectric actuators, Applied Physics Letters 75(16) (1999) 2488-2490.
[63] D.J. Bell, L. Dong, B.J. Nelson, M. Golling, L. Zhang, D. Grützmacher, Fabrication and Characterization of Three-Dimensional InGaAs/GaAs Nanosprings, Nano Letters 6(4) (2006) 725-729.

[64] K. Liu, C. Cheng, J. Suh, R. Tang-Kong, D. Fu, S. Lee, J. Zhou, L.O. Chua, J. Wu, Powerful, Multifunctional Torsional Micromuscles Activated by Phase Transition, Advanced Materials 26(11) (2014) 1746-1750.

[65] D. Valtorta, Dynamic Torsion Test for the Mechanical Characterization of Soft Biological Tissues, Cuvillier, ETH ZURICH, 2007.

[66] A. O'Halloran, F. O'Malley, P. McHugh, A review on dielectric elastomer actuators, technology, applications, and challenges, Journal of Applied Physics 104(7) (2008) 071101.

[67] J.S. Bashkin, R. Kornbluh, H. Prahlad, A. Wong-Foy, Biomedical Applications of Dielectric Elastomer Actuators, Biomedical Applications of Electroactive Polymer Actuators, John Wiley & Sons, Ltd2009, pp. 395-410.

[68] J.D. Madden, T.S. Kanigan, S. Lafontaine, I.W. Hunter, Conducting polymer actuator, US6249076 B1, Google Patents, U.S.A., 2001.

[69] K. Asai, K. Yokoyama, Conductive polymer actuator, US 7259495 B2, Google Patents, U.S.A., 2007.

[70] T.A. Skotheim, Handbook of Conducting Polymers, Second Edition, Taylor & Francis1997.

[71] Science and Applications of Conducting Polymers, Papers from the Sixth European Industrial Workshop, Taylor & Francis1991.

[72] E. Smela, Conjugated Polymer Actuators for Biomedical Applications, Advanced Materials 15(6) (2003) 481-494.

[73] A. Gürsel, M. Philippe, M.S. Geoffrey, A methodology towards geometry optimization of high performance polypyrrole (PPy) actuators, Smart Materials and Structures 15(2) (2006) 243.

[74] Y. Fang, X. Tan, G. Alici, Robust Adaptive Control of Conjugated Polymer Actuators, IEEE Transactions on Control Systems Technology 16(4) (2008) 600-612.

[75] C. Immerstrand, K. Holmgren-Peterson, K.E. Magnusson, E. Jager, M. Krogh, M. Skoglund, A. Selbing, O. Inganäs, Conjugated-polymer micro- and milliactuators for biological applications, MRS Bulletin 27(6) (2002) 461-464.

[76] Y. Wu, D. Zhou, G.M. Spinks, P.C. Innis, W.M. Megill, G.G. Wallace, TITAN: a conducting polymer based microfluidic pump, Smart Materials and Structures 14(6) (2005) 1511.

[77] Y. Fang, X. Tan, A novel diaphragm micropump actuated by conjugated polymer petals: Fabrication, modeling, and experimental results, Sensors and Actuators A: Physical 158(1) (2010) 121-131.
[78] T. James, A. Patrick, F. Timothy, C. Angela, Z. Mike Del, H. Ian, The application of conducting polymers to a biorobotic fin propulsor, Bioinspiration & Biomimetics 2(2) (2007) S6.
[79] M. Scott, A. Gursel, T. Van-Tan, S. Geoffrey, Finding NEMO (novel electromaterial muscle oscillator): a polypyrrole powered robotic fish with real-time wireless speed and directional control, Smart Materials and Structures 18(9) (2009) 095009.
[80] I.A. Anderson, T. Hale, T. Gisby, T. Inamura, T. McKay, B. O'Brien, S. Walbran, E.P. Calius, A thin membrane artificial muscle rotary motor, Applied Physics A 98(1) (2009) 75.
[81] I.A. Anderson, E.P. Calius, T. Gisby, T. Hale, T. McKay, B. O'Brien, S. Walbran, A dielectric elastomer actuator thin membrane rotary motor, 2009, pp. 72871H-72871H-10.
[82] J. Heim, R.E. Pelrine, R.D. Kornbluh, J.S. Eckerle, Electroactive polymer rotary motors, Google Patents, 2004.
[83] R. Waché, D.N. McCarthy, S. Risse, G. Kofod, Rotary Motion Achieved by New Torsional Dielectric Elastomer Actuators Design, IEEE/ASME Transactions on Mechatronics 20(2) (2015) 975-977.
[84] Y. Fang, T.J. Pence, X. Tan, Fiber-Directed Conjugated-Polymer Torsional Actuator: Nonlinear Elasticity Modeling and Experimental Validation, IEEE/ASME Transactions on Mechatronics 16(4) (2011) 656-664.
[85] M. Otake, Electroactive Polymer Gel Robots: Modelling and Control of Artificial Muscles, Springer Berlin Heidelberg2010.
[86] J.-S. Plante, S. Dubowsky, Large-scale failure modes of dielectric elastomer actuators, International Journal of Solids and Structures 43(25–26) (2006) 7727-7751.
[87] R. Balint, N.J. Cassidy, S.H. Cartmell, Conductive polymers: Towards a smart biomaterial for tissue engineering, Acta Biomaterialia 10(6) (2014) 2341-2353.
[88] K.J. Kim, S. Tadokoro, Electroactive Polymers for Robotic Applications: Artificial Muscles and Sensors, Springer London2007.

[89] B. Tondu, Modelling of the McKibben artificial muscle: A review, Journal of Intelligent Material Systems and Structures 23(3) (2012) 225-253.
[90] Z. Zhang, M. Philen, Pressurized artificial muscles, Journal of Intelligent Material Systems and Structures 23(3) (2012) 255-268.
[91] R. Tiwari, M.A. Meller, K.B. Wajcs, C. Moses, I. Reveles, E. Garcia, Hydraulic artificial muscles, Journal of Intelligent Material Systems and Structures 23(3) (2012) 301-312.
[92] B. Matthew, A.M. Michael, G. Ephrahim, Variable recruitment fluidic artificial muscles: modeling and experiments, Smart Materials and Structures 23(7) (2014) 074009.
[93] Y.K. Lee, I. Shimoyama, A skeletal framework artificial hand actuated by pneumatic artificial muscles, Proceedings 1999 IEEE International Conference on Robotics and Automation (Cat. No.99CH36288C), 1999, pp. 926-931 vol.2.
[94] G.K. Klute, J.M. Czerniecki, B. Hannaford, McKibben artificial muscles: pneumatic actuators with biomechanical intelligence, 1999 IEEE/ASME International Conference on Advanced Intelligent Mechatronics (Cat. No.99TH8399), 1999, pp. 221-226.
[95] K.E. Gordon, G.S. Sawicki, D.P. Ferris, Mechanical performance of artificial pneumatic muscles to power an ankle–foot orthosis, Journal of Biomechanics 39(10) (2006) 1832-1841.
[96] B. Verrelst, R. Van Ham, B. Vanderborght, D. Lefeber, F. Daerden, M. Van Damme, Second generation pleated pneumatic artificial muscle and its robotic applications, Advanced Robotics 20(7) (2006) 783-805.
[97] D. Sangian, S. Naficy, G.M. Spinks, B. Tondu, The effect of geometry and material properties on the performance of a small hydraulic McKibben muscle system, Sensors and Actuators A: Physical 234 (2015) 150-157.
[98] C. Xiang, M.E. Giannaccini, T. Theodoridis, L. Hao, S. Nefti-Meziani, S. Davis, Variable stiffness Mckibben muscles with hydraulic and pneumatic operating modes, Advanced Robotics 30(13) (2016) 889-899.
[99] M. Michael, C. Jordan, V. Alexander, B. Matthew, G. Ephrahim, Improving actuation efficiency through variable recruitment hydraulic McKibben muscles: modeling, orderly recruitment control, and experiments, Bioinspiration & Biomimetics 11(6) (2016) 065004.

[100] B. Tondu, P. Lopez, Modeling and control of McKibben artificial muscle robot actuators, IEEE Control Systems 20(2) (2000) 15-38.
[101] B. Tondu, S. Ippolito, J. Guiochet, A. Daidie, A Seven-degrees-of-freedom Robot-arm Driven by Pneumatic Artificial Muscles for Humanoid Robots, The International Journal of Robotics Research 24(4) (2005) 257-274.
[102] D. Villegas, M. Van Damme, B. Vanderborght, P. Beyl, D. Lefeber, Third–Generation Pleated Pneumatic Artificial Muscles for Robotic Applications: Development and Comparison with McKibben Muscle, Advanced Robotics 26(11-12) (2012) 1205-1227.
[103] D.G. Caldwell, G.A. Medrano-Cerda, M. Goodwin, Control of pneumatic muscle actuators, IEEE Control Systems 15(1) (1995) 40-48.
[104] G.K. Klute, B. Hannaford, Fatigue characteristics of McKibben artificial muscle actuators, Proceedings. 1998 IEEE/RSJ International Conference on Intelligent Robots and Systems. Innovations in Theory, Practice and Applications (Cat. No.98CH36190), 1998, pp. 1776-1781 vol.3.
[105] C. Ching-Ping, B. Hannaford, Measurement and modeling of McKibben pneumatic artificial muscles, IEEE Transactions on Robotics and Automation 12(1) (1996) 90-102.
[106] J.R. Erickson, Artificial muscle actuator assembly, US6067892 A, Google Patents, U.S.A., 2000.
[107] B. Tondu, P. Lopez, The McKibben muscle and its use in actuating robot-arms showing similarities with human arm behaviour, Industrial Robot: An International Journal 24(6) (1997) 432-439.
[108] S. Sanan, P.S. Lynn, S.T. Griffith, Pneumatic Torsional Actuators for Inflatable Robots, Journal of Mechanisms and Robotics 6(3) (2014) 031003-031003-7.
[109] F. Connolly, P. Polygerinos, C.J. Walsh, K. Bertoldi, Mechanical Programming of Soft Actuators by Varying Fiber Angle, Soft Robotics 2(1) (2015) 26-32.
[110] J. Foroughi, G.M. Spinks, G.G. Wallace, J. Oh, M.E. Kozlov, S. Fang, T. Mirfakhrai, J.D.W. Madden, M.K. Shin, S.J. Kim, R.H. Baughman, Torsional Carbon Nanotube Artificial Muscles, Science 334(6055) (2011) 494-497.
[111] C. Choi, S.H. Kim, H.J. Sim, J.A. Lee, A.Y. Choi, Y.T. Kim, X. Lepró, G.M. Spinks, R.H. Baughman, S.J. Kim, Stretchable, Weavable Coiled Carbon

Nanotube/MnO2/Polymer Fiber Solid-State Supercapacitors, Scientific Reports 5 (2015) 9387.

[112] K.-Y. Chun, S. Hyeong Kim, M. Kyoon Shin, C. Hoon Kwon, J. Park, Y. Tae Kim, G.M. Spinks, M.D. Lima, C.S. Haines, R.H. Baughman, S. Jeong Kim, Hybrid carbon nanotube yarn artificial muscle inspired by spider dragline silk, Nat Commun 5 (2014).

[113] J. Di, S. Fang, F.A. Moura, D.S. Galvão, J. Bykova, A. Aliev, M.J. de Andrade, X. Lepró, N. Li, C. Haines, R. Ovalle-Robles, D. Qian, R.H. Baughman, Strong, Twist-Stable Carbon Nanotube Yarns and Muscles by Tension Annealing at Extreme Temperatures, Advanced Materials 28(31) (2016) 6598-6605.

[114] W. Guo, C. Liu, F. Zhao, X. Sun, Z. Yang, T. Chen, X. Chen, L. Qiu, X. Hu, H. Peng, A Novel Electromechanical Actuation Mechanism of a Carbon Nanotube Fiber, Advanced Materials 24(39) (2012) 5379-5384.

[115] J.A. Lee, R.H. Baughman, S.J. Kim, High performance electrochemical and electrothermal artificial muscles from twist-spun carbon nanotube yarn, Nano Convergence 2(1) (2015) 8.

[116] J.A. Lee, Y.T. Kim, G.M. Spinks, D. Suh, X. Lepró, M.D. Lima, R.H. Baughman, S.J. Kim, All-Solid-State Carbon Nanotube Torsional and Tensile Artificial Muscles, Nano Letters 14(5) (2014) 2664-2669.

[117] M.D. Lima, N. Li, M. Jung de Andrade, S. Fang, J. Oh, G.M. Spinks, M.E. Kozlov, C.S. Haines, D. Suh, J. Foroughi, S.J. Kim, Y. Chen, T. Ware, M.K. Shin, L.D. Machado, A.F. Fonseca, J.D.W. Madden, W.E. Voit, D.S. Galvão, R.H. Baughman, Electrically, Chemically, and Photonically Powered Torsional and Tensile Actuation of Hybrid Carbon Nanotube Yarn Muscles, Science 338(6109) (2012) 928-932.

[118] S.M. Mirvakili, A. Pazukha, W. Sikkema, C.W. Sinclair, G.M. Spinks, R.H. Baughman, J.D.W. Madden, Niobium Nanowire Yarns and their Application as Artificial Muscles, Advanced Functional Materials 23(35) (2013) 4311-4316.

[119] H. Cheng, Y. Hu, F. Zhao, Z. Dong, Y. Wang, N. Chen, Z. Zhang, L. Qu, Moisture-Activated Torsional Graphene-Fiber Motor, Advanced Materials 26(18) (2014) 2909-2913.

[120] D. Li, W.F. Paxton, R.H. Baughman, T.J. Huang, J.F. Stoddart, P.S. Weiss, Molecular, Supramolecular, and Macromolecular Motors and Artificial Muscles, MRS Bulletin 34(9) (2009) 671-681.

[121] P. Kim, C.M. Lieber, Nanotube nanotweezers, Science 286(5447) (1999) 2148-50.

[122] T. Rueckes, K. Kim, E. Joselevich, G.Y. Tseng, C.L. Cheung, C.M. Lieber, Carbon nanotube-based nonvolatile random access memory for molecular computing, Science 289(5476) (2000) 94-7.

[123] V.V. Deshpande, H.Y. Chiu, H.W.C. Postma, C. Mikó, L. Forró, M. Bockrath, Carbon Nanotube Linear Bearing Nanoswitches, Nano Letters 6(6) (2006) 1092-1095.

[124] R.H. Baughman, C. Cui, A.A. Zakhidov, Z. Iqbal, J.N. Barisci, G.M. Spinks, G.G. Wallace, A. Mazzoldi, D. De Rossi, A.G. Rinzler, O. Jaschinski, S. Roth, M. Kertesz, Carbon nanotube actuators, Science 284(5418) (1999) 1340-4.

[125] U. Vohrer, I. Kolaric, M.H. Haque, S. Roth, U. Detlaff-Weglikowska, Carbon nanotube sheets for the use as artificial muscles, Carbon 42(5–6) (2004) 1159-1164.

[126] J.D.W. Madden, J.N. Barisci, P.A. Anquetil, G.M. Spinks, G.G. Wallace, R.H. Baughman, I.W. Hunter, Fast Carbon Nanotube Charging and Actuation, Advanced Materials 18(7) (2006) 870-873.

[127] M. Tissaphern, O. Jiyoung, K. Mikhail, F. Eddie Chi Wah, Z. Mei, F. Shaoli, H.B. Ray, D.W.M. John, Electrochemical actuation of carbon nanotube yarns, Smart Materials and Structures 16(2) (2007) S243.

[128] L. Qu, Q. Peng, L. Dai, G.M. Spinks, G.G. Wallace, R.H. Baughman, Carbon Nanotube Electroactive Polymer Materials: Opportunities and Challenges, MRS Bulletin 33(3) (2008) 215-224.

[129] T. Mirfakhrai, J.D.W. Madden, R.H. Baughman, Polymer artificial muscles, Materials Today 10(4) (2007) 30-38.

[130] V.H. Ebron, Z. Yang, D.J. Seyer, M.E. Kozlov, J. Oh, H. Xie, J. Razal, L.J. Hall, J.P. Ferraris, A.G. Macdiarmid, R.H. Baughman, Fuel-powered artificial muscles, Science 311(5767) (2006) 1580-3.

[131] J.D. Madden, Mobile robots: motor challenges and materials solutions, Science 318(5853) (2007) 1094-7.

[132] S.V. Ahir, E.M. Terentjev, Photomechanical actuation in polymer-nanotube composites, Nat Mater 4(6) (2005) 491-495.

[133] H. Koerner, G. Price, N.A. Pearce, M. Alexander, R.A. Vaia, Remotely actuated polymer nanocomposites--stress-recovery of carbon-nanotube-filled thermoplastic elastomers, Nat Mater 3(2) (2004) 115-20.

[134] P. Miaudet, A. Derre, M. Maugey, C. Zakri, P.M. Piccione, R. Inoubli, P. Poulin, Shape and temperature memory of nanocomposites with broadened glass transition, Science 318(5854) (2007) 1294-6.
[135] G.M. Spinks, V. Mottaghitalab, M. Bahrami-Samani, P.G. Whitten, G.G. Wallace, Carbon-Nanotube-Reinforced Polyaniline Fibers for High-Strength Artificial Muscles, Advanced Materials 18(5) (2006) 637-640.
[136] S. Courty, J. Mine, A.R. Tajbakhsh, E.M. Terentjev, Nematic elastomers with aligned carbon nanotubes: New electromechanical actuators, Europhys. Lett. 64(5) (2003) 654-660.
[137] S. Liu, Y. Liu, H. Cebeci, R.G. de Villoria, J.-H. Lin, B.L. Wardle, Q.M. Zhang, High Electromechanical Response of Ionic Polymer Actuators with Controlled-Morphology Aligned Carbon Nanotube/Nafion Nanocomposite Electrodes, Advanced Functional Materials 20(19) (2010) 3266-3271.
[138] A.M. Fennimore, T.D. Yuzvinsky, W.-Q. Han, M.S. Fuhrer, J. Cumings, A. Zettl, Rotational actuators based on carbon nanotubes, Nature 424(6947) (2003) 408-410.
[139] H. Pan, J. Li, Y. Feng, Carbon Nanotubes for Supercapacitor, Nanoscale Research Letters 5(3) (2010) 654-668.
[140] T. Chen, L. Dai, Carbon nanomaterials for high-performance supercapacitors, Materials Today 16(7–8) (2013) 272-280.
[141] P. Simon, Y. Gogotsi, Materials for electrochemical capacitors, Nat Mater 7(11) (2008) 845-854.
[142] C. Choi, K.M. Kim, K.J. Kim, X. Lepró, G.M. Spinks, R.H. Baughman, S.J. Kim, Improvement of system capacitance via weavable superelastic biscrolled yarn supercapacitors, Nature Communications 7 (2016) 13811.
[143] D. Suh, T.K. Truong, D.G. Suh, S.C. Lim, Torsional Actuator Powered by Environmental Energy Harvesting from Diurnal Temperature Variation, ACS Sustainable Chemistry & Engineering 4(12) (2016) 6647-6652.
[144] P. Chen, Y. Xu, S. He, X. Sun, S. Pan, J. Deng, D. Chen, H. Peng, Hierarchically arranged helical fibre actuators driven by solvents and vapours, Nat Nano 10(12) (2015) 1077-1083.
[145] U. Kosidlo, M. Omastová, M. Micusík, G. Ćirić-Marjanović, H. Randriamahazaka, T. Wallmersperger, A. Aabloo, I. Kolaric, T. Bauernhansl,

Nanocarbon based ionic actuators—a review, Smart Materials and Structures 22(10) (2013) 104022.
[146] S.M. Mirvakili, M.N. Mirvakili, P. Englezos, J.D.W. Madden, I.W. Hunter, High-Performance Supercapacitors from Niobium Nanowire Yarns, ACS Applied Materials & Interfaces 7(25) (2015) 13882-13888.
[147] Z. Xu, C. Gao, Graphene chiral liquid crystals and macroscopic assembled fibres, Nature Communications 2 (2011) 571.
[148] Z. Dong, C. Jiang, H. Cheng, Y. Zhao, G. Shi, L. Jiang, L. Qu, Facile Fabrication of Light, Flexible and Multifunctional Graphene Fibers, Advanced Materials 24(14) (2012) 1856-1861.
[149] H.-P. Cong, X.-C. Ren, P. Wang, S.-H. Yu, Wet-spinning assembly of continuous, neat, and macroscopic graphene fibers, Scientific Reports 2 (2012) 613.
[150] Y. Meng, Y. Zhao, C. Hu, H. Cheng, Y. Hu, Z. Zhang, G. Shi, L. Qu, All-Graphene Core-Sheath Microfibers for All-Solid-State, Stretchable Fibriform Supercapacitors and Wearable Electronic Textiles, Advanced Materials 25(16) (2013) 2326-2331.
[151] H. Cheng, Z. Dong, C. Hu, Y. Zhao, Y. Hu, L. Qu, N. Chen, L. Dai, Textile electrodes woven by carbon nanotube-graphene hybrid fibers for flexible electrochemical capacitors, Nanoscale 5(8) (2013) 3428-3434.
[152] A. Taroni, Motorizing graphene fibres, Nat Mater 13(3) (2014) 223-223.
[153] A. Cherubini, G. Moretti, R. Vertechy, M. Fontana, Experimental characterization of thermally-activated artificial muscles based on coiled nylon fishing lines, AIP Advances 5(6) (2015) 067158.
[154] C.S. Haines, N. Li, G.M. Spinks, A.E. Aliev, J. Di, R.H. Baughman, New twist on artificial muscles, Proceedings of the National Academy of Sciences 113(42) (2016) 11709-11716.
[155] C.S. Haines, M.D. Lima, N. Li, G.M. Spinks, J. Foroughi, J.D.W. Madden, S.H. Kim, S. Fang, M. Jung de Andrade, F. Göktepe, Ö. Göktepe, S.M. Mirvakili, S. Naficy, X. Lepró, J. Oh, M.E. Kozlov, S.J. Kim, X. Xu, B.J. Swedlove, G.G. Wallace, R.H. Baughman, Artificial Muscles from Fishing Line and Sewing Thread, Science 343(6173) (2014) 868-872.

[156] S. Kianzad, M. Pandit, A. Bahi, A. Rafie Ravandi, F. Ko, G.M. Spinks, J.D.W. Madden, Nylon coil actuator operating temperature range and stiffness, 2015, pp. 94301X-94301X-6.

[157] S.M. Mirvakili, A. Rafie Ravandi, I.W. Hunter, C.S. Haines, N. Li, J. Foroughi, S. Naficy, G.M. Spinks, R.H. Baughman, J.D.W. Madden, Simple and strong: twisted silver painted nylon artificial muscle actuated by Joule heating, 2014, pp. 90560I-90560I-10.

[158] G.V. Stoychev, L. Ionov, Actuating Fibers: Design and Applications, ACS Applied Materials & Interfaces 8(37) (2016) 24281-24294.

[159] S.M. Mirvakili, I.W. Hunter, Bending artificial muscle from nylon filaments, 2016, pp. 97981L-97981L-7.

[160] S.M. Mirvakili, I.W. Hunter, Multidirectional Artificial Muscles from Nylon, Advanced Materials (2016) n/a-n/a.

[161] S.H. Kim, M.D. Lima, M.E. Kozlov, C.S. Haines, G.M. Spinks, S. Aziz, C. Choi, H.J. Sim, X. Wang, H. Lu, D. Qian, J.D.W. Madden, R.H. Baughman, S.J. Kim, Harvesting temperature fluctuations as electrical energy using torsional and tensile polymer muscles, Energy & Environmental Science 8(11) (2015) 3336-3344.

[162] F.B. Fuller, The Writhing Number of a Space Curve, Proceedings of the National Academy of Sciences 68(4) (1971) 815-819.

[163] G.H.M. van der Heijden, J.M.T. Thompson, Helical and Localised Buckling in Twisted Rods: A Unified Analysis of the Symmetric Case, Nonlinear Dynamics 21(1) (2000) 71-99.

[164] K.H. Cho, M.G. Song, H. Jung, J. Park, H. Moon, J.C. Koo, J.-D. Nam, H.R. Choi, A robotic finger driven by twisted and coiled polymer actuator, 2016, pp. 97981J-97981J-7.

[165] N. Li, C.S. HAINES, M.D. LIMA, D.A.M. Jung, S. Fang, J. Oh, M.E. KOZLOV, F. GOKTEPE, O. GOKTEPE, D. SUH, Coiled and non-coiled twisted nanofiber yarn and polymer fiber torsional and tensile actuators, Google Patents, 2014.

[166] F. Carpi, S. Bauer, D. De Rossi, Stretching Dielectric Elastomer Performance, Science 330(6012) (2010) 1759-1761.

[167] A.E.H. Love, A Treatise on the Mathematical Theory of Elasticity, Dover Publications1944.

[168] M. Hiraoka, K. Nakamura, H. Arase, K. Asai, Y. Kaneko, S.W. John, K. Tagashira, A. Omote, Power-efficient low-temperature woven coiled fibre actuator for wearable applications, Scientific Reports 6 (2016) 36358.
[169] S. Kianzad, M. Pandit, J.D. Lewis, A.R. Berlingeri, K.J. Haebler, J.D.W. Madden, Variable stiffness structure using nylon actuators arranged in a pennate muscle configuration, 2015, pp. 94301Z-94301Z-5.
[170] I.M. Ward, J. Sweeney, An Introduction to the Mechanical Properties of Solid Polymers, Wiley2004.
[171] C.L. Choy, F.C. Chen, K. Young, Negative thermal expansion in oriented crystalline polymers, Journal of Polymer Science: Polymer Physics Edition 19(2) (1981) 335-352.
[172] G.M. Kerch, L.A. Irgen, Thermal expansion of oriented polyethylene, Polymer Mechanics 11(3) (1975) 468-470.
[173] L.R.G. Treloar, The Physics of Rubber Elasticity, OUP Oxford2005.
[174] Q.W. Li, Y. Li, X.F. Zhang, S.B. Chikkannanavar, Y.H. Zhao, A.M. Dangelewicz, L.X. Zheng, S.K. Doorn, Q.X. Jia, D.E. Peterson, P.N. Arendt, Y.T. Zhu, Structure-Dependent Electrical Properties of Carbon Nanotube Fibers, Advanced Materials 19(20) (2007) 3358-3363.
[175] M. Miao, Electrical conductivity of pure carbon nanotube yarns, Carbon 49(12) (2011) 3755-3761.
[176] K. Koziol, J. Vilatela, A. Moisala, M. Motta, P. Cunniff, M. Sennett, A. Windle, High-Performance Carbon Nanotube Fiber, Science 318(5858) (2007) 1892-1895.
[177] B.T. Kelly, The thermal expansion coefficients of graphite crystals—the theoretical model and comparison with 1990 data, Carbon 29(6) (1991) 721-724.
[178] J.E. McIntyre, Synthetic Fibres: Nylon, Polyester, Acrylic, Polyolefin, Elsevier Science2004.
[179] O. Olabisi, K. Adewale, Handbook of Thermoplastics, Taylor & Francis1997.
[180] P. Mitchell, G.R.S. Naylor, D.G. Phillips, Torque in Worsted Wool Yarns, Textile Research Journal 76(2) (2006) 169-180.
[181] A.D. McNaught, A. Wilkinson, I.U.o. Pure, A. Chemistry, Compendium of Chemical Terminology: IUPAC Recommendations, Blackwell Science1997.

[182] T. Shibukawa, V.D. Gupta, R. Turner, J.H. Dillon, A.V. Tobolsky, Temperature Dependence of Shear Modulus and Density of Nylon-6, Textile Research Journal 32(12) (1962) 1011-1012.
[183] P. Klemens, Thermal Conductivity 14, Springer US2013.
[184] S. Aziz, S. Naficy, J. Foroughi, H.R. Brown, G.M. Spinks, Characterisation of torsional actuation in highly twisted yarns and fibres, Polymer Testing 46 (2015) 88-97.
[185] S. Aziz, S. Naficy, J. Foroughi, H.R. Brown, G.M. Spinks, Controlled and scalable torsional actuation of twisted nylon 6 fiber, Journal of Polymer Science Part B: Polymer Physics 54(13) (2016) 1278-1286.
[186] D.M. Hall, I.R. Bruss, J.R. Barone, G.M. Grason, Morphology selection via geometric frustration in chiral filament bundles, Nat Mater advance online publication (2016).
[187] P. Weigel, Macromolecular physics. Vol. 3: Crystal melting. Von BERNHARD WUNDERLICH. New York/London/Toronto/Sydney/San Francisco: Academic Press 1980. XIII, 363 S., Lwd., $ 42.50, Acta Polymerica 32(7) (1981) 413-413.
[188] A. Boller, B. Wunderlich, Multiple melting peak analysis with gel-spun ultra-high molar mass polyethylene, Journal of thermal analysis 49(1) (1997) 343-349.
[189] F.P. Reding, The stiffness modulus of polyethylene as a function of temperature and structure, Journal of Polymer Science 32(125) (1958) 487-502.
[190] L.L. Govaert, P.P. Lemstra, Deformation behavior of oriented UHMW-PE fibers, Colloid and Polymer Science 270(5) (1992) 455 - null.
[191] G. Hartwig, Polymer Properties at Room and Cryogenic Temperatures, Springer US2013.
[192] A. Suzuki, Y. Chen, T. Kunugi, Application of a continuous zone-drawing method to nylon 66 fibres, Polymer 39(22) (1998) 5335-5341.
[193] H.P. Nadella, J.E. Spruiell, J.L. White, Drawing and annealing of polypropylene fibers: Structural changes and mechanical properties, Journal of Applied Polymer Science 22(11) (1978) 3121-3133.
[194] G. Bhat, Structure and Properties of High-Performance Fibers, Elsevier Science2016.
[195] T.D. Fornes, D.R. Paul, Crystallization behavior of nylon 6 nanocomposites, Polymer 44(14) (2003) 3945-3961.

[196] Y. Liu, L. Cui, F. Guan, Y. Gao, N.E. Hedin, L. Zhu, H. Fong, Crystalline Morphology and Polymorphic Phase Transitions in Electrospun Nylon 6 Nanofibers, Macromolecules 40(17) (2007) 6283-6290.
[197] I. Tsujimoto, T. Kurokawa, T. Takahashi, K. Sakurai, Change in fine structure of nylon 6 gut yarn in twisting, annealing, and untwisting processes. I. Observation by WAXD, SAXD, and EM, Journal of Applied Polymer Science 24(11) (1979) 2289-2301.
[198] V. Miri, O. Persyn, J.M. Lefebvre, R. Seguela, Effect of water absorption on the plastic deformation behavior of nylon 6, European Polymer Journal 45(3) (2009) 757-762.
[199] I. Boukal, Effect of water on the mechanism of deformation of nylon 6, Journal of Applied Polymer Science 11(8) (1967) 1483-1494.
[200] G. Hinrichsen, The role of water in polyamides, Colloid and Polymer Science 256(1) (1978) 9-14.
[201] N.S. Murthy, M. Stamm, J.P. Sibilia, S. Krimm, Structural changes accompanying hydration in nylon 6, Macromolecules 22(3) (1989) 1261-1267.
[202] Y.P. Khanna, W.P. Kuhn, W.J. Sichina, Reliable Measurements of the Nylon 6 Glass Transition Made Possible by the New Dynamic DSC, Macromolecules 28(8) (1995) 2644-2646.
[203] J.B. Park, K.L. Devries, W.O. Station, Structure changes caused by strain annealing of nylon 6 fibers, Journal of Macromolecular Science, Part B 15(2) (1978) 229-256.
[204] E. Richardson, G. Martin, P. Wyeth, Effects of heat on new and aged polyamide 6,6 textiles during pest eradication, Polymer Degradation and Stability 107 (2014) 262-269.
[205] L.W. McKeen, The Effect of Creep and Other Time Related Factors on Plastics and Elastomers, Second ed., Elsevier Science, Amsterdam, 2009.
[206] M.Y. Keating, L.B. Malone, W.D. Saunders, Annealing effect on semi-crystalline materials in creep behavior, Journal of Thermal Analysis and Calorimetry 69(1) (2002) 37-52.
[207] K.S. Fancey, A mechanical model for creep, recovery and stress relaxation in polymeric materials, Journal of Materials Science 40(18) (2005) 4827-4831.

[208] G.M. Spinks, Stretchable artificial muscles from coiled polymer fibers, Journal of Materials Research 31(19) (2016) 2917-2927.
[209] A.L. Ross, Cable Kinking Analysis and Prevention, Journal of Engineering for Industry 99(1) (1977) 112-115.
[210] H. Xin, S.Z. Saricilar, H.R. Brown, P.G. Whitten, G.M. Spinks, Effect of First Network Topology on the Toughness of Double Network Hydrogels, Macromolecules 46(16) (2013) 6613-6620.
[211] J.E. McIntyre, T. Institute, Synthetic Fibres: Nylon, Polyester, Acrylic, Polyolefin, First ed., CRC Press, U.S.A. , 2005.